



**CALIFORNIA
ENERGY COMMISSION**



**CALIFORNIA
natural
resources
AGENCY**

California Energy Commission
Clean Transportation Program

FINAL PROJECT REPORT

Development of High Energy Density Lithium Batteries

Prepared for: California Energy Commission

Prepared by: Envia



**Gavin Newsom, Governor
November 2019 | CEC-600-2019-071**

California Energy Commission

Herman Lopez

Michael Sinkula

Primary Authors

Envia Systems

7979 Gateway Blvd. Suite 101

Newark, CA 94560

510-962-3682

[Envia Systems Website](http://www.enviasystems.com) (www.enviasystems.com)

Agreement Number: ARV-09-004

Charles Smith

Project Manager

Charles Smith

Office Manager

TRANSPORTATION POLICY AND ANALYSIS OFFICE

Kevin Barker

Deputy Director

FUELS AND TRANSPORTATION

Drew Bohan

Executive Director

Disclaimer

Staff members of the California Energy Commission prepared this report. As such, it does not necessarily represent the views of the Energy Commission, its employees, or the State of California. The Energy Commission, the State of California, its employees, contractors and subcontractors make no warrant, express or implied, and assume no legal liability for the information in this report; nor does any party represent that the uses of this information will not infringe upon privately owned rights. This report has not been approved or disapproved by the Energy Commission nor has the Commission passed upon the accuracy or adequacy of the information in this report.

PREFACE

Assembly Bill 118 (Núñez, Chapter 750, Statutes of 2007) created the Clean Transportation Program, formerly known as the Alternative and Renewable Fuel and Vehicle Technology Program. The statute authorizes the California Energy Commission (CEC) to develop and deploy alternative and renewable fuels and advanced transportation technologies to help attain the state's climate change policies. Assembly Bill 8 (Perea, Chapter 401, Statutes of 2013) reauthorizes the Clean Transportation Program through January 1, 2024, and specifies that the CEC allocate up to \$20 million per year (or up to 20 percent of each fiscal year's funds) in funding for hydrogen station development until at least 100 stations are operational.

The Clean Transportation Program has an annual budget of about \$100 million and provides financial support for projects that:

- Reduce California's use and dependence on petroleum transportation fuels and increase the use of alternative and renewable fuels and advanced vehicle technologies.
- Produce sustainable alternative and renewable low-carbon fuels in California.
- Expand alternative fueling infrastructure and fueling stations.
- Improve the efficiency, performance and market viability of alternative light-, medium-, and heavy-duty vehicle technologies.
- Retrofit medium- and heavy-duty on-road and nonroad vehicle fleets to alternative technologies or fuel use.
- Expand the alternative fueling infrastructure available to existing fleets, public transit, and transportation corridors.
- Establish workforce-training programs and conduct public outreach on the benefits of alternative transportation fuels and vehicle technologies.

To be eligible for funding under the Clean Transportation Program, a project must be consistent with the CEC's annual Clean Transportation Program *Investment Plan Update*. The CEC issued solicitation PON-08-010 to provide funding opportunities under the Clean Transportation Program for American Recovery and Reinvestment Act of 2009 Cost Share Projects. In response to PON-08-010, the recipient submitted application 119, which was proposed for funding in the CEC's Notice of Proposed Awards on November 16, 2009. The agreement was executed as ARV-09-004 on September 1, 2010 for \$933,854.

ABSTRACT

Envia Systems, in partnership with Argonne National Laboratory, proposed to develop and scale-up high energy density lithium ion batteries using nano silicon-carbon composite anodes and high capacity manganese rich layered-layered composite cathodes. Silicon coated carbon nanotubes and fibers and silicon and porous silicon-carbon composite anodes were developed. The novel anode composites targeted a high specific capacity ($\geq 1000\text{mAh/g}$), low irreversible capacity loss ($\leq 200\text{mAh/g}$) and improved cycle life. Envia also developed cathodes with high specific capacity ($\geq 250\text{mAh/g}$) and an irreversible capacity loss that is tailored to match the irreversible capacity loss of the anodes. Integration of both novel anode and cathodes electrodes will take place in the form of approximately 40Ah capacity commercial format pouch cells. Energy density of the commercial pouch cells is expected to be over 400Wh/Kg, which is almost double the energy density of what is available commercially in laptop batteries and three times the energy density of automotive batteries, making widespread adoption of plug-in-hybrid electric vehicles and electric vehicles possible.

Keywords: Energy density, lithium ion battery, silicon-carbon composite anodes, manganese rich layered-layered composite cathodes, 400 Wh/kg, battery electric vehicle, plug-in hybrid vehicle, large format cell, Argonne National Laboratory, ARPA-E.

Please use the following citation for this report:

Lopez, Herman, Michael Sinkula. (Envia Systems). 2019. *High Energy Density Lithium Batteries*. California Energy Commission. Publication Number: CEC-600-2019-071.

TABLE OF CONTENTS

	Page
Preface.....	i
Abstract	ii
Table of Contents.....	iii
List of Figures.....	iii
List of Tables	vii
Executive SUMMARY	1
CHAPTER 1: Purpose and Approach	3
CHAPTER 2: Anode Development.....	5
Development of Silicon-Coated and Alloyed Intermetallic Carbon Fiber Anodes.....	5
Development of Silicon-Coated Aligned Carbon Nanotube and Graphene Anodes.....	14
Development of Silicon-Carbon Alloy Anodes by Electrochemical Anodization of Silicon	17
Chemical Synthesis of Porous Silicon.....	23
Anode Materials Scale Up.....	47
CHAPTER 3: Cathode Development.....	53
CHAPTER 4: Large Cell Integration.....	60
CHAPTER 5: Independent Cell Testing Validation	72
CHAPTER 6: Thermal Stability and Abuse Testing	75
CHAPTER 7: Future Direction.....	77
Glossary	78

LIST OF FIGURES

	Page
Figure 1: CF Charge Capacity versus Cycles for the Various Screened CFs	6
Figure 2: SEM Micrograph of a Si-CF Composite Anode Material after High Energy Mechanical Milling	6
Figure 3: Charge Capability versus Cycles for the CF-Si Composites with Increasing Content of Si in the Composite	7
Figure 4: A) Charge Capacity versus Cycles for the Sdcf-Si Composites Prepared by Various Methods; B) Half Cell Electrochemical Performance of High Energy Mechanically Milled Si-CF Composite	7
Figure 5: Full Cell Electrochemical Performance of the High Energy Mechanically Milled Si-CF Anode with Envia’s High Capacity Manganese Rich Cathode Based on the (a) Cathode and (b) Anode Active Weight.....	8
Figure 6: SEM Micrographs of (a) Pristine Nanosilicon and (b) Nanosilicon after the Carbon Coating Process	9

Figure 7: Half Cell Electrochemical Performance of the Carbon Coated Nanosilicon Mixed with CF Anodes	10
Figure 8: Full Cell Electrochemical Performance of the Carbon Coated Nanosilicon-Cf Anode WITH Envia’s High Capacity Manganese Rich Cathode based on the (a) Cathode and (b) Anode Active Weight	11
Figure 9: Half Cell Electrochemical Performance of Various Si-Fe-CF Intermetallic Anode Alloys	13
Figure 10: Full Cell Electrochemical Performance of a Si-Fe-CF Intermetallic Alloy with Envia’s HCMR™ Cathode	14
Figure 11: SEM Image (A) and Half Cell Electrochemical Performance (B) Of ACNT-Si Nanoparticle Anode Composites Grown by CVD	15
Figure 12: SEM Images of Varying Si Nanoparticle Size and Coverage Deposited Over Graphene	16
Figure 13: Half-Cell Electrochemical Cycling Performance of the Si-Graphene Composite Material (A) and Full Cell Electrochemical Performance of the Si-Graphene Anode Composite Paired with Argonne’s High Capacity Cathode (B).....	17
Figure 14: (A) Schematic of the Electrochemical Anodization Setup and (B) Actual Electrochemical Anodization Setup Used to Produce Porous Si	18
Figure 15: Cross-Section SEM Images of Porous Si (P+) at Various Current Densities: A) 150ma/Cm ² for 20min in 35 Percent HF Solution and B) 50ma/Cm ² For 1hr in 35 Percent HF Solution.....	18
Figure 16: Cross-Section SEM Images of Porous Si (P+) Produced at Various HF Concentrations: A) At 50ma/Cm ² in 25 Percent HF Solution and B) At 50ma/Cm ² in 45 Percent HF Solution.....	19
Figure 17: Cross-Section SEM Images of Porous Si Produced From Different Types of Si Wafers: A) 50ma/Cm ² , 60 Min, 35 Percent HF, P+ And B) 50ma/Cm ² , 30min, 35 Percent HF, N+	19
Figure 18: Half Cell Electrochemical Performance of Porous Si and Pristine P+ Si Anodes	20
Figure 19: Half Cell Electrochemical Performance versus Cycles for Different Porous Si Composites Anodes Which Are Carbon Coated	21
Figure 20: Electrochemical Performance of Oxidized Porous Silicon	22
Figure 21: Electrochemical Performance of Oxidized and Carbonized Porous Silicon	23
Figure 22: Schematic Showing the Hydrothermal Synthesis Approach to Produce Carbon-Coated Nanosilicon.....	23
Figure 23: Hydrothermal Synthesis Reactor	24
Figure 24: SEM Micrographs of Porous Si Prepared by the Hydrothermal Process: (A) 50wt Percent HF, 140°C, 6 H And (B) 50wt Percent HF, 160°C, 2 H.....	24
Figure 25: Electrochemical Performance of Porous and Pristine Silicon	25
Figure 26: SEM Micrographs of Chemically Produced Porous Si Anode Via a Solid State Process	25

Figure 27: XRD Patterns of Porous Si Synthesized by Solid State Method. The Sample Numbers Refer to the Experimental Condition in Table 4	27
Figure 28: Half Cell Specific Capacity versus Cycles for Chemically Produced Porous Si Anodes. The Number Refers to the Experimental Condition in Table 4	27
Figure 29: Half Cell Specific Capacity versus Cycles for Chemically-Produced Porous Si and Porous Silicon-Carbon Anodes.....	28
Figure 30: Full Cell Specific Capacity (Based On Cathode And Anode Active Weight) and Columbic Efficiency Versus Cycles for Chemically Produced Porous Si Anodes	29
Figure 31: Specific Capacity versus Cycles for Chemically Produced Porous Silicon-Carbon Composite Anodes	30
Figure 32: Half Cell Specific Capacity versus Cycles for Chemically Produced Porous Silicon-Carbon Anodes	31
Figure 33: Full Cell Specific Capacity (Based On Cathode and Anode Active Weight) and Columbic Efficiency versus Cycles For Chemically Produced Porous Silicon-Carbon Anodes And Lithium Additive	33
Figure 34: Schematic of the Chemical Synthesis of Porous Si-C-O Anodes Via Liquid Phase Route	33
Figure 35: A) Half Cell and B) Full Cell Electrochemical Performance from Chemically Synthesized Si-C-O Anodes via Carbonization of Cross-Linked Polysiloxane Precursors.....	34
Figure 36: XRD Spectra of Magnesium Reduction of A) Polydiethoxysiloxane and B) Sodium Silicate	35
Figure 37: Cyclic Performance of Porous Si Anode Synthesized From Magnesium Reduction of Sodium Silicate	35
Figure 38: A) Half Cell and B) Full Cell Electrochemical Performance versus Cycles for Porous Si Based Anodes Synthesized Based On TEOS	36
Figure 39: High Energy Planetary Ball Mill Used to Form Alloy Materials.....	37
Figure 40: A) Capacity versus Cycles and Voltage versus Capacity For C-Si-Hard Carbon Alloys and B) Charge-Discharge Performance of Si-Fe-C Alloys Prepared By HEMM.....	37
Figure 41: Half Cell Capacity versus Cycling Performance of Sio-Based Anodes Prepared by HEMM	38
Figure 42: Sem Images of Carbon-Sio-Hard Carbon at Different Magnifications.....	38
Figure 43: Particle Size Distribution of Pristine and Mechanically Milled (HEMM) Sio	39
Figure 44: A) Cycling Performance in a Half Cell Configuration And B) XRD Analysis of Sio at Different Mechanical Milling (HEMM) Times	39
Figure 45: A) XRD Analysis and B) Half Cell Electrochemical Behavior of Sio-Ni and Sio-Ni-CNF Anode Composites	40
Figure 46: Full Cell Electrochemical Performance of Sio-Ni-CNF Anode and HCMR Cathode Based on Anode and Cathode Active Weights	41
Figure 47: Half Cell Electrochemical Cycling Performance of Sio-Graphite Composite Anodes with Higher Sio Percent. Different Electrode Loading Densities Are Shown.....	42

Figure 48: Full Cell Electrochemical Cycling Performance of Sio-Graphite Composite Anodes Based on the Cathode and Anode Active Weights. Anode Loading Is 2.47mg/Cm ²	43
Figure 49: Full Cell Electrochemical Cycling Performance of Sio-Graphite Composite Anodes Based on the Cathode and Anode Active Weights. Anode Loading Is 2.08mg/Cm ²	43
Figure 50: Half Cell Cycling Performance of Sio-Si-Gr-HC Anode Composites with Varying Amounts of Si	44
Figure 51: Full Cell Electrochemical Cycling Performance of Envia’s Si _α -Gr _β -Si _γ -M _δ -HC _ε -CF _ζ Anode and HCMR™ Cathode with Different Anode Electrode Loading Levels	45
Figure 52: Full Cell Electrochemical Data from Single Layer Pouch Cells with Different Cell Balance and Anode Electro Loading	46
Figure 53: Particle Size Distribution of Si Monoxide Obtained From HEMM in Small and Large Milling Jars Along With the Pristine Sio Material	47
Figure 54: Half Cell Specific Capacity of Si Monoxide Milled at Different HEMM Conditions	48
Figure 55: XRD Patterns of Si Monoxide Milled at Different HEMM Conditions	48
Figure 56: Half Cell Specific Capacity of Sio-Graphite Anode Milled for Different Times in a Large Jar	49
Figure 57: XRD Patterns of Sio-Graphite Anode Composites Milled at Different HEMM Conditions	50
Figure 58: Half Cell Electrochemical Performance from the Sio-Gr Scaled-Up 2Kg Batch, Small Jar Material and Individual Large Jars	51
Figure 59: Specific Discharge Capacity versus Cycles for Optimized Cathode Materials	53
Figure 60: XRD Patterns of Different High Capacity Manganese Rich Cathodes	54
Figure 61: Half Cell Electrochemical Performance from the Optimized HCMR™ Cathode Material	55
Figure 62: Half Cell Electrochemical Performance from the Scale-Up 10Kg Cathode Batch	56
Figure 63: Half Cell Electrochemical Performance of HCMR™ Cathode with 2 Electrode Compositions at an Electrode Loading of Approximately 22mg/Cm ²	57
Figure 64: Half Cell Electrochemical Performance of HCMR Cathode with Various Electrode Loading Levels at an Electrode Density of 2.7g/Cc	58
Figure 65: Half Cell Electrochemical Performance of an HCMR™ Cathode with an Electrode Loading of 26mg/Cm ² and Electrode Density of 2.4g/Cc	58
Figure 66: Relationship of Cycling Capability and Cell Balance.....	60
Figure 67: Relationship of (a) Specific Capacity versus Cycles and (b) Energy Versus Cycles for Different Voltage Windows	61
Figure 68: Schematic Representation of Single Layer Pouch Cells.....	62
Figure 69: Electrochemical Performance of the Single Layer Pouch Cells with Heavy Loading Levels of the Cathode.....	63
Figure 70: Electrochemical Performance from 10Ah Capacity Pouch Cells With and Without Supplemental Lithium.....	64
Figure 71: Electrochemical Performance of 20Ah Cells With Envia’s HCMR™ Cathode and High Capacity Silicon-Based Anode	65

Figure 72: Energy Density and Average Voltage Versus Cycles for the 20Ah Capacity Pouch Cells with Envia’s HCMR™ Cathode and High Capacity Silicon-Based Anode.....	65
Figure 73a: First C/20 Charge-Discharge Curves from 37Ah Capacity Pouch Cells Incorporating Envia’s HCMR™ Cathode and High Capacity Silicon-Based Anode.....	66
Figure 73b: C/3 Charge-Discharge Curves from 35Ah Capacity Pouch Cells Incorporating Envia’s HCMR™ Cathode and High Capacity Silicon-Based Anode.....	67
Figure 74: (A) Charge and Discharge Curves for the First Formation Cycle at a C/20 Rate and (B) Third Cycle Corresponding to a C/3 Rate.....	70
Figure 75: Energy Density versus Cycles at a C/20, C/10 and C/3 Rate Cycled at 100 Percent DOD (4.6V to 1.5V).....	70
Figure 76: Normalized Energy Density versus Cycles for a 45Ah Cell Cycled at 80 Percent DOD at a C/3 Rate.....	71
Figure 77: Energy Density Versus Cycles for the 5 Cells Delivered to the NSWC (Cell #5, #6, #9, #11 & #12) Comparing to Cell #7 Which Was Tested at Envia.....	72
Figure 78: Energy Density versus Cycles for Cell #9 Tested at the NSWC in Crane.....	73
Figure 79: Comparison of the Normalized Energy Density Versus Cycles for 3 Cells Tested at NSWC (Cell #9, #11 And #12) and Tested at Envia (Cell #2).....	74
Figure 80: Thermal Characteristics of a (Approximately 45Ah) Silicon-Based Cell in Comparison to a (Approximately 20Ah) Graphite Based Cell.....	75

LIST OF TABLES

	Page
Table 1: Target Performance	3
Table 2: Summary and Status of CEC Project Milestones and Deliverables	4
Table 3: Summary of Different Si-CF Alloy Anodes Prepared by HEMM	12
Table 4: Experimental Conditions and the Resulting Surface Area of the Porous Si Formed....	26
Table 5: Experimental Conditions and the Resulting Surface Area of the Si Anodes	29
Table 6: Electrochemical Summary of Chemically Synthesized Porous Silicon-Carbon Composite Anodes.....	30
Table 7: Electrochemical Summary of Chemically Synthesized Porous Si Based Anodes	32
Table 8: Summary of Physical, Structural and Electrochemical Parameters of the Scale-up SiO-Gr Anode.....	52
Table 9: Energy Density Calculations at C/3 With Respect to the Cathode Electrode Density and Electrolyte Density (The Cell Modeling Was Done by Assuming a Fixed Cathode and Anode Loading Level and a Specific Ah for The Cell Capacity)	68
Table 10: Energy Density Calculations at C/3 With Respect to the Cathode and Anode Specific Capacities at a C/3 Rate (The Cell Modeling Was Done by Assuming a Fixed Cathode Loading Level and 30 Percent Excess Anode Balancing)	69

EXECUTIVE SUMMARY

In January 2010, Envia Systems began the development and scale-up of high energy density lithium ion batteries using nano silicon-carbon composite anodes and high capacity manganese rich layered composite cathodes. This work was co-funded by the CEC's Clean Transportation Program. The goal of the project was to develop, build, test and independently validate the highest energy density lithium ion batteries in the world and show reasonable cycle life. The energy density target of the program was 300 watt-hours per kilogram (Wh/kg) (later increased to 400 Wh/kg) with a cycle life target of 500 cycles.

At the U.S. Department of Energy's Advanced Research Projects Agency – Energy (ARPA-E) summit meeting in Washington in February, 2012, Envia announced the achievement of 400 Wh/kg lithium-ion batteries beyond 200 cycles with independent validation from a third party, the Naval Surface Warfare Center in Crane, Indiana. The high energy density results were measured from approximately 48 Ah capacity pouch cells. Electrochemical results from these cells showed an energy density of 430Wh/Kg at a C/20 discharge rate (meaning discharged over twenty hours). At a C/3 rate, the measured energy density is 390Wh/Kg with a corresponding cell capacity of approximately 45Ah. The energy density values of 390Wh/Kg at C/3 are nearly reaching the final cell target of 400Wh/Kg. With respect to cycle life, the cells show a cycle life of nearly 200 cycles at 80 percent depth of discharge before reaching 80 percent of the initial C/3 energy density.

The achievement of the program goal has tremendous implications for the emerging battery electric vehicle and plug-in hybrid electric vehicle market, which currently depends on batteries with energy densities in the range of 100-200Wh/kg. Because of the lower energy density of these cells, a very large battery pack is required to achieve a reasonable driving range, which adds significant costs to the automobile. High costs have limited the adoption of electric vehicles. Envia believes that its invention, as a result of this program, can eventually reduce the cost of electric vehicle batteries by over 50 percent, making widespread adoption of battery electric vehicles and plug-in hybrid electric vehicles possible.

CHAPTER 1:

Purpose and Approach

The CEC issued solicitation PON-08-010 to provide funding opportunities under the Clean Transportation Program for American Recovery and Reinvestment Act of 2009 Cost Share funding. In response to PON-08-010, Envia Systems (Envia) submitted application 119, which was proposed for funding in the CEC’s Notice of Proposed Awards on November 16, 2009. The agreement was executed as ARV-09-004 on September 1, 2010 for \$933,854, with another \$452,000 in private matching funds. Envia would develop a low cost, high energy density, and high performance battery system that could be utilized in the future by electric and plug-in hybrid electric vehicles.

The project focused on the development and testing of numerous anode technologies, as well as the synthesis of the best anodes with advanced cathodes into large format cells. Table 1 summarizes the performance goals for these anodes, cathodes and integrated cells.

Table 1: Target Performance

Anode Development Metrics	Rnk	Target
Specific Capacity	1	1000 mAh/g
IRCL	1	<200 mAh/g
Cycle life at C/3 rate, 80% DoD, >80% efficiency (half cell)	1	>50 cycles
Cycle life at C/3 rate, 80% DoD, >80% efficiency (full cell)	1	>100 cycles
Tap density	2	>1g/cc
Manufacturability	2	Yes
Cathode Development Metrics	Rnk	Target
Specific Capacity	1	260 mAh/g
IRCL	1	Tailored to Anode
Cycle life at C/3 rate, 80% DoD, >80% efficiency (half cell)	1	>50 cycles
Cycle life at C/3 rate, 80% DoD, >80% efficiency (full cell)	1	>100 cycles
Tap density	2	>1.8g/cc
Manufacturability	2	Yes
Large Format Cell Metrics	Rnk	Target
Gravimetric Energy Density	1	>400 Wh/kg
Cycle life at C/3 rate, 80% DoD, >80% efficiency	1	>500 cycles
Volumetric Energy Density	2	>850 Wh/L
Specific Power - Discharge, 80% DOD/30 sec	2	>570 W/kg
Power Density	2	>920W/L

Source: Envia Systems

Throughout the project, Envia explored multiple approaches on materials development, scale-up, cell design, engineering, building and testing of cells. Table 2 shows the various anode development approaches, summarizing which approaches were stopped, and which approaches continued through scale-up and large capacity cell development.

Table 2: Summary and Status of CEC Project Milestones and Deliverables

Task	Project	Description	Project Deliverables	Status
1 Phase I	Silicon Carbon Fiber Alloy & Composites Anodes	C. Form and test CF-Si alloy anodes	Stopped development	
		D. Form and test CF-Si composite anodes	Stopped development	
2 Phase I	Silicon Coated Aligned Carbon Nanotube & Silicon Graphene Composite Anodes	C. Form and test Si-ACNT anodes	Stopped development	
		C.L. Form and test Si-Graphene anodes	Stopped development	
3 Phase I	Electrochemical Synthesis of Silicon Nanostructure Composites	C. Form and Test PSi Carbon Intermetallic Alloy based Anodes	Stopped development	
4 Phase I	Chemical Synthesis of Silicon Nanostructure Composites	C. Form and Test PSi Carbon composite Anodes	Stopped development	
5 Phase I	High Surface Area Carbon Intermetallic Alloy Anodes	B. Form and test HSA Carbon Intermetallic Alloy Anodes	Q4 Milestone: Demonstrate capacity >1000 mAh/g, IRCL <200mAh/g of reversible capacity, and cycle life >50 cycles in a full cell configuration	Complete
			Q5 Milestone: Demonstrate capacity >1000 mAh/g, IRCL <200mAh/g and cycle life >100 cycles in a full cell configuration	Complete
		C. Produce down selected ANODE material for large format cell build	Q6 Milestone: Deliver 2kg of down selected anode material for large format cell demonstration (iteration #1)	Complete
			Q7 Milestone: Deliver 2kg of down selected anode material for large format cell demonstration (iteration #2-#3)	Complete
			Q8 Milestone: Deliver 2kg of down selected anode material for large format cell demonstration (iteration #4)	Complete
1 Phase II	Cathode Development	A. Develop and Optimize Cathode Compositions, Dopants, and Nanocoatings	Q3 Milestone: Demonstrate capacities >260mAh/g and a cycle life >30 cycles in a half cell configuration	Complete
		B. Test Advanced Cathode with Promising Advanced Anodes	Q4 Milestone: Demonstrate anode capacity >1000 mAh/g, IRCL <200mAh/g of reversible capacity, and cycle life >50 cycles in a full cell configuration	Complete
			Q5 Milestone: Deliver 3kg of down selected cathode material for large format cell demonstration (iteration #1)	Complete
		C. Produce down selected cathode material for large format cell build	Q6 Milestone: Deliver 3kg of down selected cathode material for large format cell demonstration (iteration #2)	Complete
			Q7 Milestone: Deliver 3kg of down selected cathode material for large format cell demonstration (iteration #3)	Complete
			Q8 Milestone: Deliver 3kg of down selected cathode material for large format cell demonstration (iteration #4)	Complete
1 Phase III	Large Cell Integration	A. Finalize design for commercial large format (10-40Ah) pouch cells	Q4 Milestone: Finalize the cell design for commercial large format 10-40Ah capacity pouch cells	Complete
			Q5 Milestone: Build 10-40Ah capacity pouch cells and demonstrate energy density >250 Wh/kg and a cycle life >100 cycles (iteration #1)	Complete
		B. Produce commercial large format (10-40Ah capacity) pouch cells	Q6 Milestone: Build 10-40Ah capacity pouch cells and demonstrate energy density >300 Wh/kg and a cycle life >200 cycles (iteration #2)	Complete
			Q7 Milestone: Build 10-40Ah capacity pouch cells and demonstrate energy density >350 Wh/kg and a cycle life >300 cycles (iteration #3)	In Progress
			Q8 Milestone: Build 10-40Ah capacity pouch cells and demonstrate energy density >400 Wh/kg and a cycle life >500 cycles (iteration #4)	In Progress
			Q8 Milestone: Deliver two (2) 10-40Ah capacity pouch cells to the Naval Warfare Center for independent testing	Complete

Source: Envia Systems

CHAPTER 2:

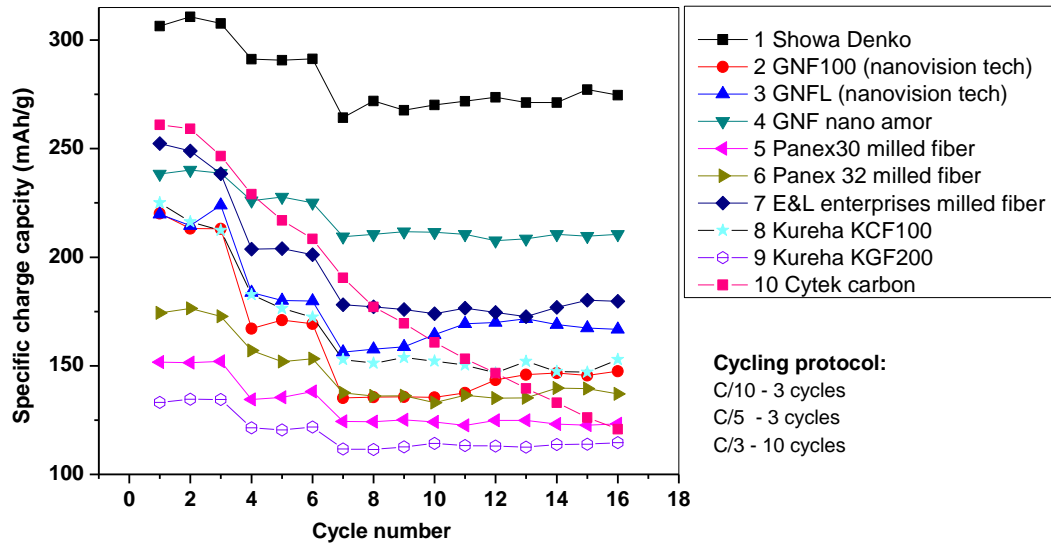
Anode Development

With respect to the anode, Envia has taken a multi-faceted approach where a variety of material compositions, synthesis techniques and morphologies were explored. While the various techniques are summarized in the following sections, over 20 different material approaches were comprehensively examined.

Development of Silicon-Coated and Alloyed Intermetallic Carbon Fiber Anodes

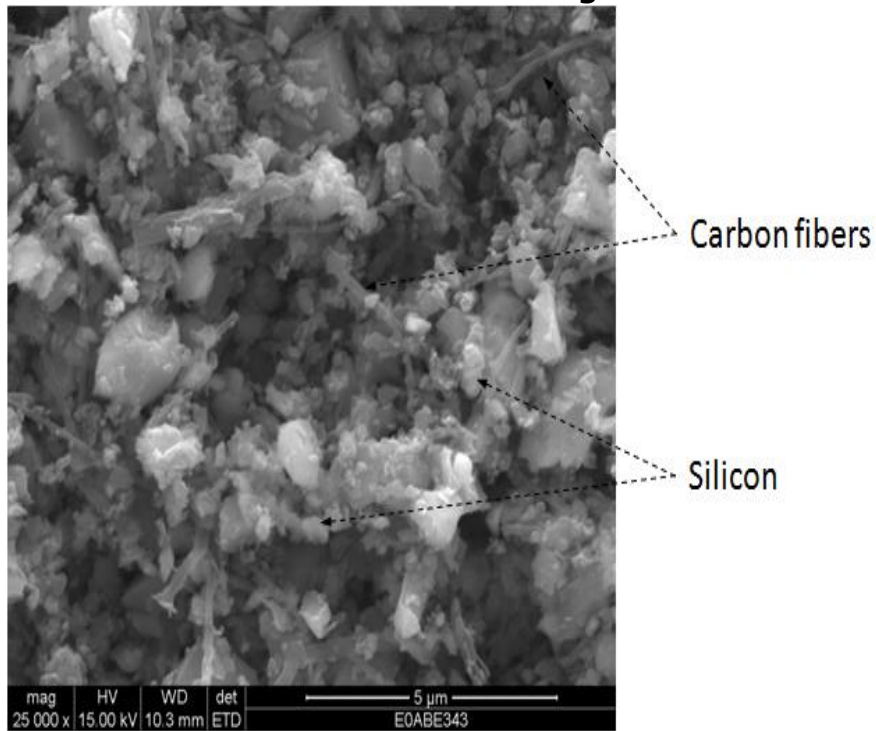
For Task 1, Envia developed a high-energy ball milling technique that utilized Nobilta mixing and Jar mill mixing to prepare the composites of carbon fiber (CF) and silicon (Si) material. Milling is a mechanical fusion method that can produce solid-solid composite materials in a dry process without the use of a binder and by only applying mechanical force. Both CF and Si powder in this task were commercially received and carefully down-selected from the sample lists and electrochemical performance as shown in Figure 1. Figure 2 shows the morphology of a Si-CF composite anode material after high-energy mechanical milling via a scanning electron microscope (SEM). CFs and Si powder were homogeneously mixed together. To reach the capacity goal, the content of Si was tuned to reach higher capacity. Figure 3 shows composites with more Si delivering higher capacity. But simply mixing Si powder with CFs didn't enhance the cycling stability of Si materials as indicated in Figure 4a and Figure 4b. By optimized the cell design, full cells with Si-CF anode and high capacity manganese rich (HCMR) cathode were surprisingly able to deliver decent capacity and good cycling capability. Figure 5 shows improved performance for the full cell with 54 percent excess anode and excess lithium, with a fade of about 5 percent in the first 50 cycles (cycles 7 through 57) at a C/3 rate. The corresponding capacity of this cell based on the anode active weight (figure 5b) is above the target 1000mAh/g at C/3 in 50 cycles with an efficiency of 95 percent and a first cycle irreversible capacity loss (IRCL) of 114mAh/g.

Figure 1: CF Charge Capacity versus Cycles for the Various Screened CFs



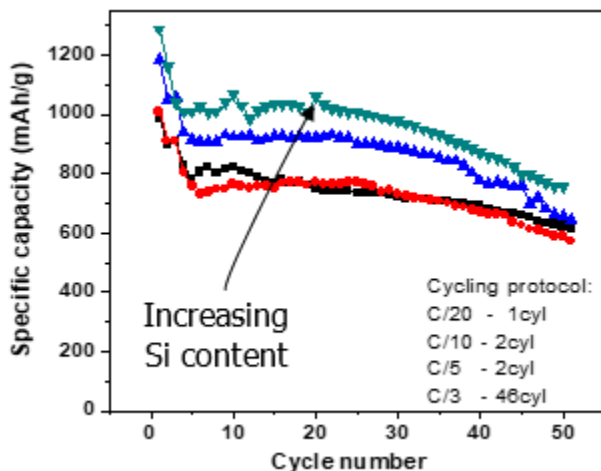
Source: Envia Systems

Figure 2: SEM Micrograph of a Si-CF Composite Anode Material after High Energy Mechanical Milling



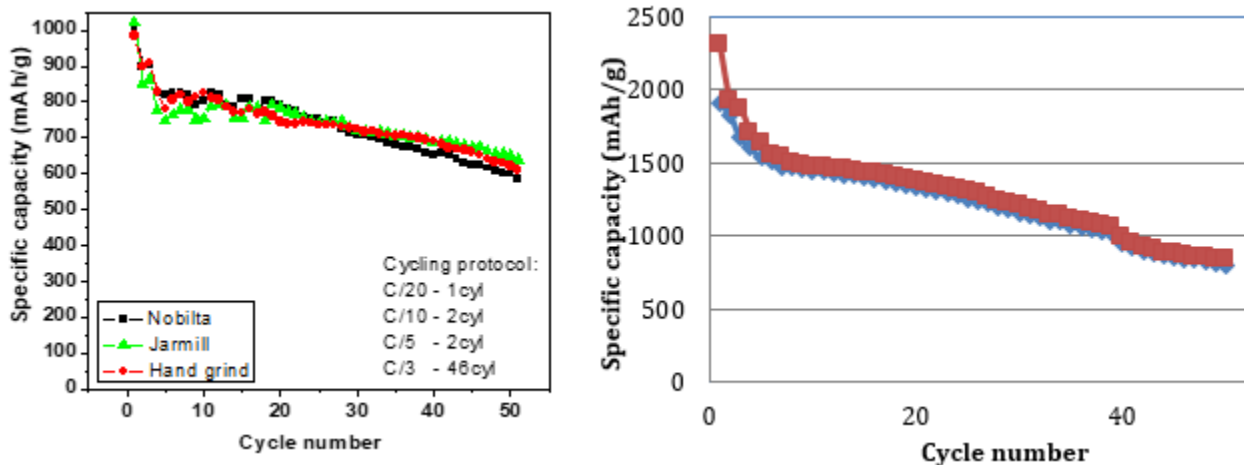
Source: Envia Systems

Figure 3: Charge Capability versus Cycles for the CF-Si Composites with Increasing Content of Si in the Composite



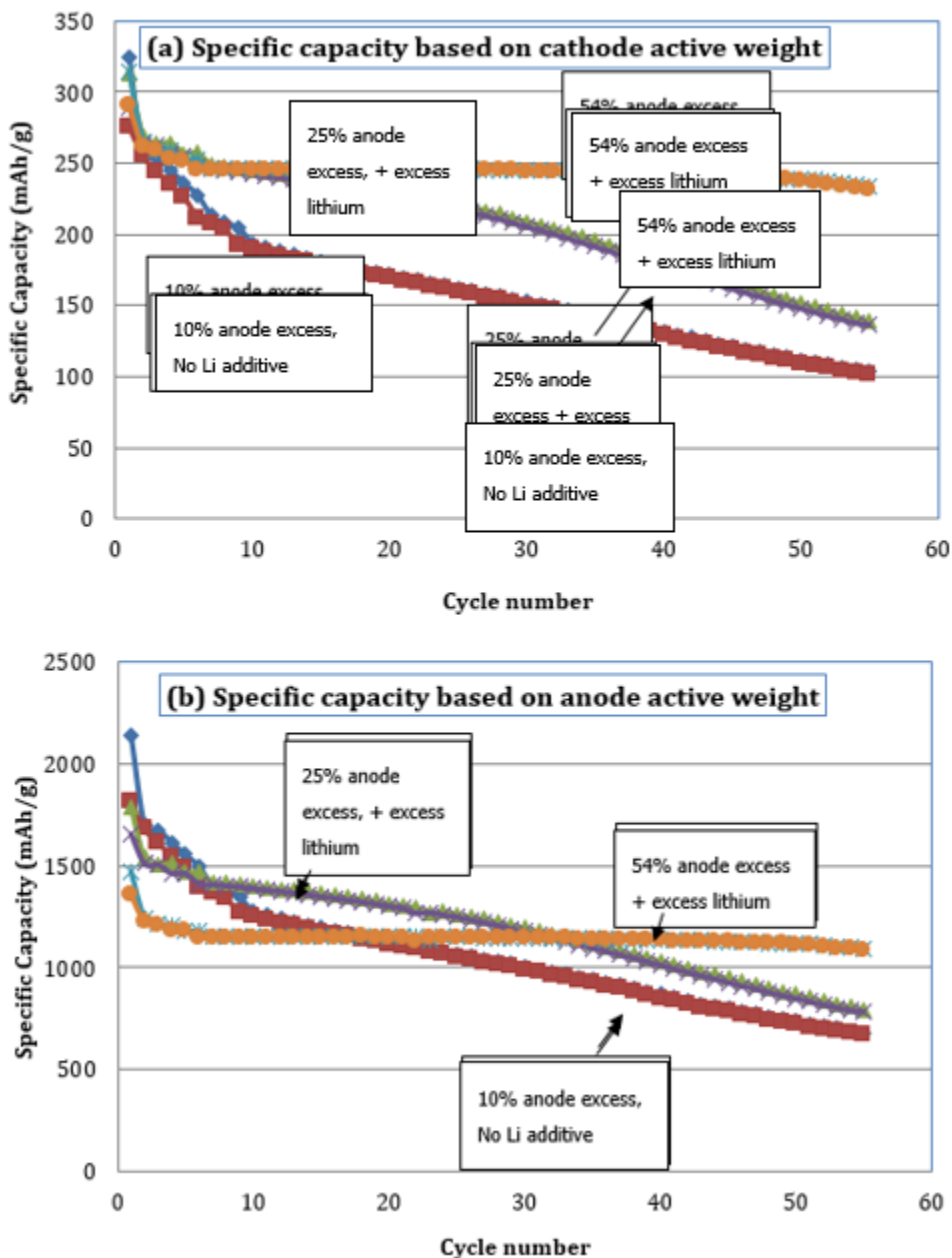
Source: Envia Systems

Figure 4: A) Charge Capacity versus Cycles for the Sdcf-Si Composites Prepared by Various Methods; B) Half Cell Electrochemical Performance of High Energy Mechanically Milled Si-CF Composite



Source: Envia Systems

Figure 5: Full Cell Electrochemical Performance of the High Energy Mechanically Milled Si-CF Anode with Envia's High Capacity Manganese Rich Cathode Based on the (a) Cathode and (b) Anode Active Weight

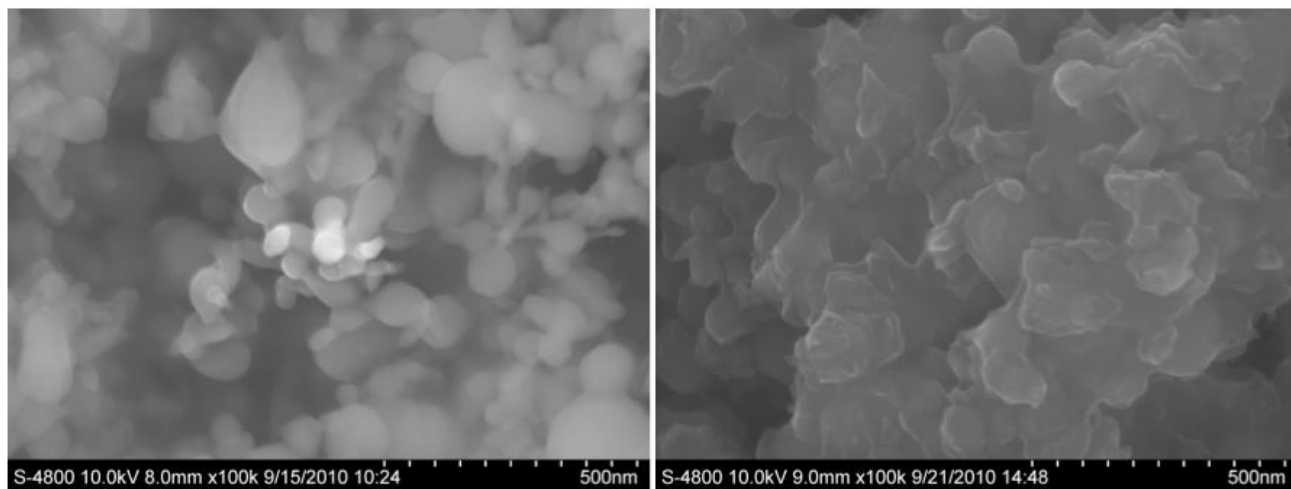


Source: Envia Systems

Carbonization and alloys with other elements were also tried to further improve the Si-CF composite cycling stability. Figure 6 shows the image of pristine Si and carbonized Si powders. After the coating process, no Si particles can be identified individually as the carbon coating is assumed to completely cover all of the nanosilicon. Candidates of carbon sources included glucose, sucrose, polyvinyl chloride or poly-acrylonitrile in a suitable solvent. Carbonation was performed at temperatures ranging from 700-1000 degrees Celsius ($^{\circ}\text{C}$) under an inert

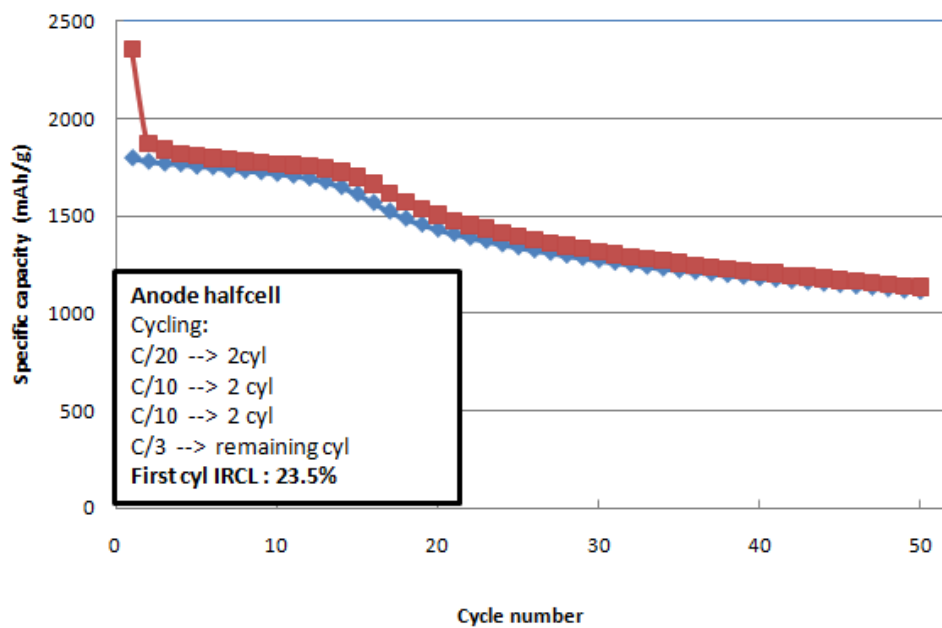
atmosphere. After carbonation, Si-CF composites showed improved cycling performance but the cycling stability was not enough to meet the demanding project targets, as shown by the half cell electrochemical data seen in Figure 7. With an optimized cell design, the full cell performance with carbonized Si-CF could not show better performance as indicated in Figure 8. Figure 8a shows the full cell capacity based on cathode active weight versus cycles where Figure 8b shows the similar data where the capacity is based on the anode active weight. In both cases the cycling performance has improved specially for the case where a lithium additive has been added to the cell.

Figure 6: SEM Micrographs of (a) Pristine Nanosilicon and (b) Nanosilicon after the Carbon Coating Process



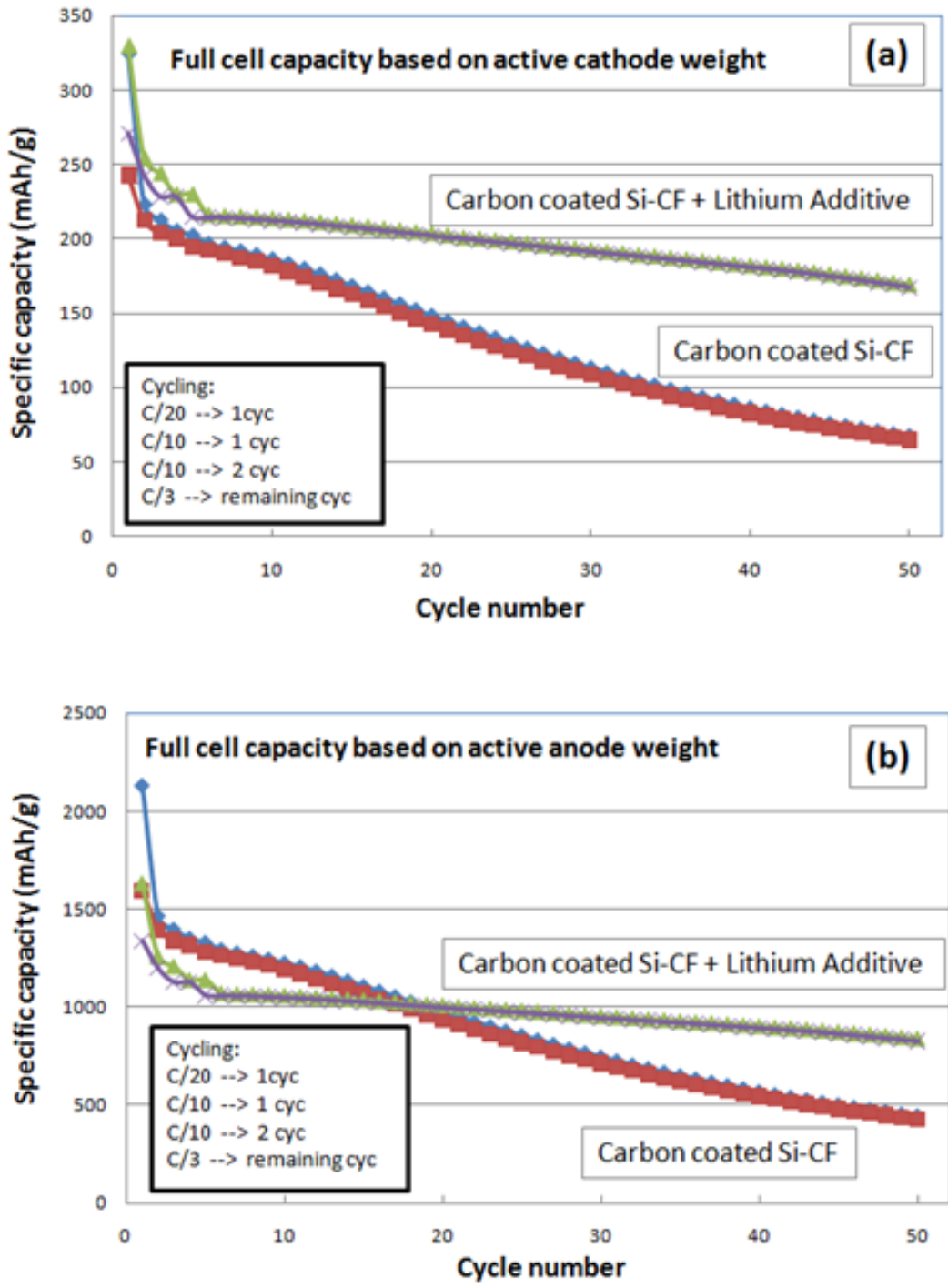
Source: Envia Systems

Figure 7: Half Cell Electrochemical Performance of the Carbon Coated Nanosilicon Mixed with CF Anodes



Source: Envia Systems

Figure 8: Full Cell Electrochemical Performance of the Carbon Coated Nanosilicon-Cf Anode WITH Envia's High Capacity Manganese Rich Cathode based on the (a) Cathode and (b) Anode Active Weight



Source: Envia Systems

For alloyed intermetallic CF anodes, Si-CF-M compositions were explored where metal M corresponds to copper (Cu), nickel (Ni) and iron (Fe). The various anode components were alloyed in a high-energy planetary ball mill. The idea was to develop a material that will yield a low first cycle irreversible capacity loss and show good cycling stability. Various compositions have been prepared by mixing the respective material ratios at different rotations per minute and times in the high-energy mechanical mill. Several intermetallic alloy compositions containing Si and CF with Fe and Cu are shown in Table 3.

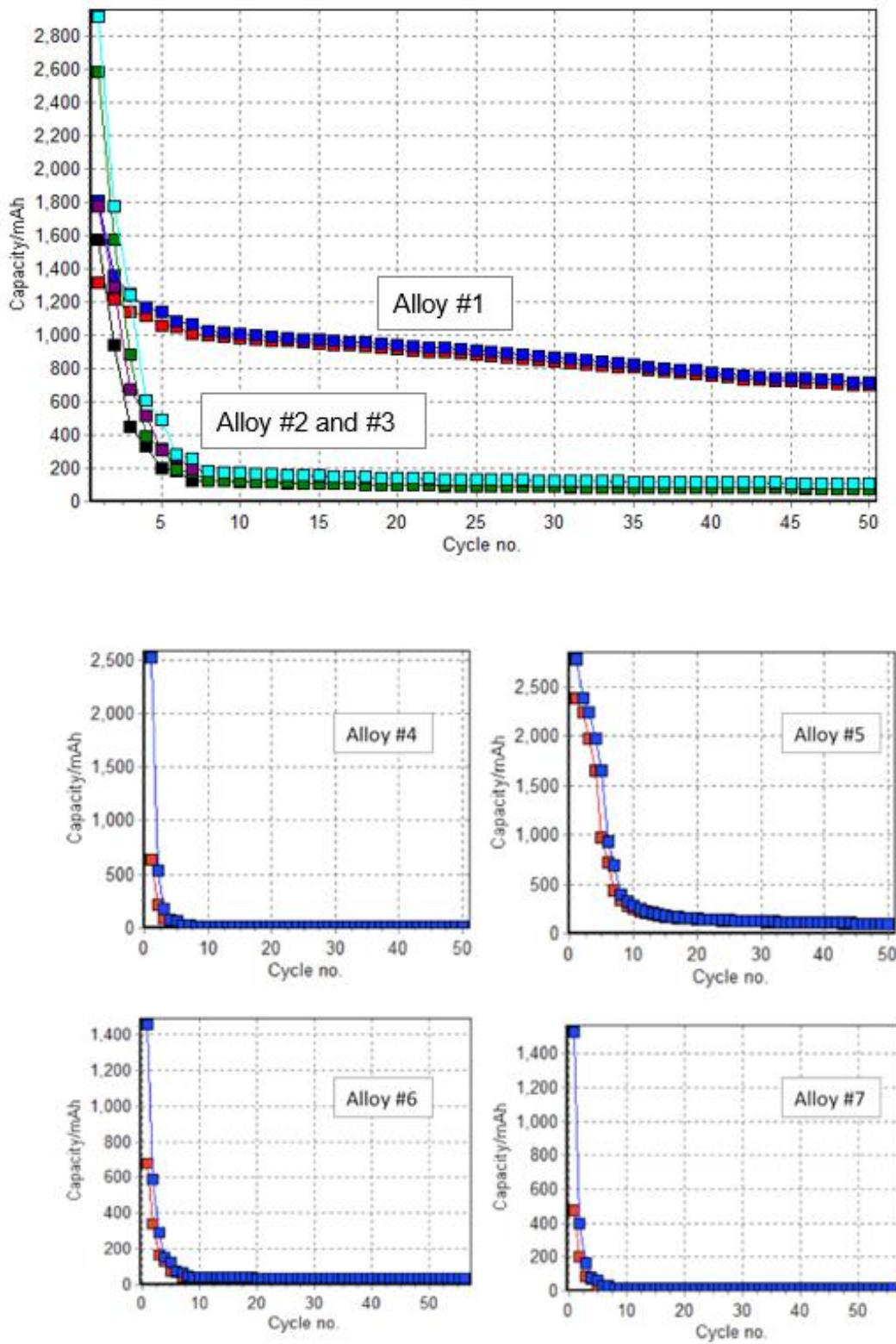
Table 3: Summary of Different Si-CF Alloy Anodes Prepared by HEMM

System	Alloy	Composition
Silicon-Iron-Carbon Fiber Alloy Anode	#1	$Si_{\alpha} Fe_{\beta} CF_{\gamma}$
	#2	$Si_{\alpha-x} Fe_{\beta} CF_{\gamma+z}$
	#3	$Si_{\alpha-x} Fe_{\beta-\gamma} CF_{\gamma+z}$
Silicon-Copper- Carbon Fiber Alloy Anode	#4	$Si_{\alpha-xa} Cu_{\beta-\gamma} CF_{\gamma+zc}$
	#5	$Si_{\alpha-xd} Cu_{\beta-e} CF_{\gamma+zf}$
	#6	$Si_{\alpha} Cu_{\beta} CF_{\gamma}$
	#7	$Si_{\alpha-x} Cu_{\beta-\gamma} CF_{\gamma+z}$

Source: Envia Systems

Figure 9 shows the half cell electrochemical performance of the various Si-Fe-CF and Si-Cu-CF intermetallic anode alloys. It is very clear from the data that except for alloy #1 ($Si_{\alpha}Fe_{\beta}CF_{\gamma}$), the specific capacity of all others anodes fade rapidly with cycles.

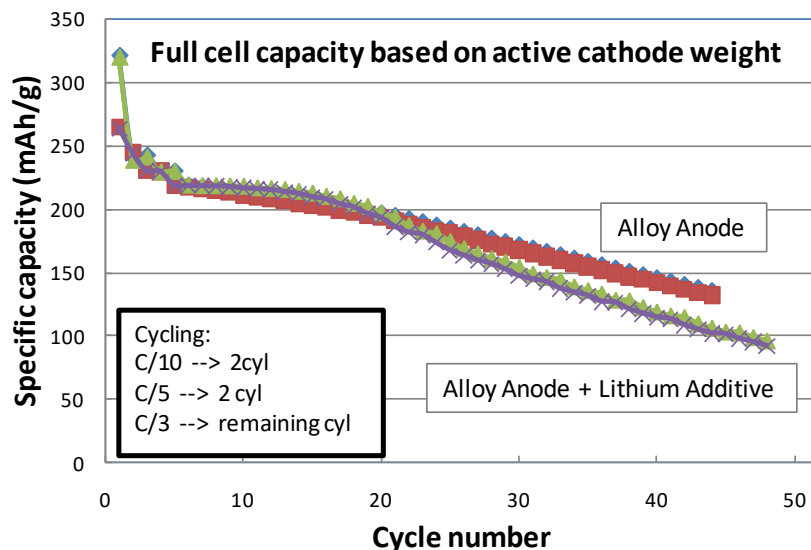
Figure 9: Half Cell Electrochemical Performance of Various Si-Fe-CF Intermetallic Anode Alloys



Source: Envia Systems

Full cells were assembled with the most promising alloy #1 (Figure 10); unfortunately, the obtained electrochemical data was not able to meet the performance goals. Due to this poor performance, the development on Si-CF intermetallic alloy anodes was stopped and resources shifted to more promising approaches.

Figure 10: Full Cell Electrochemical Performance of a Si-Fe-CF Intermetallic Alloy with Envia's HCMR™ Cathode



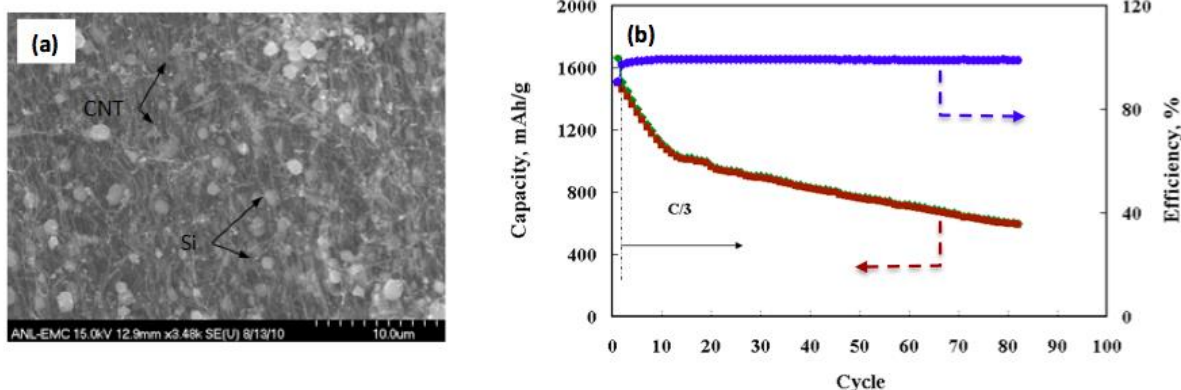
Source: Envia Systems

Development of Silicon-Coated Aligned Carbon Nanotube and Graphene Anodes

Task 2 was performed in partnership with Argonne National Laboratory (ANL). Their task was to develop Si coated aligned carbon nanotubes (Si-ACNT) and Si-Graphene anodes. Argonne developed an approach to synthesis aligned carbon nanotubes (CNTs) with open end structure by a chemical vapor deposition method. A variety of shapes and sizes of multiple walled CNT bundles with identical spatial orientation were prepared through a one-step, chemical vapor deposition (CVD) process using inexpensive aromatic hydrocarbons and transition metal compounds.

Figure 11a shows the morphology where n-Si particles were homogeneously distributed throughout the CNT matrix. The electrochemical data in Figure 11b shows a first cycle IRCL of 20 percent but with significant capacity fading over cycles. The Si coated aligned carbon nanotube (Si-ACNT) method shows promise in terms of capacity and low IRCL, but the cycling performance is very poor. In addition, considering the scale up challenges and costs associated with this approach, the Argonne along with the Envia team decided to stop the work and focus the efforts on more scalable processes like Si-graphene materials.

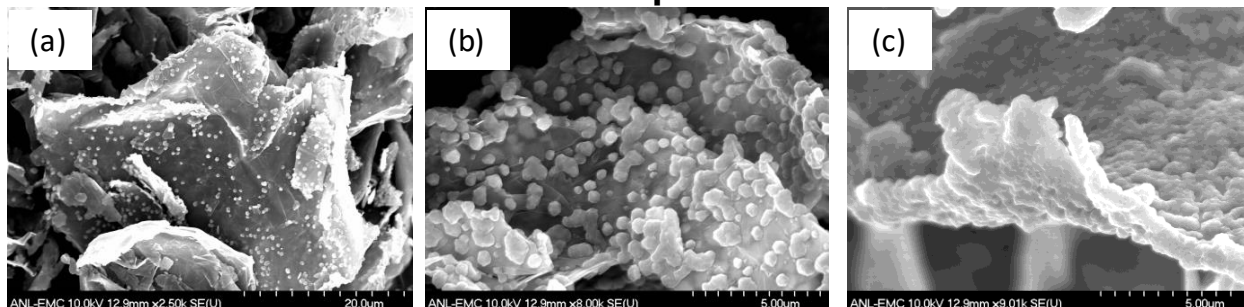
Figure 11: SEM Image (A) and Half Cell Electrochemical Performance (B) Of ACNT-Si Nanoparticle Anode Composites Grown by CVD



Source: Envia Systems

Silicon-graphene composites anodes were explored by ANL. In the beginning, Graphene was synthesized onsite by Argonne and later ANL decided to purchase graphene from an outside vendor. The purchased graphene was made by a method where natural graphite was subjected to an intercalation/oxidation treatment under a condition comparable to what has been commonly employed to prepare the so-called expandable graphite or stable graphite intercalation compound (GIC). This was accomplished by immersing graphite powder in a solution of concentrated sulfuric acid or nitric acid, for 1-2 hours. The subsequently dried product, a GIC, is then subjected to a thermal shock (e.g., 1,000° C. for 15-30 seconds) to obtain exfoliated graphite worms, which are networks of interconnected exfoliated graphite flakes with each flake comprising one or a multiplicity of graphene sheets. The exfoliated graphite is then subjected to ultrasonication treatment to break up the exfoliated graphite flakes and separate the graphene sheets. ANL focused on optimizing the Si incorporated in the anode composites. Figure 12 shows SEM images of the Si-graphene anode composites prepared through a CVD process with various levels of Si loading. ANL tried to increase the first cycle efficiency by controlling the graphene structure and optimizing the CVD process to control the deposition size and coverage of the Si particle over the graphene. By varying the CVD process parameters, the size of the Si nanoparticle deposition varies in the range of 100–200 nanometers (nm) (Figure 12a), around 800nm (Figure 12b), and a thin film (Figure 12c) on graphene.

Figure 12: SEM Images of Varying Si Nanoparticle Size and Coverage Deposited Over Graphene

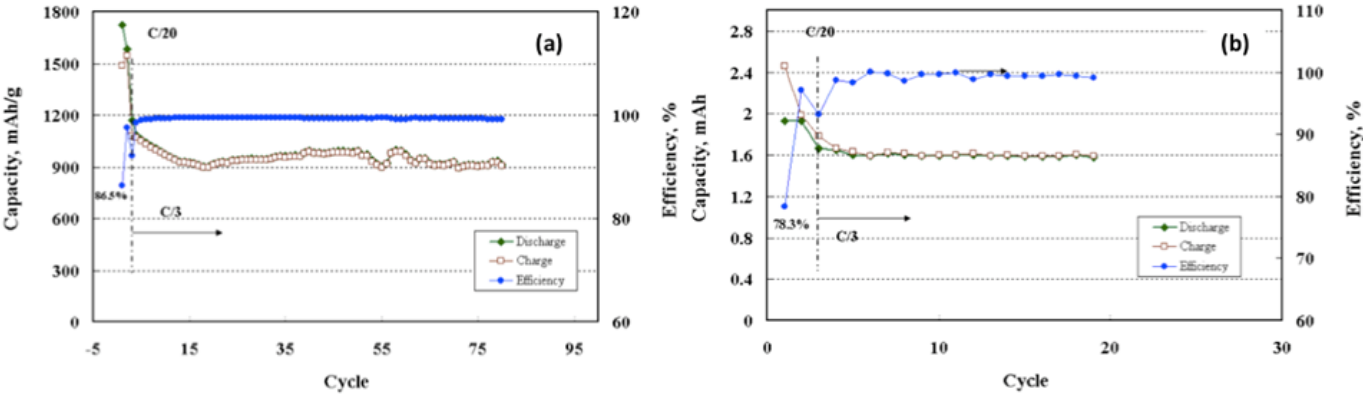


Source: Envia Systems

Figure 13a shows the half cell electrochemical cycling performance of the optimized Si-Graphene anode material containing approximately 35 percent Si (shown in Figure 12b). The IRCL of the material is shown to be 13.5 percent when the half cell is cycled from 2.5V to 20mV. If the cell is cycled from 1.5V to 5mV, which is more representative of operation in a full cell, the IRCL is 15.3 percent. The IRCL of <20 percent is a good characteristic of this anode material since the lower the IRCL the less lithium that is consumed from the cathode resulting in higher cell energy density. The cycling behavior shows that the capacity remains at approximately 900mAh/g after 75 cycles at a rate of C/3. The loading and density of the anode electrode low (e.g. 0.66g/cc and approximately 0.95mg/cm²) though, in comparison to what is required to reach the target cell energy density (>1g/cc electro density and 2-5mg/cm² electrode loading).

Figure 13b shows the preliminary full cell data from the Si-graphene anodes paired with Argonne's high capacity cathodes. The figure shows only 19 cycles with a first cycle IRCL of 21.7 percent. Similar to the half cell, the electrode loading and electrode density are lower than what is required to reach the desired energy density from the large format cells. It is critical to test the electrodes with the proper target loading and density values, because what is important is to show cycle life under the more aggressive target electrode specifications. If a material fails to cycle under heavier electrode loading and electrode densities, it will be nearly impossible to reach the target cell energy density and cycle life. It was also noted that the balancing of the full cells was still not optimized.

Figure 13: Half-Cell Electrochemical Cycling Performance of the Si-Graphene Composite Material (A) and Full Cell Electrochemical Performance of the Si-Graphene Anode Composite Paired with Argonne’s High Capacity Cathode (B)



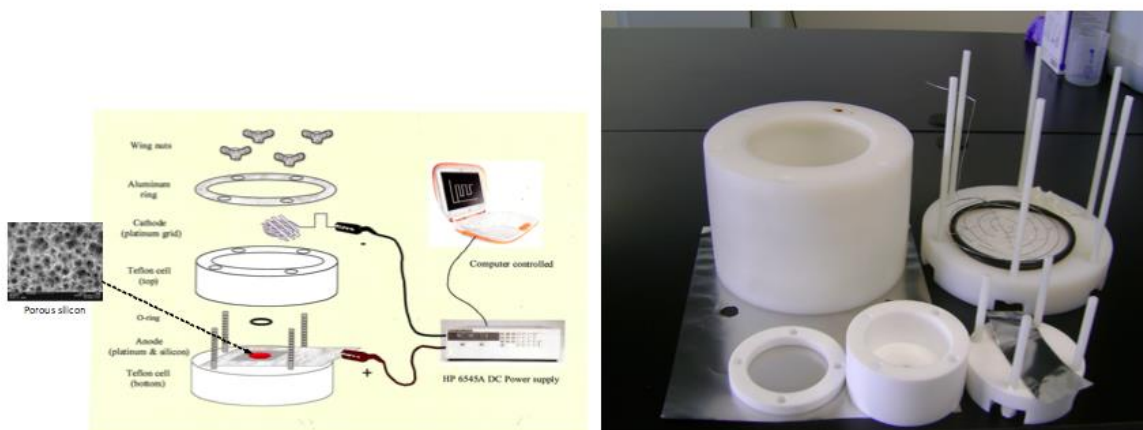
Source: Envia Systems

Based on the aggressive targets and limited timeline of the project, some promising approaches still had to be stopped. This is the case for the silicon-graphene anode composite work, where the limited initial data looks promising but there are still many unanswered questions on the material as well as concerns on the scalability. More effort still would be required to properly evaluate the material in full cell configurations with proper cell balancing and more aggressive loading and electrode densities to see if this is still a valid approach. The silicon-graphene anode approach is a promising candidate for more fundamental studies, but under the time constraints and targets of the project it was critical to focus on the most promising and ready approaches that have higher chances for success. For these reasons this development approach was stopped.

Development of Silicon-Carbon Alloy Anodes by Electrochemical Anodization of Silicon

The approach for Task 3 involved electrochemically synthesizing porous Si. Electrochemical methods were designed and manufactured to make porous Si from Si wafers. Figure 14 shows a schematic and the actual equipment used during the electrochemical anodization of crystalline Si to produce porous Si. The porous structure of the Si anode was expected to minimize the stress due to the volume change during charge and discharge and increase cycle life of the batteries. Envia carefully designed the morphology of porous Si by tuning the electrochemical etching conditions including HF concentration, current density and time, and choosing different types of Si wafers (type and resistivity).

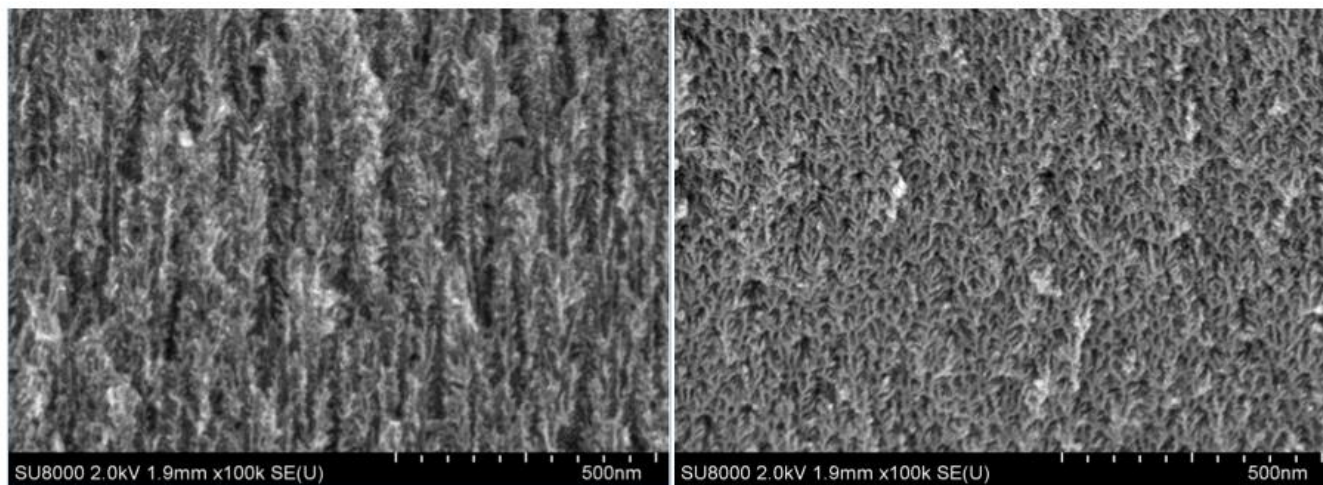
Figure 14: (A) Schematic of the Electrochemical Anodization Setup and (B) Actual Electrochemical Anodization Setup Used to Produce Porous Si



Source: Envia Systems

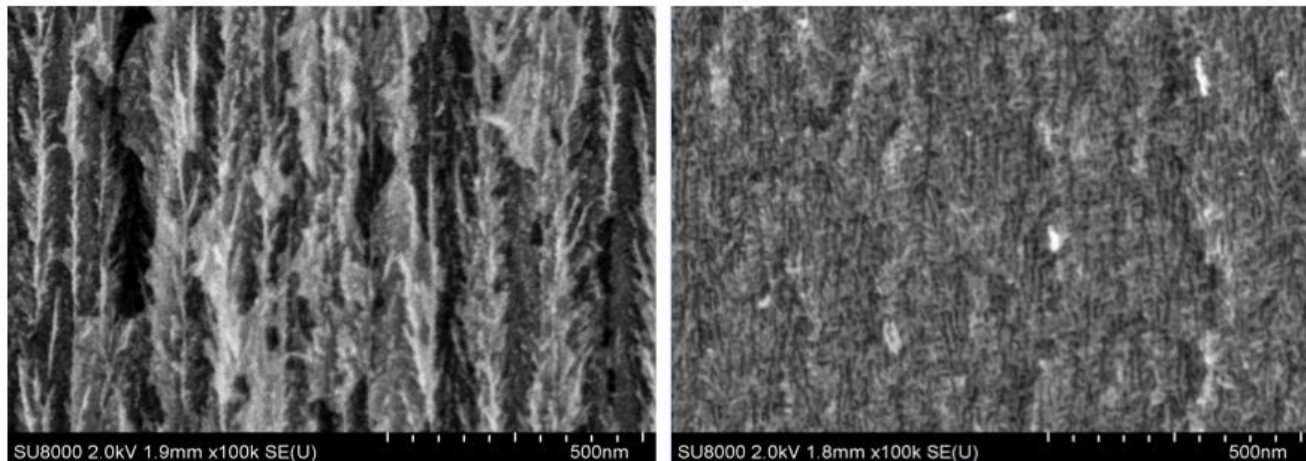
Figure 15, 16 and 17 shows the morphology characteristics of Envia's prepared porous Si. Depending on the preparation conditions and type of starting substrate, the morphology of the porous Si samples can be precisely controlled. The following figures show the various porous Si morphologies obtained by varying the preparation current densities (Figure 15), HF concentrations (Figure 16) and Si substrate types (Figure 17).

Figure 15: Cross-Section SEM Images of Porous Si (P+) at Various Current Densities: A) 150ma/Cm² for 20min in 35 Percent HF Solution and B) 50ma/Cm² For 1hr in 35 Percent HF Solution



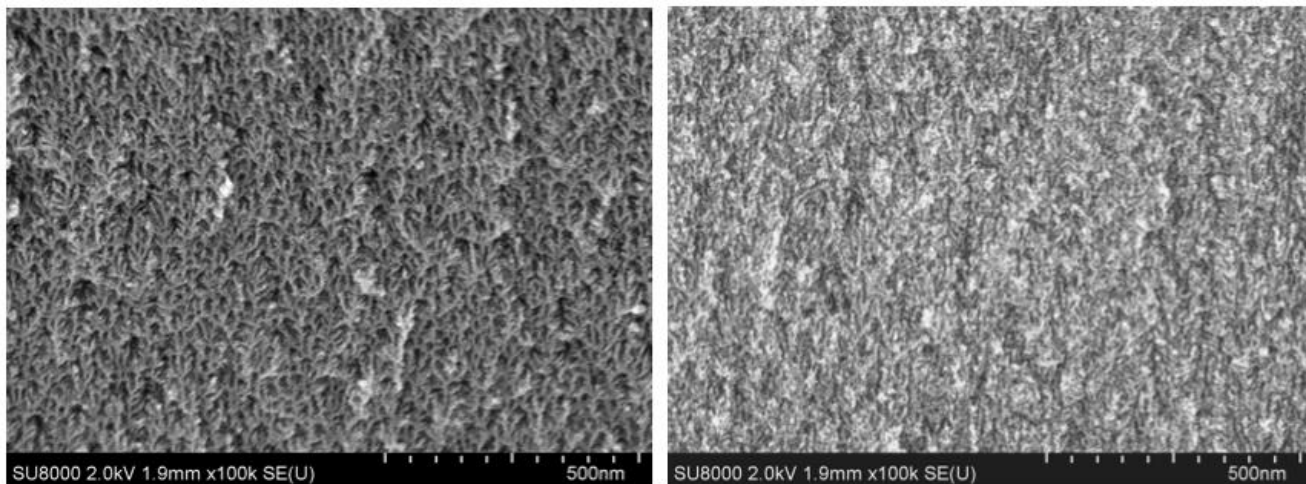
Source: Envia Systems

Figure 16: Cross-Section SEM Images of Porous Si (P+) Produced at Various HF Concentrations: A) At 50ma/Cm² in 25 Percent HF Solution and B) At 50ma/Cm² in 45 Percent HF Solution



Source: Envia Systems

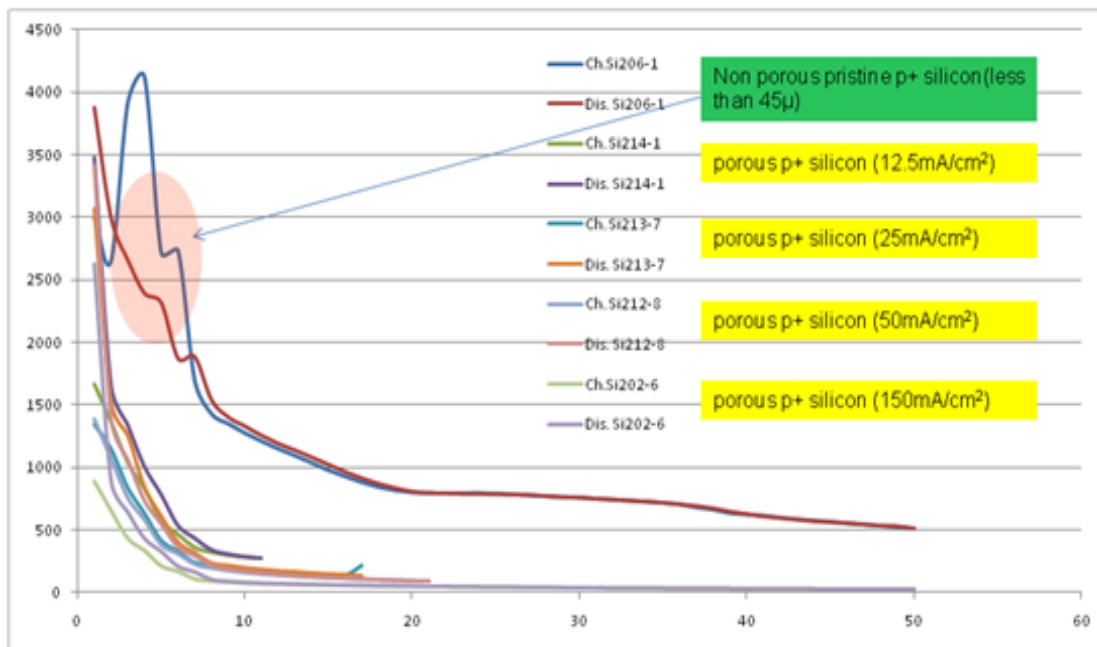
Figure 17: Cross-Section SEM Images of Porous Si Produced From Different Types of Si Wafers: A) 50ma/Cm², 60 Min, 35 Percent HF, P+ And B) 50ma/Cm², 30min, 35 Percent HF, N+



Source: Envia Systems

With respect to the electrochemical performance of the porous Si samples, a rapid capacity fade and large IRCL (approximately 50 percent) was observed for all the porous Si samples as shown in Figure 18. The high surface area of the porous Si anodes did not serve as a cushion against the high volume expansion of Si during alloying and de-alloying of Li. On the other hand, the high surface area appeared to have defects, impurities and surface states that could irreversibly trap lithium causing a severe reduction of capacity.

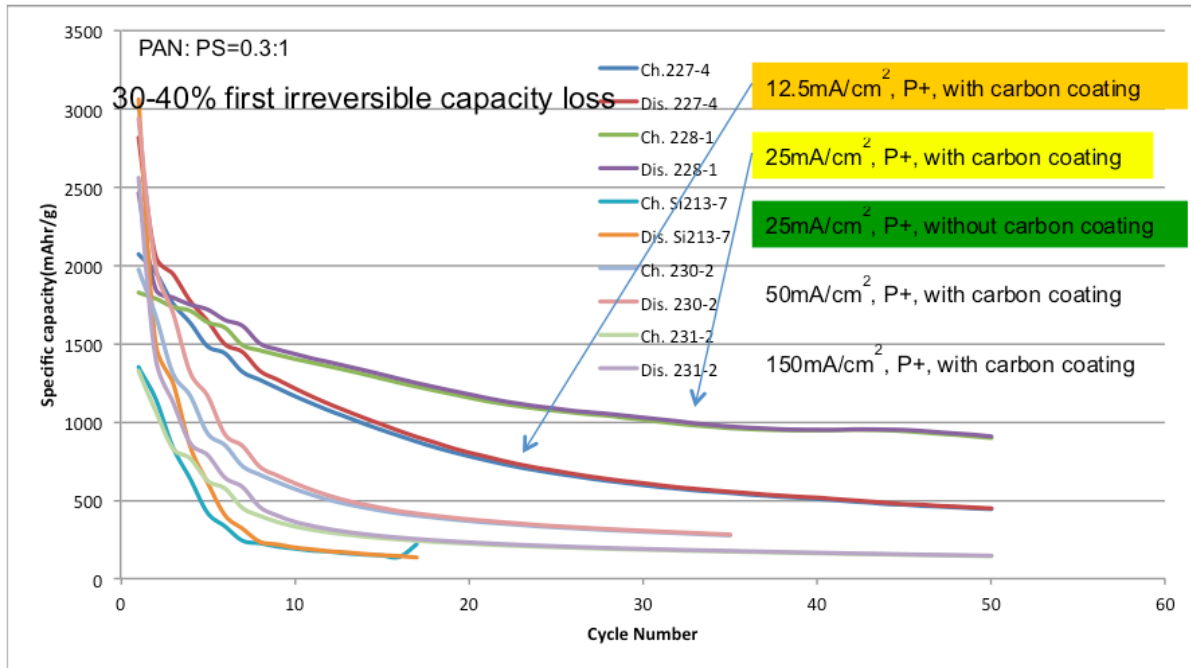
Figure 18: Half Cell Electrochemical Performance of Porous Si and Pristine P+ Si Anodes



Source: Envia Systems

In an attempt to stabilize the porous Si structure, copper, silver, and carbon coatings or CFs were added to the porous Si materials. Figure 19 shows that after carbon coating, the irreversible capacity loss of porous Si decreased. However, a large fade in capacity versus cycles was still observed for the carbon coated porous silicon-based materials. Metal coatings (Cu and Au) were also not successful in improving the poor cycle life of the porous Si composite anode materials.

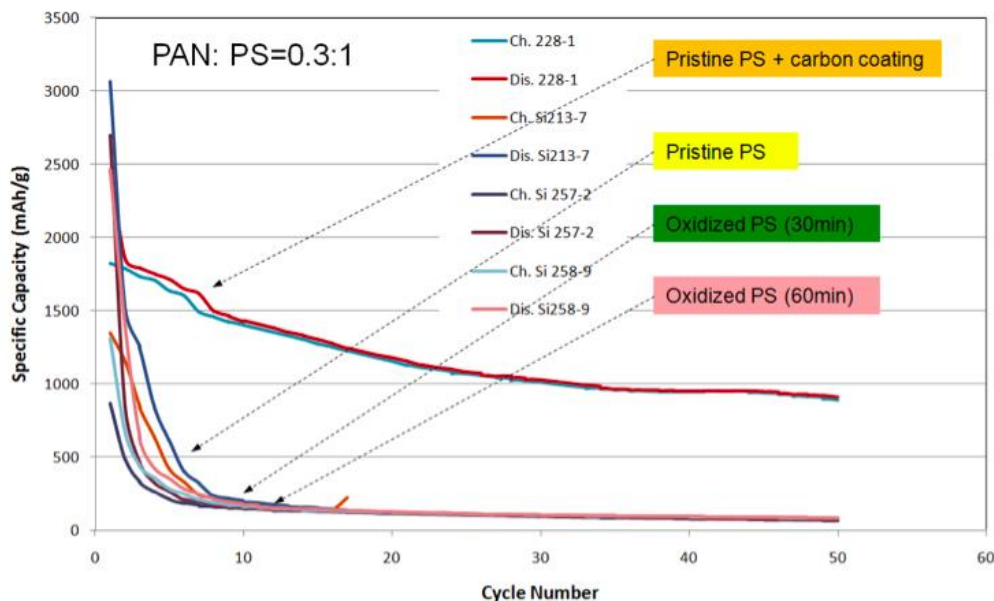
Figure 19: Half Cell Electrochemical Performance versus Cycles for Different Porous Si Composites Anodes Which Are Carbon Coated



Source: Envia Systems

In a final attempt to solve the proposed defect, conductivity and stress problems of porous Si, three different approaches were explored. The first approach was to passivate and neutralize the unstable surface states by oxidation of the porous Si anode. The second approach also oxidizes the PS surface followed by carbon coating to reduce the resistance of the nano branches and to support their mechanical strength. The third approach was to freshly etch porous Si and avoid oxidation followed by passivation of the surface with organic chemicals via Si-C bonding reaction and carbonize the material. The porous Si samples were oxidized under air flow at 800°C for 30min and 60min respectively. After oxidation, the final products have a 15 percent to 25 percent increase of weight indicating the oxidation of the surface of porous Si. These powders were mixed with binder and conducting carbons and laminated on copper foil. The composition of the composite anode was 80 percent oxidized PS, 10 percent binder, and 10 percent conductive additive. Figure 20 shows the electrochemical performance of the oxidized porous Si along with pristine and carbon coated pristine porous Si samples. It is clearly observed that oxidation alone of the porous Si surface does not eliminate the severe capacity fade.

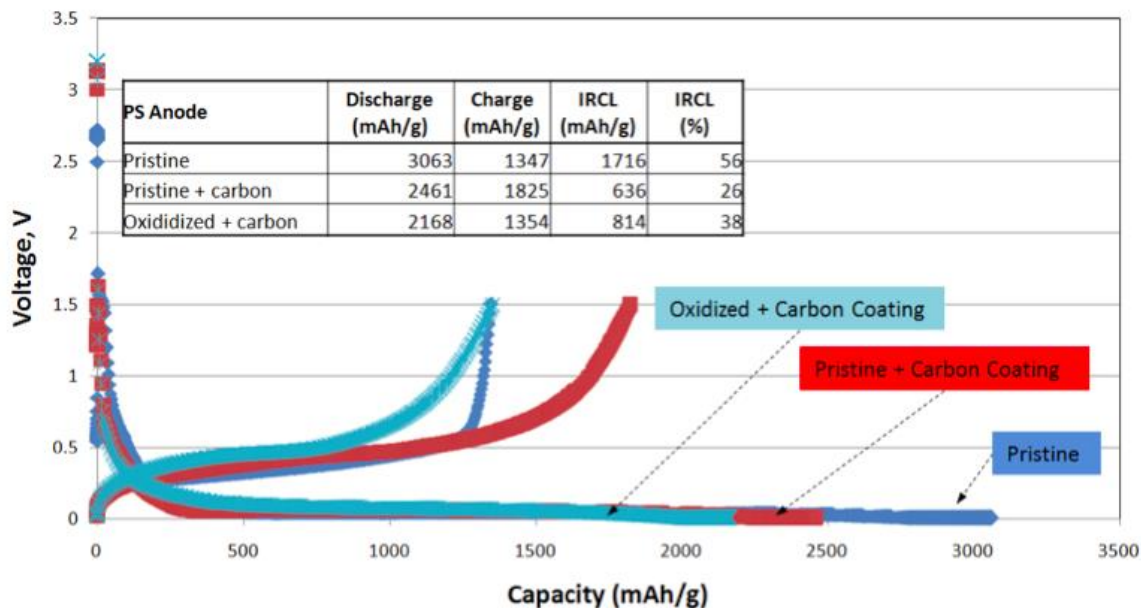
Figure 20: Electrochemical Performance of Oxidized Porous Silicon



Source: Envia Systems

The oxidized porous Si in Figure 20 was mixed with phenyltrimethoxysilane in ethanol solvent. A small amount of water and HCl was used to activate the surface of the oxidized Si powder and form Si-OH groups, which can react with phenyltrimethoxysilane. After the oxide surface layer of porous Si powders was coated with phenylsiloxanes, they are carbonized at 900°C in an inert atmosphere and then used for anode composite. Figure 21 shows the first cycle charge and discharge profiles for the carbon coated oxidized PS sample. Unfortunately the oxidized carbon coated porous Si sample shows lower reversible capacity (1354mAh/g) and higher IRCL (38 percent) versus the pristine carbon coated samples. After numerous unsuccessful attempts to improve the cycle life and IRCL, the electrochemical method to prepare porous Si was stopped to focus effort on other more promising methods.

Figure 21: Electrochemical Performance of Oxidized and Carbonized Porous Silicon

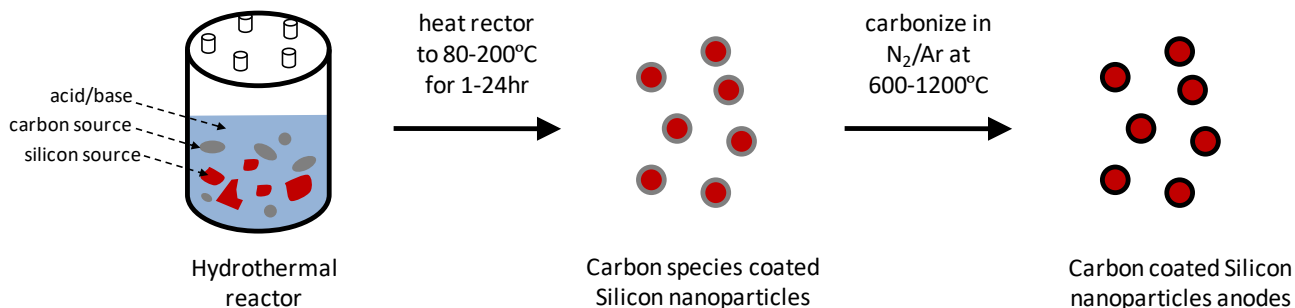


Source: Envia Systems

Chemical Synthesis of Porous Silicon

The fourth anode development approach utilized a hydrothermal route to synthesize porous Si. The process is illustrated in Figure 22, where Si and hydrofluoric acid in the presence of high temperature and pressure result in a porous Si nanostructure material. The stainless steel hydrothermal reactor shell along with the Teflon inner cup is shown in figure 23. The hydrothermal process was able to produce a porous Si powder as shown in Figure 24, but unfortunately it could not convert the entire Si material into a porous structure.

Figure 22: Schematic Showing the Hydrothermal Synthesis Approach to Produce Carbon-Coated Nanosilicon



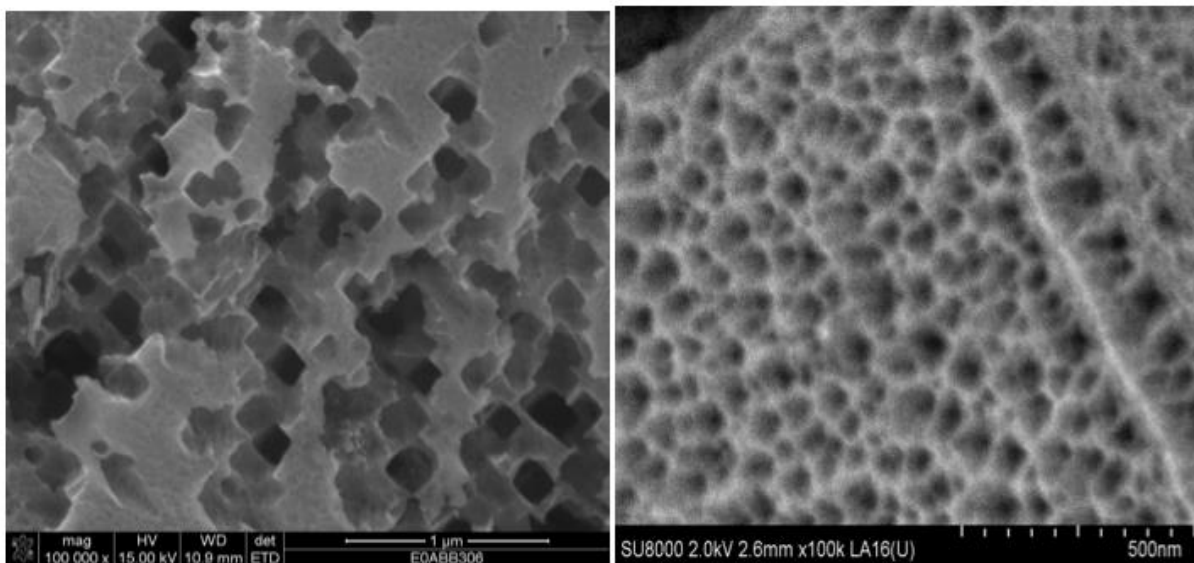
Source: Envia Systems

Figure 23: Hydrothermal Synthesis Reactor



Source: Envia Systems

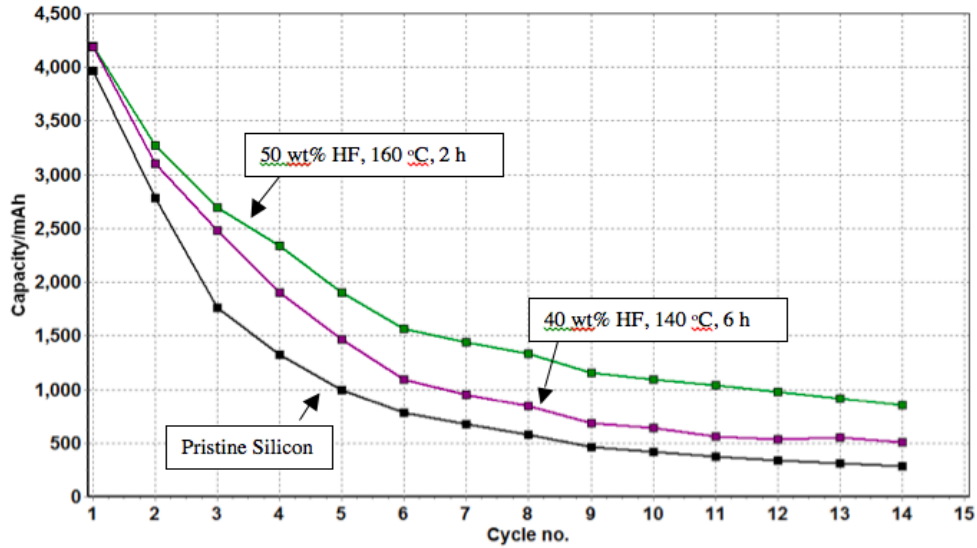
**Figure 24: SEM Micrographs of Porous Si Prepared by the Hydrothermal Process:
(A) 50wt Percent HF, 140°C, 6 H And (B) 50wt Percent HF, 160°C, 2 H**



Source: Envia Systems

The electrochemical performance of the porous Si prepared by the hydrothermal process only slightly improved when compared to an untreated Si control as shown in Figure 25. As mentioned before, it was believed that the hydrothermal process only created a porous structure on the surface of the Si substrate leaving a large part of the bulk untouched. Further carbon coating on these porous Si samples did not improve the cycling performance (data not shown here). Considering the results and remaining challenges with the process control and scale-up of this process, Envia stopped this approach to focus on more promising anode development approaches.

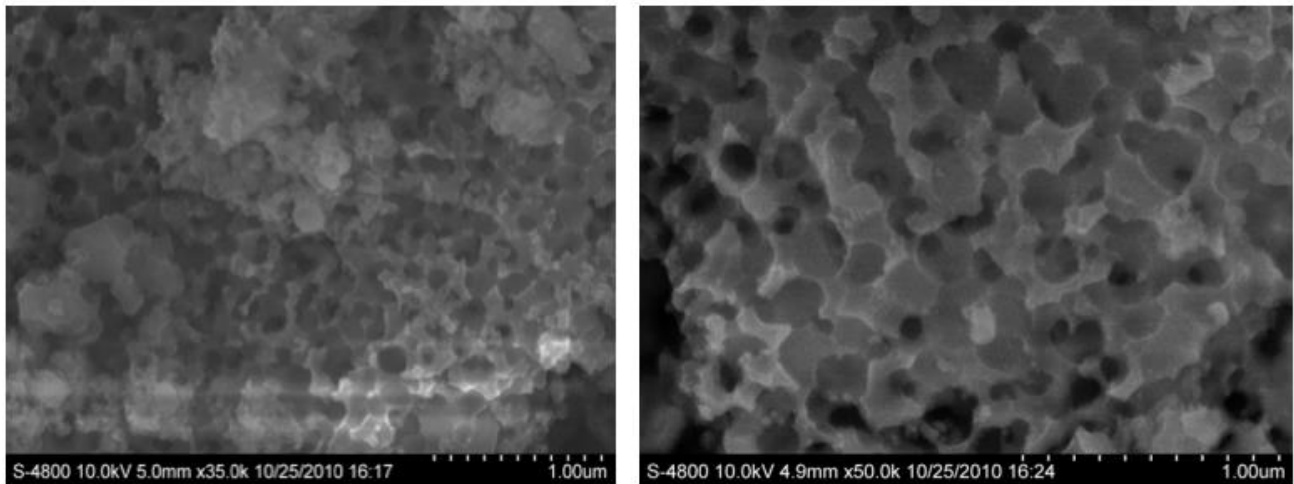
Figure 25: Electrochemical Performance of Porous and Pristine Silicon



Source: Envia Systems

Another approach to chemically form porous Si structures used Si oxide and a reducing metal. In this approach, Si monoxide and/or SiO₂ plus metal powders (aluminum, magnesium, etc.) were taken as the starting materials, and were mixed in a high energy ball mill at different rotation rates and times. During the milling process, the metal reduces the Si monoxide/silica into Si and forms a metal oxide. The metal oxide is removed by treating the ball milled samples in hydrochloric acid solution. During the etching process, the metal oxide is etched out leaving behind a porous Si material. Figure 26 shows the morphology of chemically produced porous Si anode via a solid state process.

Figure 26: SEM Micrographs of Chemically Produced Porous Si Anode Via a Solid State Process



Source: Envia Systems

In one specific case, silica is reduced to Si using a reducing agent (aluminum or magnesium metal) followed by acid leaching. In the first step, commercially available silica and magnesium powder were intimately mixed using a high energy ball mill. The mixed sample was heat treated in an inert atmosphere. During the heat treatment process, magnesium reduces silica into pure Si and gets oxidized to form magnesium oxide. Magnesium oxide is removed by etching with an acid and the resulting material results in a porous Si structure.

Various concentrations of magnesium and different heating rates have been explored to control the morphology of the porous Si. The different experimental conditions and the resulting surface area of the Si formed are tabulated in Table 4. The surface area remains more or less the same for all conditions (22-40 m²/g), except for the Si which is produced at a very low heating rate of 2°C/min. The high surface area obtained could be attributed to the small grain size of Si formed during the slow heating process.

Table 4: Experimental Conditions and the Resulting Surface Area of the Porous Si Formed

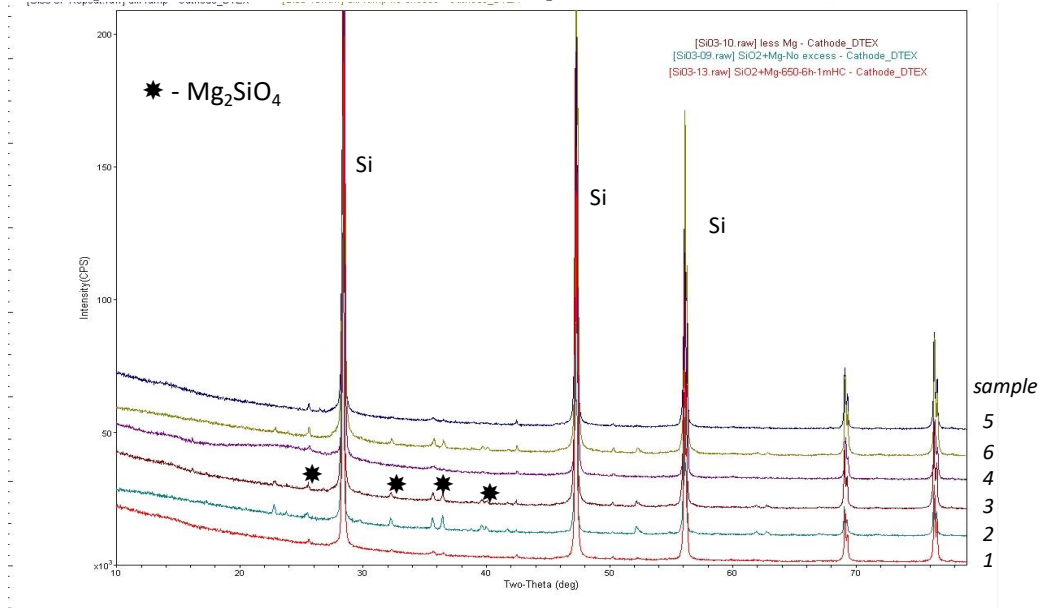
Sample	Processing Conditions	Mg Concentration	IRCL (%)	Electrode Loading (g/cm ²)	Surface Area (m ² /g)
1	650°C, 5°C/min, 6hr run	High	38	1.7	45
2	650°C, 5°C/min, 6hr run	Medium	22	1.7	22
3	650°C, 5°C/min, 6hr run	Low	27	2	27
4	650°C, 5°C/min, 6hr run	Lowest	32	3.3	24
5	650°C, 2°C/min, 6hr run	High	47	1.4	151
6	MHS, 5°C/min	High	29	2.3	28
7	MHS, 5°C/min	Medium	25	1.3	24

Note: MHS corresponds to a stepwise temperature ramp up to 700 °C

Source: Envia Systems

The X-ray diffraction (XRD) patterns of the porous Si formed at different conditions are shown in Figure 27. It is evident from Figure 27 that pure crystalline Si is formed along with some amounts of magnesium silicate. Both peaks are clearly seen in the figure.

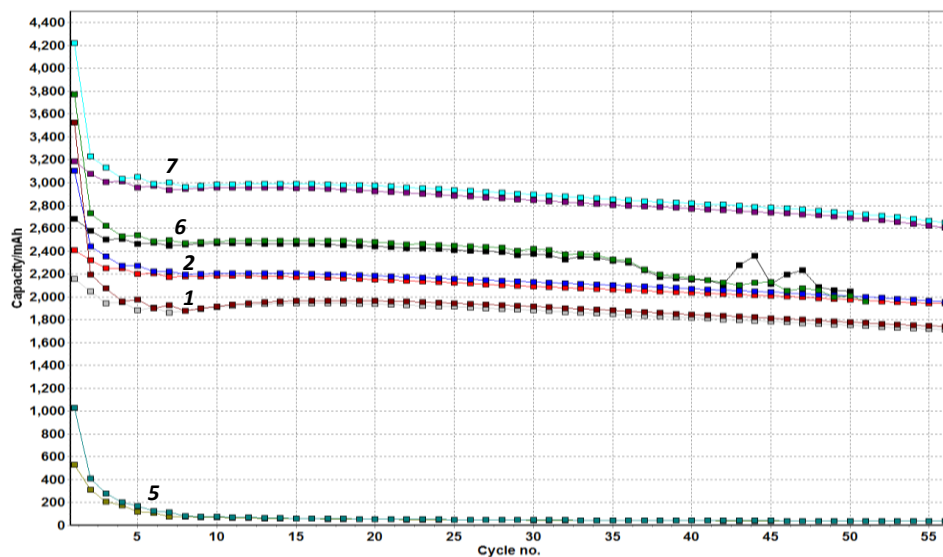
Figure 27: XRD Patterns of Porous Si Synthesized by Solid State Method. The Sample Numbers Refer to the Experimental Condition in Table 4



Source: Envia Systems

The half cell electrochemical performance of the porous Si synthesized under select conditions is shown in Figure 28. With the exception of the Si produced at 2°C/min ramp rate, all the samples cycled well at high discharge capacity values. The enhanced stability of the Si anodes could be due to its porous nature, which offsets the volume changes associated with the Si during cycling. The first cycle IRCLs of these samples are also summarized in Table 4.

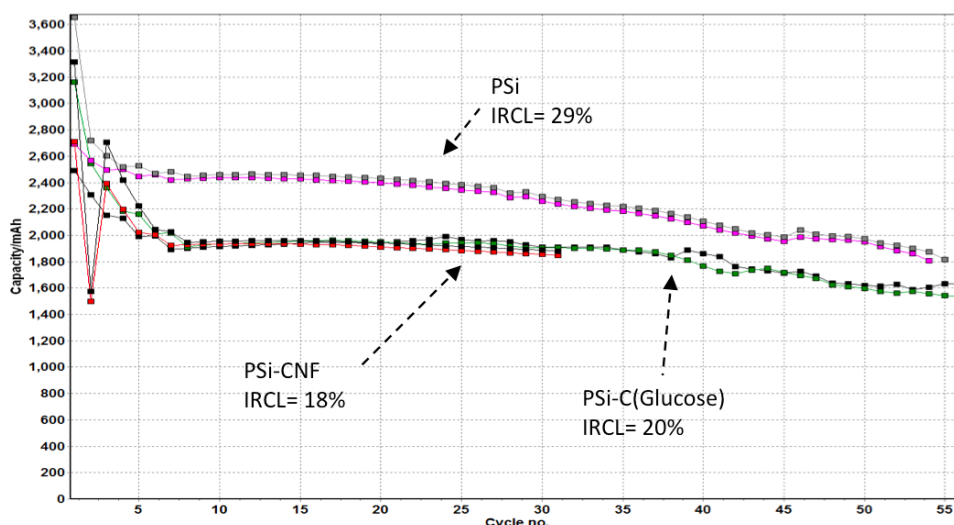
Figure 28: Half Cell Specific Capacity versus Cycles for Chemically Produced Porous Si Anodes. The Number Refers to the Experimental Condition in Table 4



Source: Envia Systems

Ideally, Envia needs an anode with low irreversible capacity loss, stable cycle life and specific capacity above 1000mAh/g at a C/3 rate. The previous figure shows high capacity and good cycle life up to 55 cycles, but the irreversible lithium loss remains a concern. In this regard, pyrrolytic carbon coating on the surface of the Si using a hydrothermal approach was employed. Also, carbon nanofibers (CNF) were also used to form silicon-carbon composites. The half cell performance of these composite electrodes is shown in Figure 29. The addition of CNF reduces the IRCL from 29 percent to 18 percent, while the hydrothermal carbon coating reduces it to 20 percent. Apart from reducing the IRCL, the silicon-carbon composite anodes perform well versus cycles even at higher electrode loadings levels. As a result of the promising half cell electrochemical performance, full cells from these materials were made and evaluated.

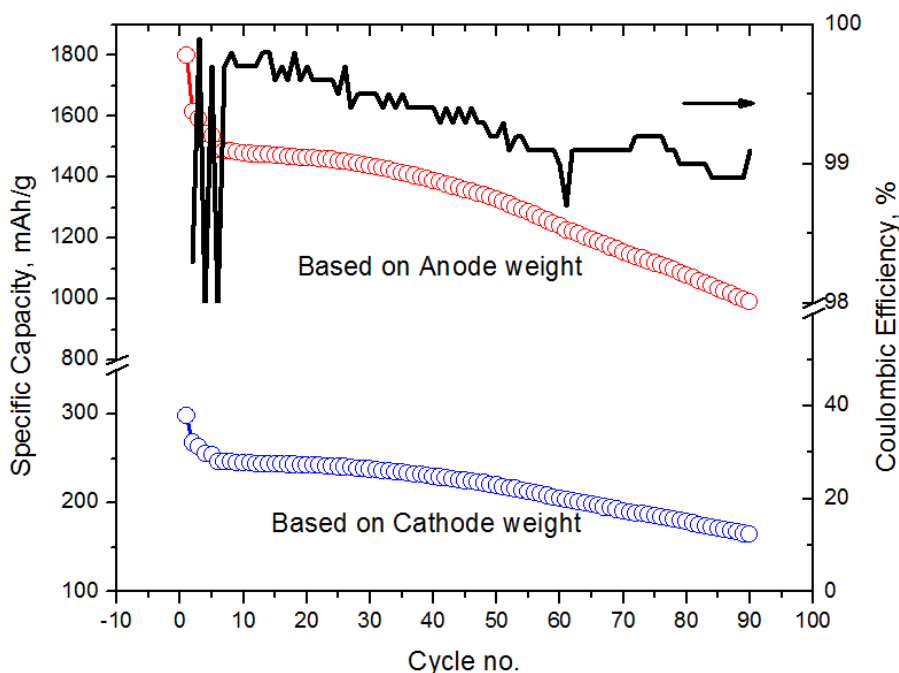
Figure 29: Half Cell Specific Capacity versus Cycles for Chemically-Produced Porous Si and Porous Silicon-Carbon Anodes



Source: Envia Systems

The porous Si obtained via the magnesium reduction route was made into full cells by pairing it with Envia's high capacity manganese rich (HCMR™) cathode. The full cell performance of the porous silicon-HCMR™ cells tested with the lithium additive is shown in Figure 30. The full cell with porous Si anode cycled well at a constant capacity at C/3 rate for 40 cycles, after which the capacity starts to fade. About 80 percent of the capacity is retained until 66 cycles. It was observed that the promising half cell performance from chemically produced porous Si could not be observed in full cells.

Figure 30: Full Cell Specific Capacity (Based On Cathode And Anode Active Weight) and Coulombic Efficiency Versus Cycles for Chemically Produced Porous Si Anodes



Source: Envia Systems

Various concentrations of metals and different heating rates were tried to control the morphology of the porous Si so as to obtain the best performing Si anodes. The different experimental conditions and the resulting surface area of the Si anodes is tabulated in Table 5. The surface area remains more or less the same for all conditions (22-40 m²/g), except for the Si anode produced at a lower heating rate that results in a higher surface area of 151 m²/g (sample 5). The high surface area obtained could be attributed to the small grain size of Si formed during the slow heating process. Unfortunately, the same inferior full cell performance was observed for these samples.

Table 5: Experimental Conditions and the Resulting Surface Area of the Si Anodes

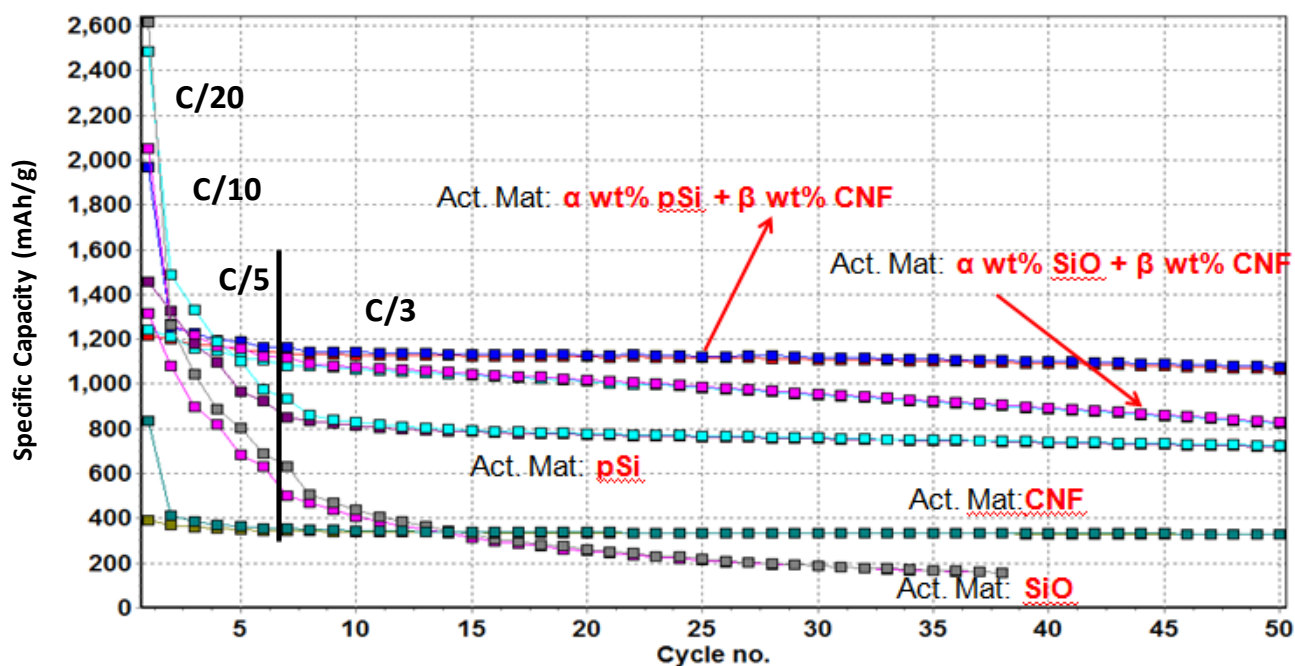
Sample	Processing Conditions	Metal Concentration	Li Deintercalation Capacity (mAh/g)	IRCL (%)	Electrode Loading (g/cm ²)	Surface Area (m ² /g)
1	Temp #1, Rate #1, Time #1	High	2159	38	1.7	45
2	Temp #1, Rate #1, Time #1	Medium	2408	22	1.7	22
3	Temp #1, Rate #1, Time #1	Low	2678	27	2	27
4	Temp #1, Rate #1, Time #1	Lowest	2279	32	3.3	24
5	Temp #1, Rate #2, Time #1	High	531	47	1.4	151
6	Temp #2, Rate #1, Time #2	High	2682	29	2.3	28
7	Temp #2, Rate #1, Time #2	Medium	3187	25	1.3	24

Source: Envia Systems

In another case, Si monoxide was reduced by Al to also produce porous Si anode materials. Figure 31 and Table 6 summarized the electrochemical performance of these porous Si composites with/without CNF. The irreversible lithium loss in the first cycle is significantly high

for all the samples (33-51 percent). Relatively high lithium loss for porous Si (41 percent) indicates the presence of metal oxides and unreacted Si oxides. The cycling stability of the porous Si is remarkably good; however the charge capacity value is approximately 800mAh/g which is lower than the target 1000mAh/g. At the end of 50 cycles, 84 percent of the capacity is retained. Superior cycling performance at high reversible capacity values are observed for the porous silicon-CNF composite. The cells cycle at around 1100mAh/g reversible capacity, with 94 percent of the initial capacity retained at the end of 50 cycles. The increased rate capability is attributed to the presence of CNF in the composite.

Figure 31: Specific Capacity versus Cycles for Chemically Produced Porous Silicon-Carbon Composite Anodes



Source: Envia Systems

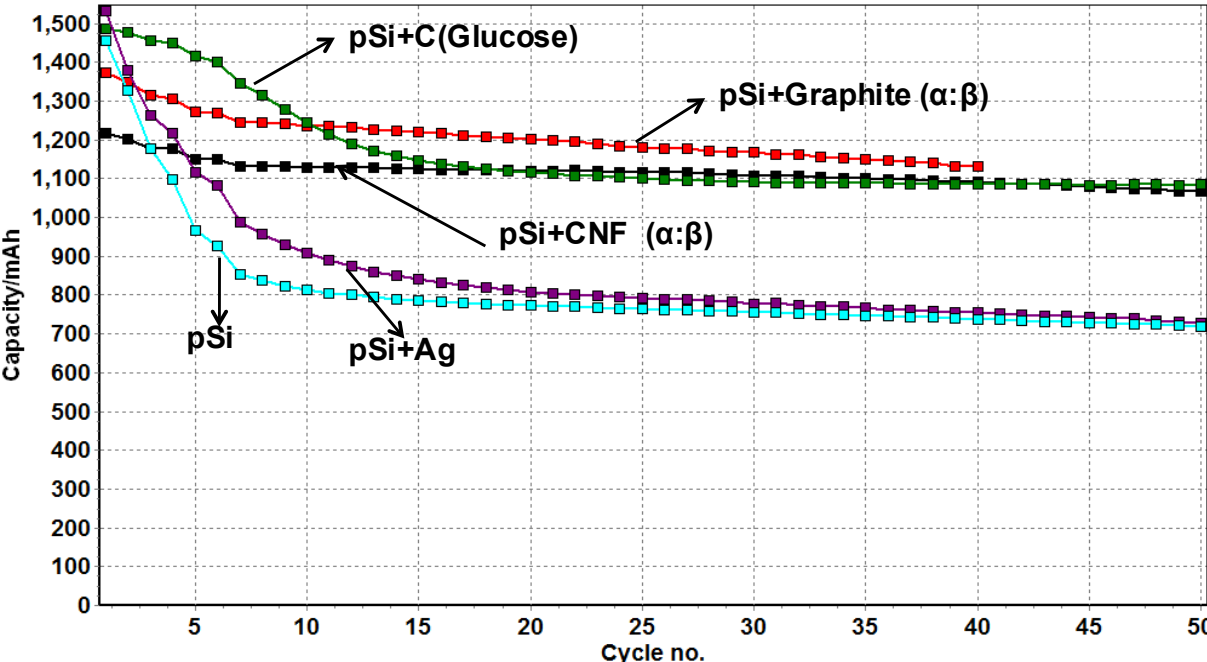
Table 6: Electrochemical Summary of Chemically Synthesized Porous Silicon-Carbon Composite Anodes

Sample	First cycle irreversible capacity loss (%)	Specific capacity at initial C/3 cycle (mAh/g)	Capacity retention after 50 cycles (%)
SiO	33	136	10
CNF	51	343	96
SiO+CNF (α : β)	40	1083	76
pSi	41	854	84
pSi+CNF (α : β)	38	1131	94

Source: Envia Systems

Composites were subsequently formed by mixing the porous Si material in this approach with graphite or carbonized using glucose. In another study, silver metal was deposited on the surface of the porous Si. All these samples were tested in half cell configuration to choose the best recipe which gives the best cycling performance with low first cycle irreversible capacity loss. The electrochemical data are plotted in the Figure 32 and summarized in Table 7. The first cycle RCL of all the samples varied between 34 percent and 41 percent. There is only a marginal reduction in this value with carbon surface coating or Ag metal deposition. Of all the compositions, porous silicon-CNF composites gave the best cycling performance with 94 percent of the capacity retained at the end of 50 cycles.

Figure 32: Half Cell Specific Capacity versus Cycles for Chemically Produced Porous Silicon-Carbon Anodes



Source: Envia Systems

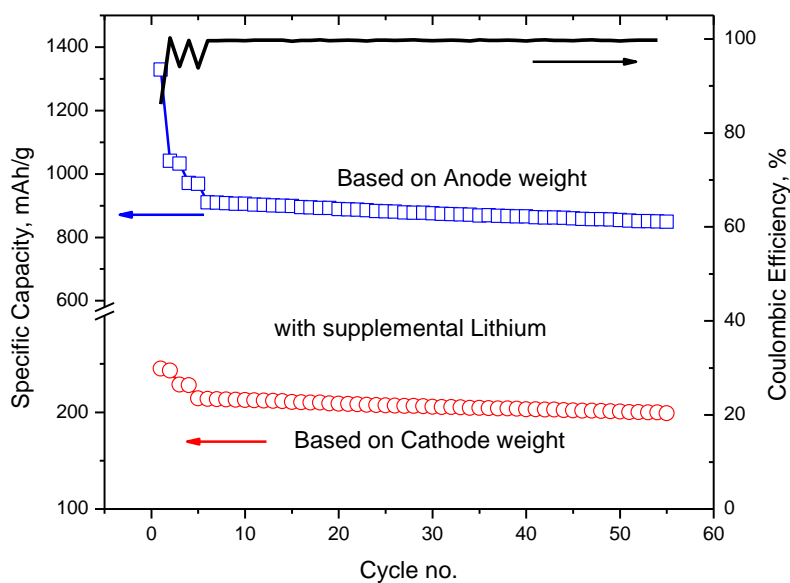
Table 7: Electrochemical Summary of Chemically Synthesized Porous Si Based Anodes

Anode System	First Intercalation Capacity, mAh/g	First Cycle Lithium Loss %	Capacity Fade after 50 cycles (C/3)	Loading, mg/cm²
pSi (BM)	2488	41	16 percent	1.7
pSi(BM)+CNF	1969	38	6 percent	1.6
pSi(BM)+Graphite	2089	34	12 percent	2.9
pSi(BM)+Glucose	2269	34	19 percent	2.2
pSi(BM)+Ag	2361	35	26 percent	1.8

Source: Envia Systems

Full cells were assembled using the porous silicon-CNF composite anodes and Envia's HCMR™ cathode material. To mitigate the high irreversible capacity loss associated with the anodes, supplemental lithium additive was used. The excess lithium was introduced either by physical or by electrochemical methods. Figure 33 shows the full cell specific capacity and columbic efficiency versus cycle number wherein the capacities have been calculated based on the cathode and anode active weights with supplemental lithium. The capacity retention is 93 percent up to 50 cycles. The cell capacity based on anode weight is less than the target 1000mAh/g C/3 reversible capacity. Even though the cycle life of these materials was very promising, the low capacity of the materials produced by chemically reduced Si oxides did not meet the required specifications to reach the desired cell energy density. As a result of the low capacity, this approach was eventually stopped.

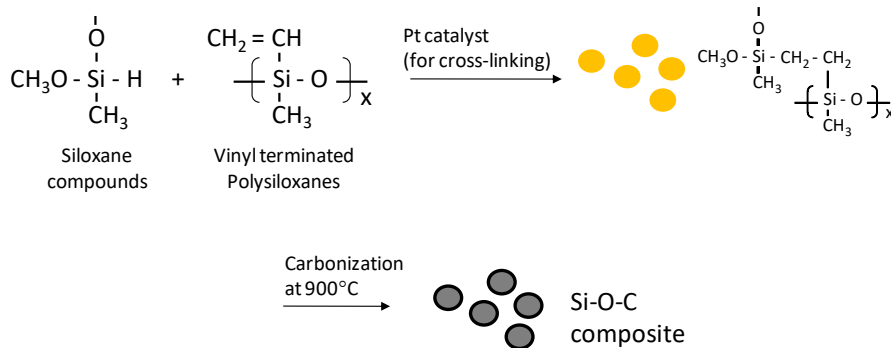
Figure 33: Full Cell Specific Capacity (Based On Cathode and Anode Active Weight) and Coulombic Efficiency versus Cycles For Chemically Produced Porous Silicon-Carbon Anodes And Lithium Additive



Source: Envia Systems

Porous silicon-carbon-oxygen (Si-C-O) anode composites were also synthesized from liquid phase precursors, which are composed of polymethylhydrogen siloxane and vinylmethoxysilane. The advantages of a liquid phase precursor route are the ease to control the morphology and chemical composition of the Si-C-O composites, cheaper than other precursors, and easily applicable in mass production. Figure 34 shows a schematic of the chemical synthesis of Si-C-O anodes via a liquid precursor route. The reaction involves a platinum catalyst for the cross-linking of the precursors followed by carbonization at high temperatures (>700°C) to complete the synthesis of the anodes.

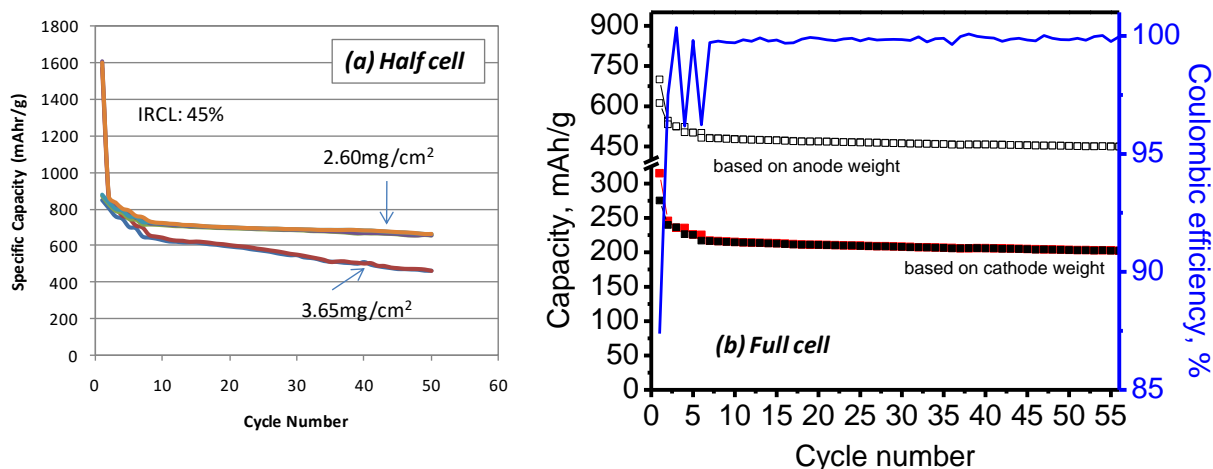
Figure 34: Schematic of the Chemical Synthesis of Porous Si-C-O Anodes Via Liquid Phase Route



Source: Envia Systems

The most promising data obtained from a material via polysiloxane precursors showed a reversible capacity of 700mAh/g over 50 cycles with higher than 85 percent coulombic efficiency in a half cell configuration. Unfortunately the IRCL of this material is approximately 45 percent. Figure 35 show the half cell and full cell electrochemical performance from anodes prepared by the polysiloxane precursor route. Figure 35a shows the half cell data for two different cells with different anode electrode loading. As expected for the cell with the higher loading, larger fade in capacity with cycles is observed. Figure 35b shows the full cell electrochemical performance of the Si anodes with a capacity >600mAh/g, IRCL <50 percent and cycle life >50 cycles before reaching 80 percent efficiency. Unfortunately the specific capacity of these materials is well below the target capacity target of 1000mAh/g.

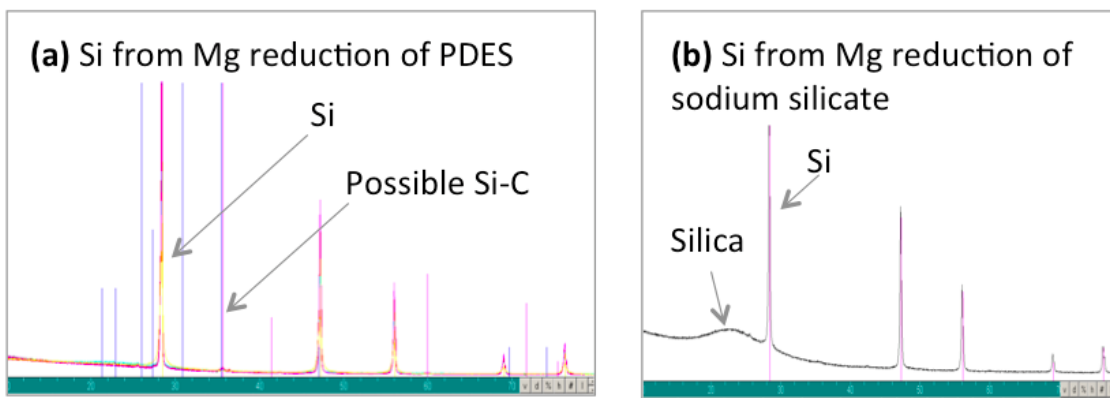
Figure 35: A) Half Cell and B) Full Cell Electrochemical Performance from Chemically Synthesized Si-C-O Anodes via Carbonization of Cross-Linked Polysiloxane Precursors



Source: Envia Systems

In the further advancement of this topic, Envia focused on developing porous Si anodes from the magnesium reduction of sodium silicate or polydiethoxysiloxane, as well as, nano Si/Si-C-O composite anodes from cross-linkable polysiloxanes. Porous Si anodes were synthesized from the magnesium reduction of sodium silicate and polydiethoxysiloxanes. Figure 36 shows the XRD spectra of both samples clearly confirming that magnesium reduction produced crystalline Si even though amorphous silica remained in the final powder. The surface areas of these Si powders are found to be higher than 100m²/g measured by the Brunauer–Emmett–Teller method.

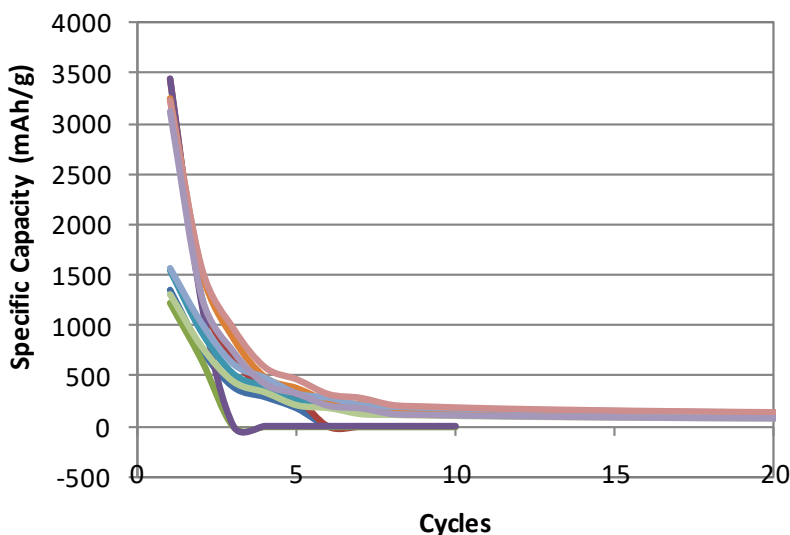
Figure 36: XRD Spectra of Magnesium Reduction of A) Polydiethoxysiloxane and B) Sodium Silicate



Source: Envia Systems

Figure 37 shows the electrochemical cycling performance of the Si anodes synthesized from the magnesium reduction of sodium silicate. Interestingly, the first discharge capacity is close to 3500mAh/g, which indicates that the porous Si anode is almost pure silicon, even though the XRD shows signs of unreduced silica. From the previous work of Mg reduction of SiO_2 , Envia had found that the best cyclic performance is obtained when the surface area of the porous Si anodes is in the range of 20-30 m^2/g . If the surface area becomes higher than approximately 50 m^2/g , porous Si anodes showed very poor cycling performance. In general, the high surface area of the samples could also cause poor adhesion of the Si anode on the copper current collector and result in poor cycling performance.

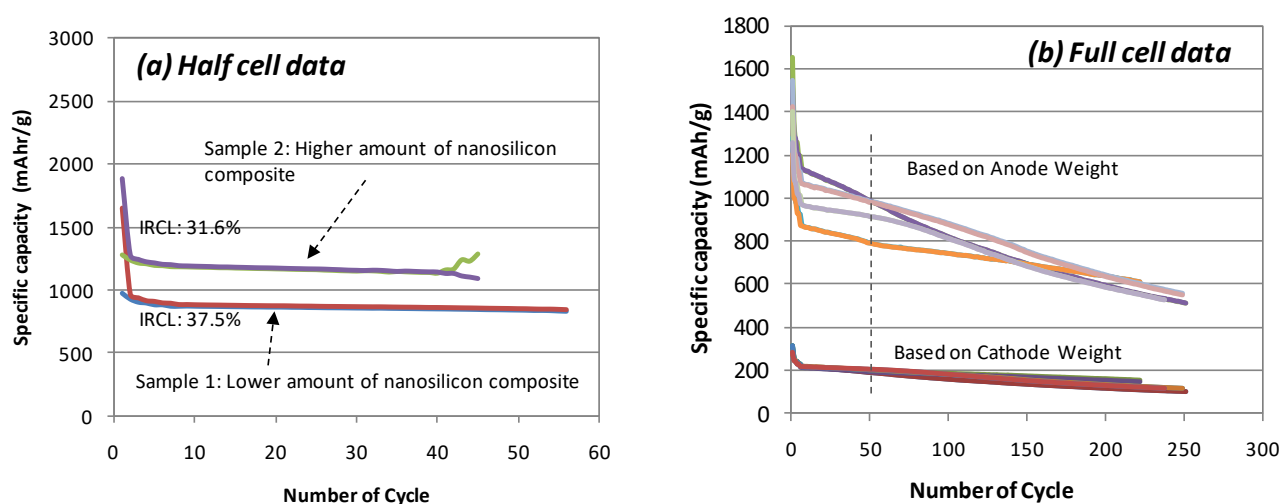
Figure 37: Cyclic Performance of Porous Si Anode Synthesized From Magnesium Reduction of Sodium Silicate



Source: Envia Systems

In order to make nano Si/Si-C-O composites, nano Si powder and graphite were mixed by a high energy ball mill at 300rpm for 3hr. The ball milled powder was dispersed in tetraethyl orthosilicate (TEOS) and diphenyldiethoxysilane solution. The mixed solution was cross-linked with a small amount of diluted hydrochloric acid (HCl) and then dried under vacuum at 80°C. Solid product was obtained and then carbonized under an argon atmosphere. Figure 38a shows that the carbonized Si-O-C composite has a reversible capacity of 1200mAh/g in a half cell configuration. Figure 38b shows the full cell electrochemical performance from the Si-C-O composites, but unfortunately not satisfying the project targets due to the low capacity and poor cycle life.

Figure 38: A) Half Cell and B) Full Cell Electrochemical Performance versus Cycles for Porous Si Based Anodes Synthesized Based On TEOS



Source: Envia Systems

Development of High Surface Area Carbon Intermetallic Alloy Anodes

The last approach involved using high surface area carbons to form carbon-Si composite and carbon-Si intermetallic alloy anodes through a high energy mechanical milling (HEMM) process. The HEMM equipment is shown in Figure 39.

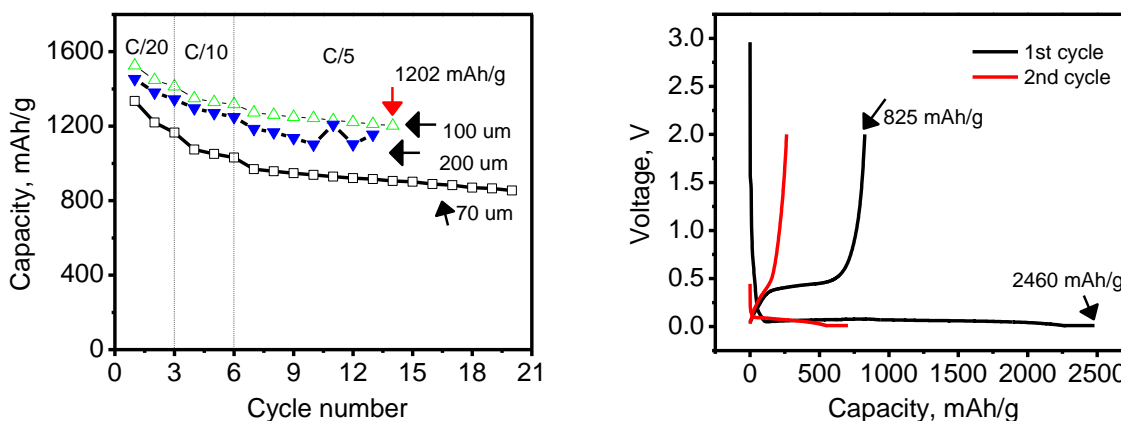
Figure 39: High Energy Planetary Ball Mill Used to Form Alloy Materials



Source: Envia Systems

Figure 40a shows the electrochemical performance data for a typical carbon-silicon-hard carbon composite showing a reversible capacity up to 1500mAh/g with a 17 percent initial IRCL at a C/20 rate and a capacity of 1202mAh/g at C/5. Under the same conditions, Si-Fe-C alloys showed much lower reversible capacity as indicated in Figure 40b. Under the experiment conditions of this work, the initial irreversible capacity loss of Si-Fe-C reached 85 percent.

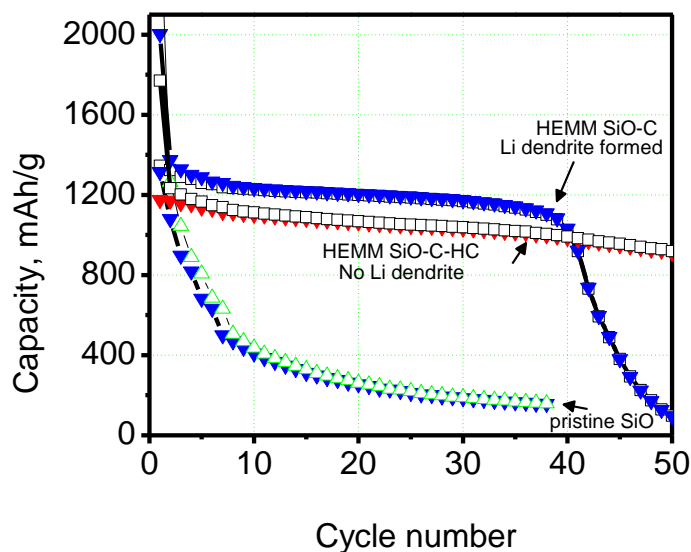
Figure 40: A) Capacity versus Cycles and Voltage versus Capacity For C-Si-Hard Carbon Alloys and B) Charge-Discharge Performance of Si-Fe-C Alloys Prepared By HEMM



Source: Envia Systems

Figure 41 demonstrates the superior half cell cycling performance of the carbon-Si monoxide composite anodes compared to the silicon-based anodes shown above. In spite of the formation of lithium dendrite in the heavy loaded electrodes (approximately 40cycles), the SiO-based composite electrodes reach 80.1 percent capacity retention after 50 cycles at C/3 (from the 7th cycle to 50th cycle).

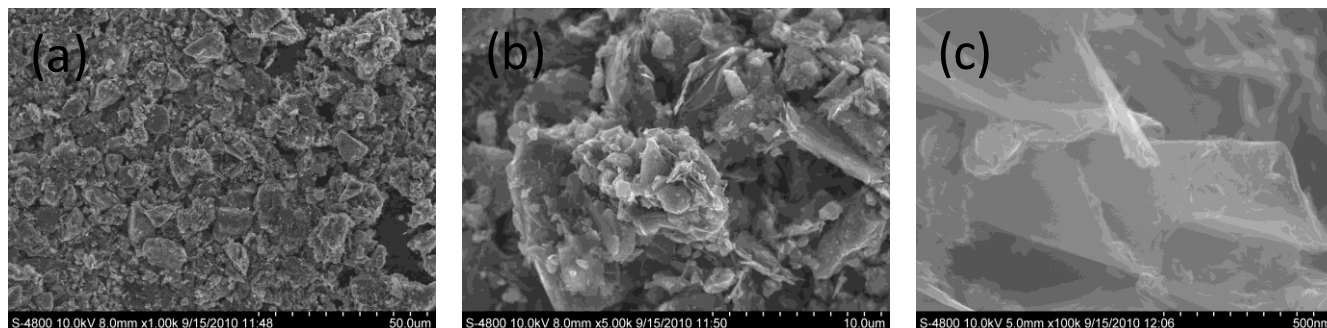
Figure 41: Half Cell Capacity versus Cycling Performance of SiO-Based Anodes Prepared by HEMM



Source: Envia Systems

Figure 42 shows SEM images of the SiO-carbon composite anodes showing homogeneous mixing of the carbon and SiO. The high magnification SEM in Figure 42(c) shows that some of the carbon has resulted formation of possibly low dimensional carbon structures. The possible presence of the low dimensional carbon structures, should improve the electronic conductivity and structural stability of the SiO-carbon anode.

Figure 42: Sem Images of Carbon-Sio-Hard Carbon at Different Magnifications

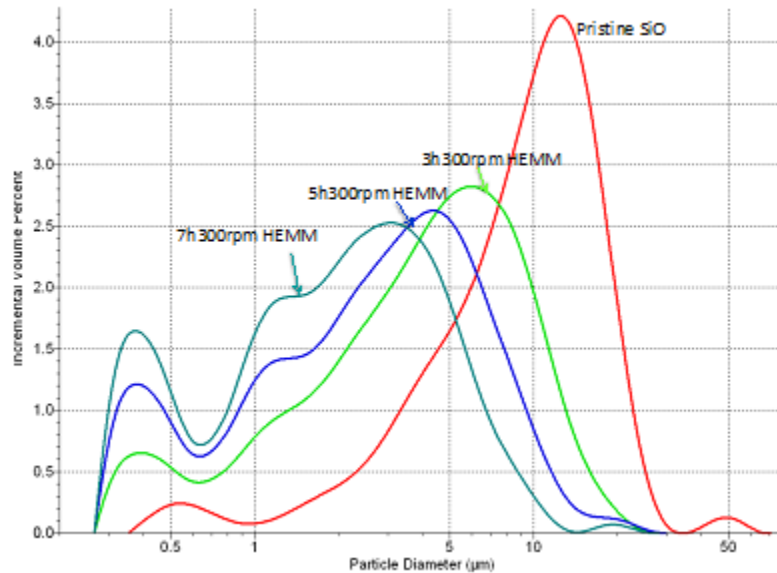


Source: Envia Systems

It is also believed that Si particles are formed, mixed and are possibly embedded within the low dimensional carbon structures. This could explain the resistance of this material against the large volume expansion and pulverization concerns of silicon. This enhanced mechanical stability could be the reason for the improved cycle life observed from the silicon-based anode composites. One of the ways to further improve the performance of SiO-Gr composite is to reduce the particle size of the powder. Pristine micro-sized SiO was milled by the high energy mechanical miller for different times. As shown in the particle size distribution plot in Figure

43, the longer mechanical milling times produced smaller SiO particles. Significant particles less than a micron were obtained for the longer milling times.

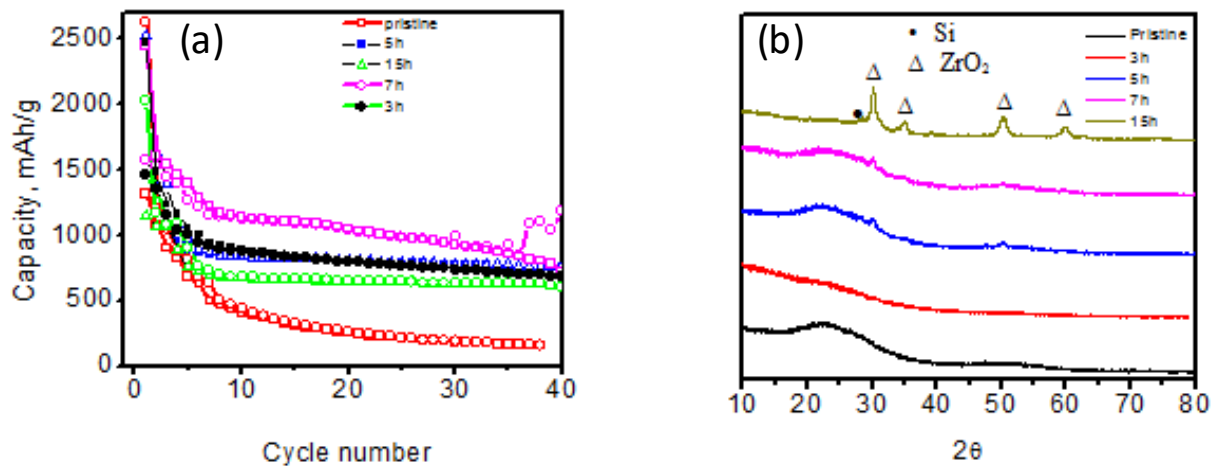
Figure 43: Particle Size Distribution of Pristine and Mechanically Milled (HEMM) SiO



Source: Envia Systems

Improved electrochemical performance was observed with smaller SiO particles as shown in Figure 44a. Figure 44b shows XRD patterns of these SiO materials. Crystalline Si/SiO peaks can be observed. With extended HEMM time, ZrO₂ contaminants from the HEMM jars are also presented in the samples.

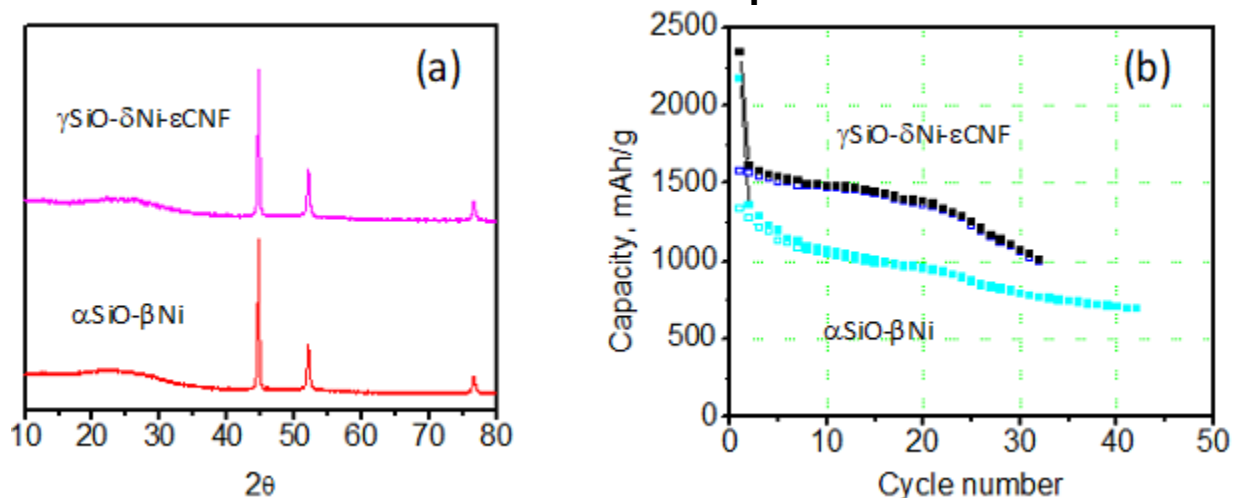
Figure 44: A) Cycling Performance in a Half Cell Configuration And B) XRD Analysis of SiO at Different Mechanical Milling (HEMM) Times



Source: Envia Systems

SiO was also used to compose alloys with metals, such as Ni, Cu and Li. As for Ni, two different compositions SiO-Ni and SiO-Ni-CNF were prepared by HEMM. Figure 45a shows the XRD of both SiO-Ni and SiO-Ni-CNF anode materials. No crystalline SiO-Ni was formed in both cases. Figure 45b shows the electrochemical performances of both anode composites in the half cell configuration. The half cell results showed better performance for the SiO-Ni-CNF anode composite in comparison to the SiO-Ni material .

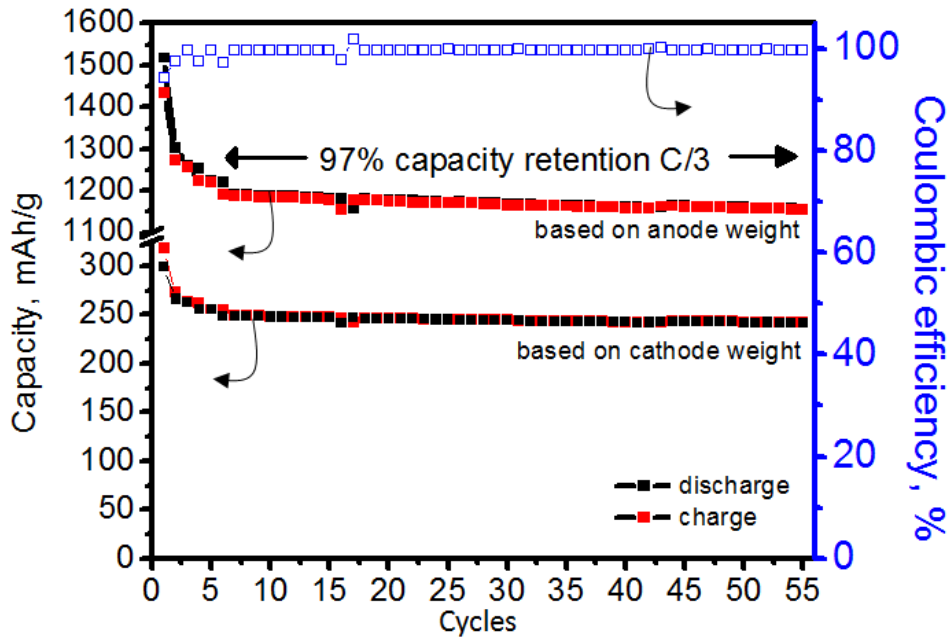
Figure 45: A) XRD Analysis and B) Half Cell Electrochemical Behavior of SiO-Ni and SiO-Ni-CNF Anode Composites



Source: Envia Systems

Figure 46 shows the full cell performance of SiO-Ni-CNF with Envia's HCMR™ cathode based on the active weight of the cathode and anode. Excess lithium additive was used in the full cells. The cells were cycled at a voltage of 4.6V-1.0V for the 1st cycle and 4.5V-1.0V for the remaining cycles. The figure shows a reversible capacity of 1153mAh/g after 50 cycles at a rate of C/3 which exceeds the >1000mAh/g target. The irreversible capacity loss was 85mAh/g, which is less than the <200mAh/g target. The capacity retention after 50 cycles at a C/3 rate is 97 percent which is well above the required capacity retention >80 percent of initial reversible capacity in the full. Anodes that did not show promising electrochemical performance were the alloy anode materials like Si-Li, SiO-Li and SiO-Cu which failed to form laminates due to the incompatibility with the *N*-Methyl-2-pyrrolidone-based binder.

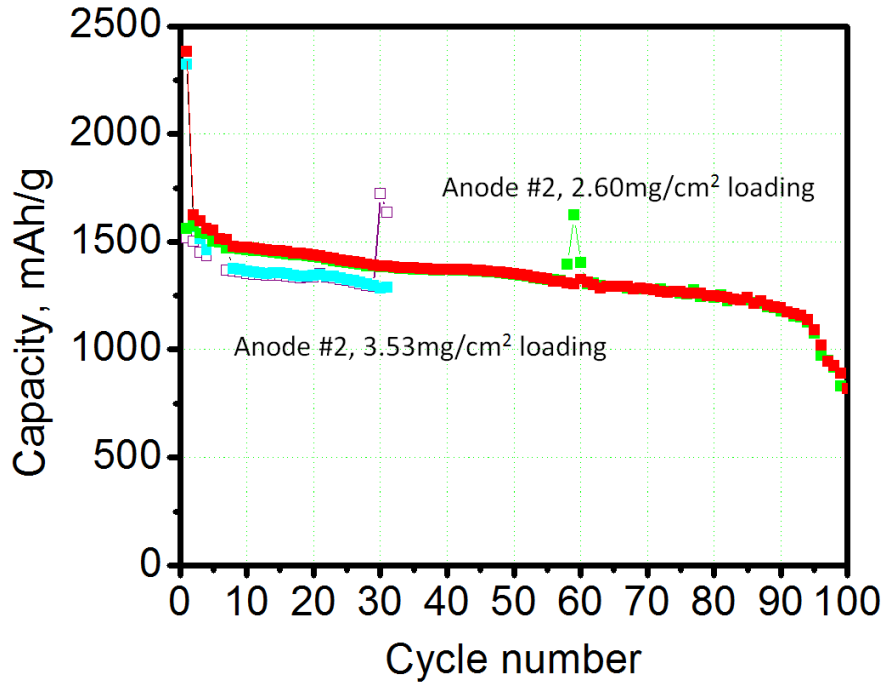
Figure 46: Full Cell Electrochemical Performance of SiO-Ni-CNF Anode and HCMR Cathode Based on Anode and Cathode Active Weights



Source: Envia Systems

In order to increase the capacity of the anode composites and keep reasonable cycling capability, Envia increased the ratio of SiO in the composite. It was found that increasing the ratio of SiO in SiO-Ni-CNF led to inferior cycling performance (not shown here); however in a SiO-Gr composite, the same cycling capability can be better retained. Figure 47 shows the half cell performance of the higher percent SiO anode composites with graphite. The reversible capacity increased from 1264mAh/g to 1560mAh/g when the ratio of SiO increased by approximately 45 percent. The IRCL remained at approximately 34 percent. At a higher loading of 3.53mg/cm², the cell cycled with a capacity of 1366mAh/g at C/3. A reversible specific capacity of 1468mAh/g was achieved at a lower electrode loading level of 2.60mg/cm².

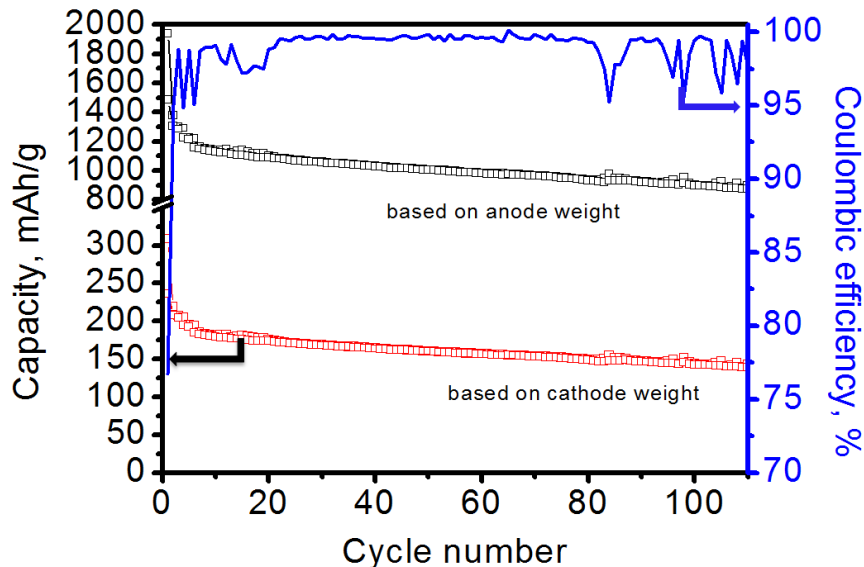
Figure 47: Half Cell Electrochemical Cycling Performance of Sio-Graphite Composite Anodes with Higher Sio Percent. Different Electrode Loading Densities Are Shown



Source: Envia Systems

In the full cell, anodes with the higher amount of SiO showed more than 1160mAh/g capacity at C/3 as shown in Figure 48. The 1st charge capacity is 1941mAh/g and the first discharge capacity is 1489mAh/g based on the whole active weight of anode. In the 100th cycle, the capacity was retained to 79 percent. The IRCL is high (452mAh/g), possibly due to the low cell balance of anode to cathode (120 percent) as well as the lower loading of lithium additive (covering only 30 percent of the IRCL of anode), which cannot effectively and sufficiently compensate the IRCL.

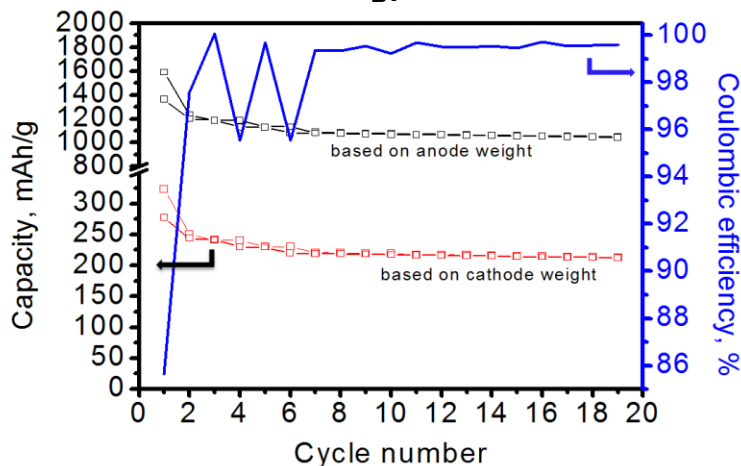
Figure 48: Full Cell Electrochemical Cycling Performance of Sio-Graphite Composite Anodes Based on the Cathode and Anode Active Weights. Anode Loading Is 2.47mg/Cm²



Source: Envia Systems

The electrochemical performance can be successfully improved by tuning the full cell balance to 126 percent and incorporating larger amounts of excess lithium to cover more of the anodes IRCL (70 percent covering IRCL) as shown in Figure 49. In the 1st cycle, 1591mAh/g charge capacity was obtained. The 1st discharge capacity is 1362mAh/g at a loading density of 2.08mg/cm². The IRCL was effectively reduced to 229mAh/g in this means. At C/3, 1081mAh/g reversible capacity was obtained. It is reasonable to expect the cell to cycle for more than 100 cycles.

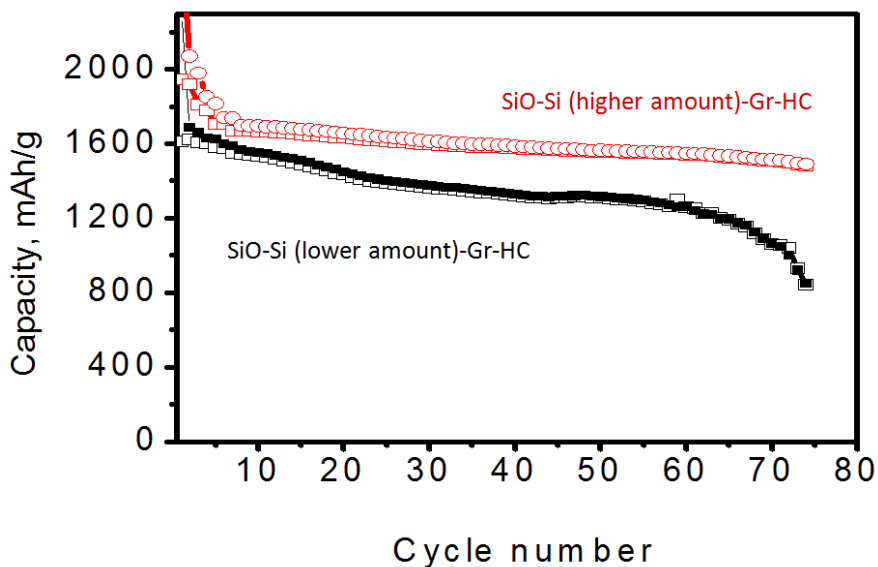
Figure 49: Full Cell Electrochemical Cycling Performance of Sio-Graphite Composite Anodes Based on the Cathode and Anode Active Weights. Anode Loading Is 2.08mg/Cm²



Source: Envia Systems

To achieve even higher capacity and improved cycling performance, Si powder was added to the SiO-Gr composite and hard carbon was coated on the composite. Figure 50 shows the half cell electrochemical performance of two anodes one of which contains higher Si/SiO amounts. It is clear that more capacity can be obtained by increasing the Si amount.

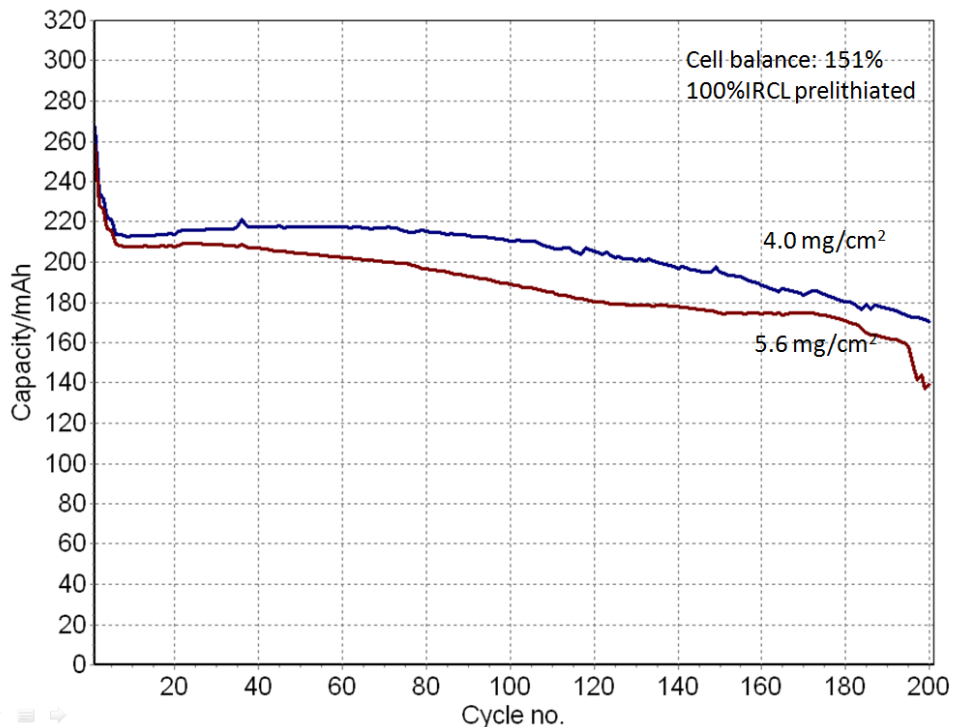
Figure 50: Half Cell Cycling Performance of SiO-Si-Gr-HC Anode Composites with Varying Amounts of Si



Source: Envia Systems

Considerable efforts have been made on selecting the optimal graphite source (natural graphite vs. artificial graphite), using CNF to partly or fully replace graphite, adding graphene paper (commercial sample), and trying different hard carbons. In summary, artificial graphite showed better performance than natural graphite. Composites with CNF showed very competitive electrochemical performance to artificial graphite, with one big advantage of the SiO-CNF anode showing approximately 10 percent higher electrode density. Among the investigated SiO-based high capacity anode composites (SiO-Gr-Si-M-HC-CF), SiO-Gr composite anodes present superior physical and electrochemical properties when compared to other candidates. Figure 51 shows that at the loading density of 4.0mg/cm^2 of this composite, a higher anode to cathode balance of 151 percent (blue curve) shows longer cycling life (199 cycles vs. 150 cycles) when compared to the results observed for 137 percent cell balance. The improvement in cycle life due to higher cell balance comes at a price of higher cell weight due to more anode, supplemental lithium and electrolyte resulting in lower energy density. Envia has also demonstrated that SiO-Gr anodes can work at a high electrode loading of 5.6mg/cm^2 . The cell can be cycled for 180 cycles at such a high loading. All reported cycle life numbers are values obtained when the specific capacity of the cell decreases to 80 percent of the initial C/3 capacity value.

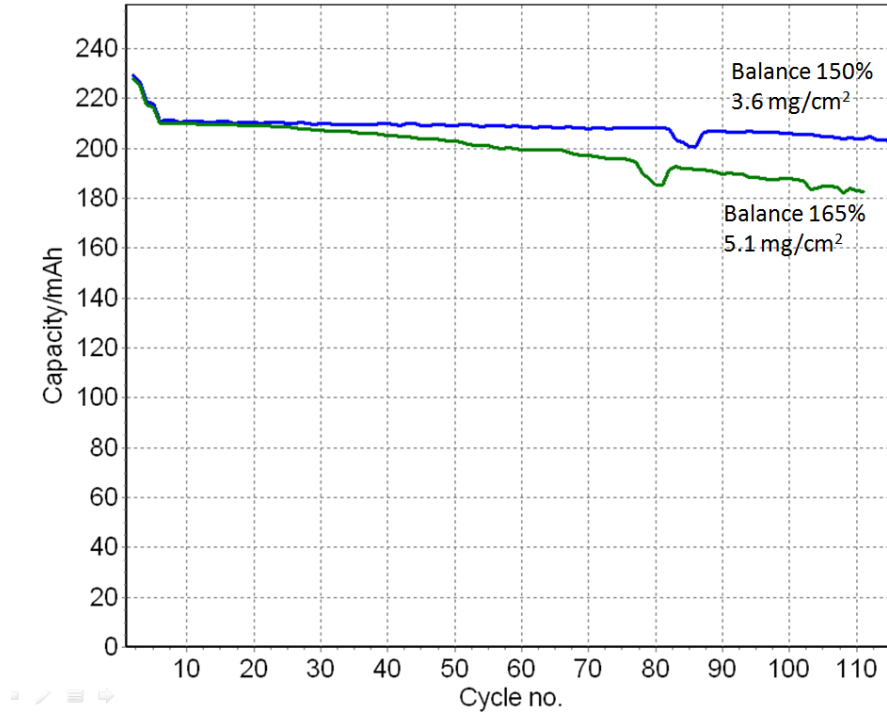
Figure 51: Full Cell Electrochemical Cycling Performance of Envia's $\text{SiO}_\alpha\text{-Gr}_\beta\text{-Si}_\gamma\text{-M}_\delta\text{-HC}_\varepsilon\text{-CF}_\zeta$ Anode and HCMR™ Cathode with Different Anode Electrode Loading Levels



Source: Envia Systems

SiO-Gr-Si-M-HC-CF composite anodes were made into low capacity single layer pouch cells. Figure 52 shows the electrochemical performance of the single layer pouch cells. The cell at 5.1 mg/cm² anode electrode loading completed 110 cycles with 87 percent capacity retention. At the lower anode electrode loading of 3.6 mg/cm², 96 percent capacity is still retained after 110 cycles. It can be expected that these pouch cells will cycle for at least 200 times before the capacity fade reaches 80 percent of the initial C/3 capacity.

Figure 52: Full Cell Electrochemical Data from Single Layer Pouch Cells with Different Cell Balance and Anode Electro Loading



Source: Envia Systems

SiO-Gr-Si-M-HC-CF was down-selected as the anode of choice to build large format cells. SiO-Gr-Si-M-HC-CF anode composites have the advantage of high reversible capacity, good rate capability, stable cycle life, high loading capability and manufacturable via a high energy mechanical milling (HEMM) process. Even though this anode material is very promising, cell design optimization continued to be a critical aspect to reach the aggressive electrochemical project targets. Even with the best electrode materials, if the electrode loading, cell balance, electrode density, cycling voltage window, etc. are not completely optimized the cells will not cycle or meet the energy density targets.

Envia Systems explored 20 significantly different anode materials and production/synthesis approaches, which were summarized into the five categories discussed previously in this section. During this time, the most promising anode with respect to material capacity, IRCL, cycle life, manufacturability and cathode compatibility were selected. Out of the 20 approaches, most of the approaches were stopped due to poor specific capacity, poor cycle life and high IRCL. Other approaches were discontinued due to scalability concerns and lack of data, which could suggest the approaches were promising, but not appropriate for the aggressive targets and timeline of the project. As a result of this extensive selection process, Envia decided to focus all of its effort on the development of mechanically milled SiO to form various anode composites (SiO-Gr-Si-M-HC-CF).

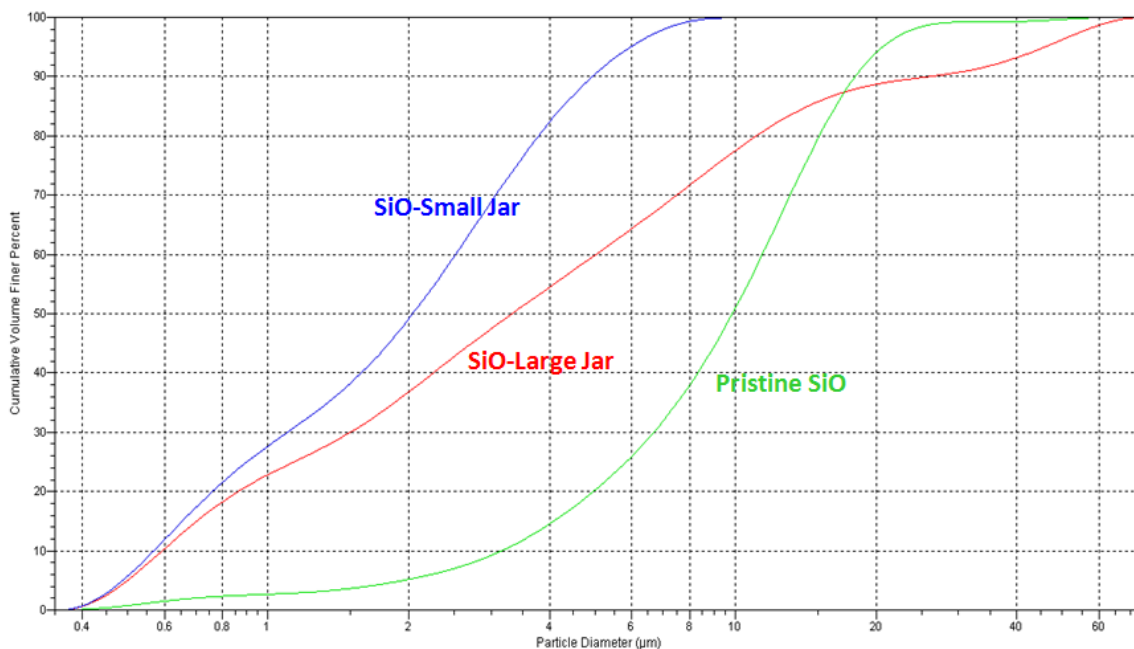
Anode Materials Scale Up

Envia had a target to deliver 2kg of down-selected SiO-graphite anode material for large format cell demonstration. The 2kg anode target was established from the cathode requirement of 3kg since the anode has higher surface area and much higher capacity than the cathode, thereby requiring less anode for the large cell build.

To scale up the process, large 500mL HEMM jars were used instead of the standard 50mL jars. An important challenge during the scaling-up process was to reduce the contamination of the anode material by zirconium oxide, which originates from the walls of the milling jars and from the milling media. During the initial scaling up process, large amounts of zirconium oxide were noticed in the milled samples. As a result, the electrochemical performance of the anode materials significantly dropped because of the presence of the zirconia impurities. To overcome this problem, it was decided to change to dry milling (without any liquid media) instead of wet milling. The disadvantage associated with the dry milling is that it is not as effective as wet milling for the reduction of the particle size. To match up with the material characteristics obtained in a small jar, Envia had to optimize the milling time, milling speed, loading, and the number of media used.

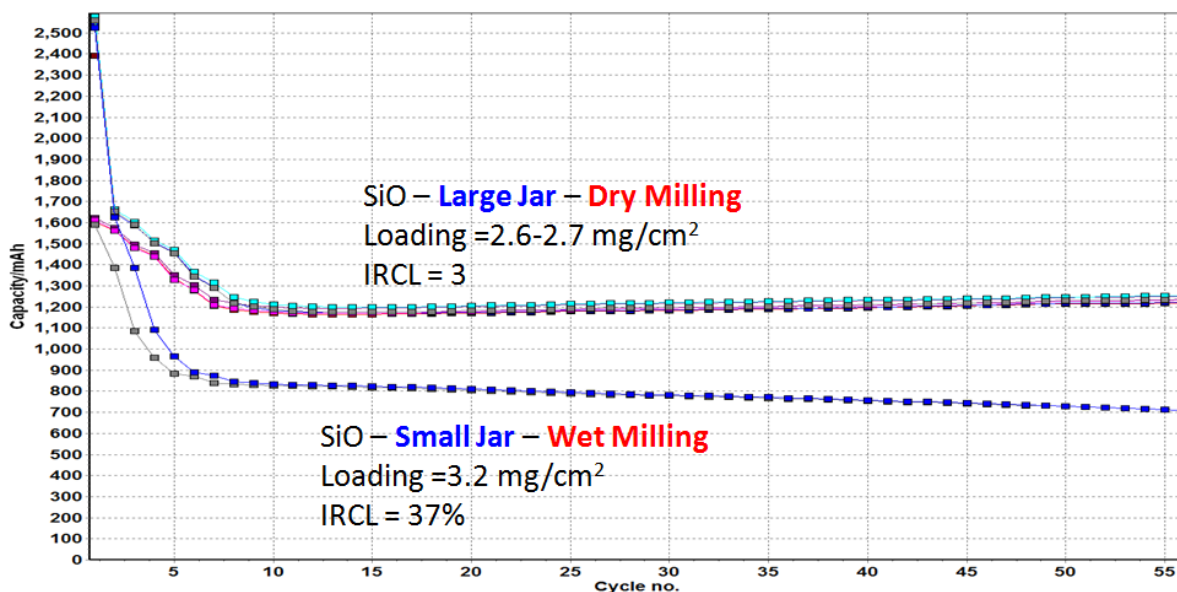
The cumulative particle size distribution of the optimized large jar condition along with the control data from the small jar are shown in figure 53. Although the average particle size of the milled SiO from the large jar is slightly bigger than that obtained from the small jar, there was no difference in the electrochemical performance as evident in figure 54. In fact, the SiO milled in the large jars had better rate capability than those milled in the small jars.

Figure 53: Particle Size Distribution of Si Monoxide Obtained From HEMM in Small and Large Milling Jars Along With the Pristine SiO Material



Source: Envia Systems

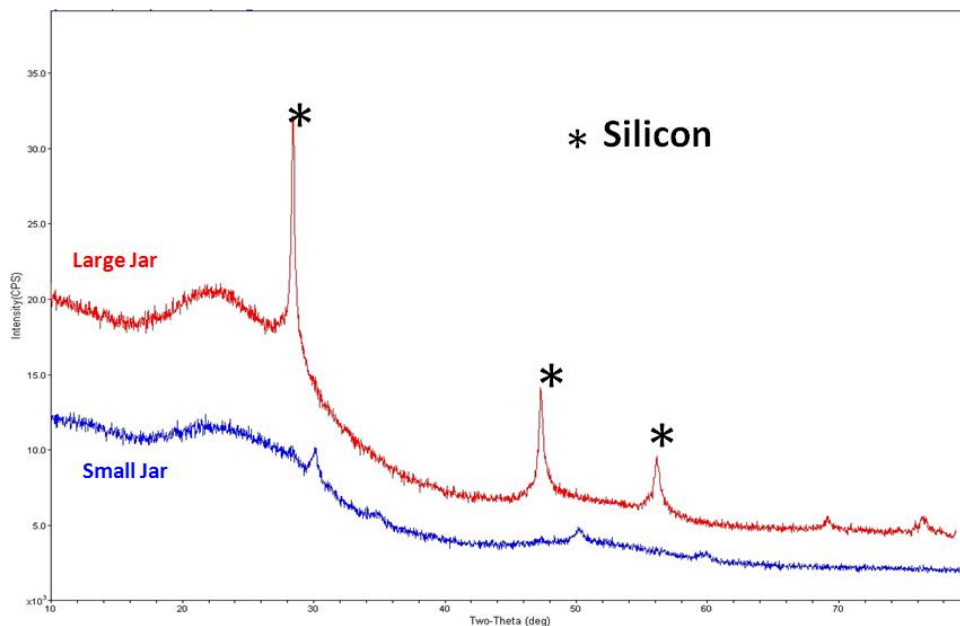
Figure 54: Half Cell Specific Capacity of Si Monoxide Milled at Different HEMM Conditions



Source: Envia Systems

The formation of Si as substantiated by the XRD patterns (figure 55) in the SiO obtained from the large jars could have improved the electrochemical performance. Figure 55 clearly shows the presence of sharp Si peaks for the large jar where they are smaller or less apparent from the small jar processing.

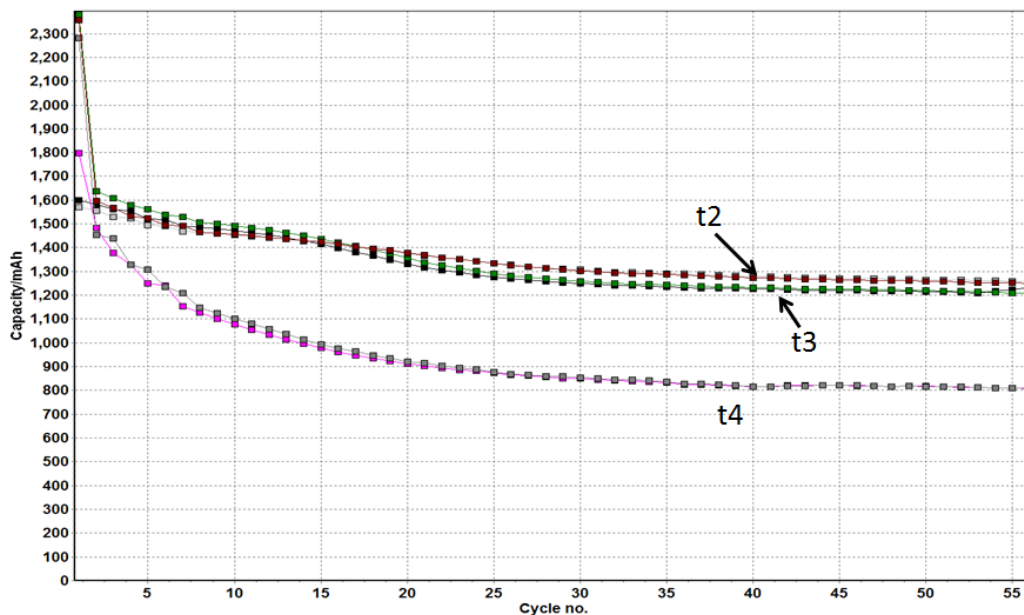
Figure 55: XRD Patterns of Si Monoxide Milled at Different HEMM Conditions



Source: Envia Systems

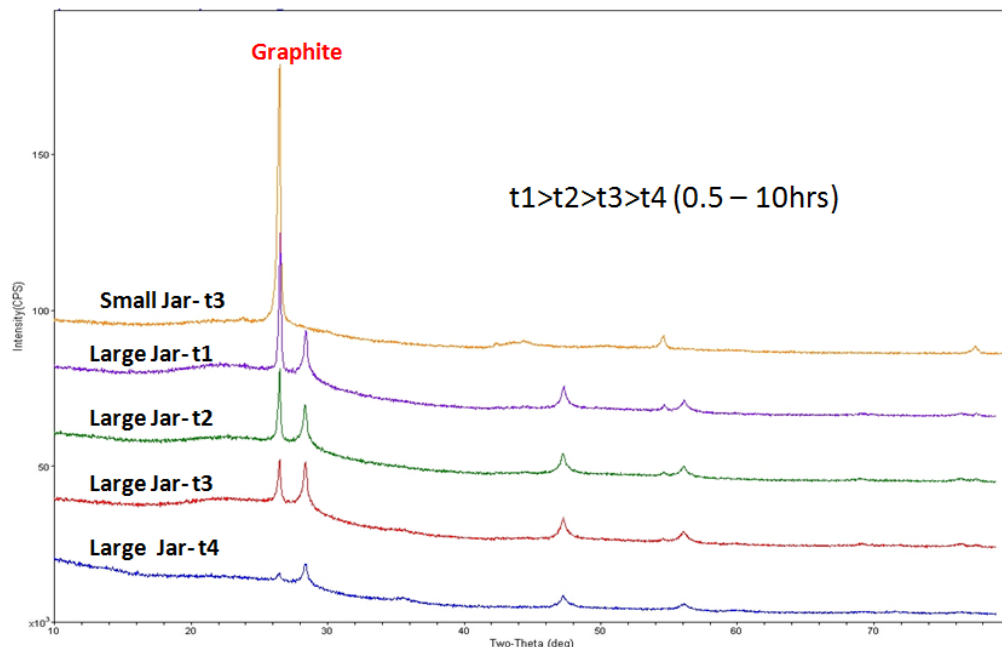
With the processing conditions for the starting SiO material optimized, the next step was to form the SiO-graphite composite anode. Once again, different parameters were fine tuned in the HEMM to obtain the best anode performance. The cycling data for the composite materials as a function of milling time (0.5hr-10hr) is shown in figure 56. With higher milling times, the graphite becomes amorphous deteriorating the electrochemical performance. This claim is further substantiated by the XRD patterns in figure 57, where there is a clear reduction in the graphite peak with milling time.

Figure 56: Half Cell Specific Capacity of Sio-Graphite Anode Milled for Different Times in a Large Jar



Source: Envia Systems

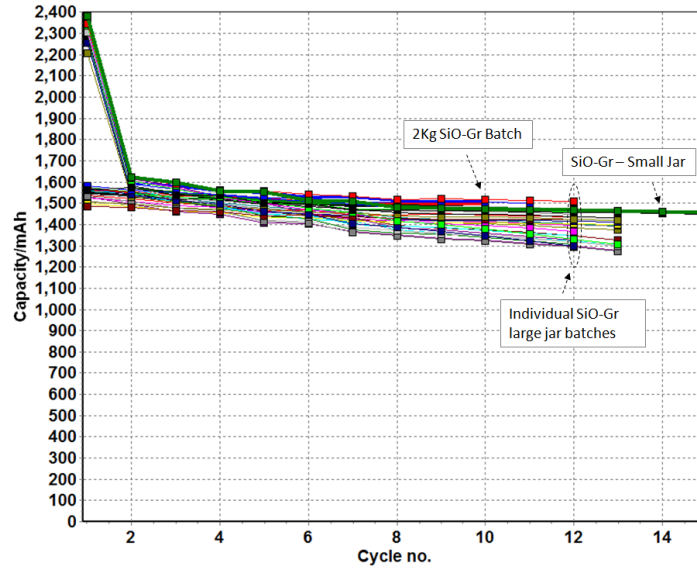
Figure 57: XRD Patterns of SiO-Graphite Anode Composites Milled at Different HEMM Conditions



Source: Envia Systems

Based on the optimized SiO and SiO-Graphite HEMM conditions, 2Kg of SiO-Graphite were produced and shipped to Envia's cell facility to build large capacity pouch cell. In order to make the 2Kg batch of SiO-Gr anode, the material from 12 different large jars was mixed. Figure 58 shows the half cell electrochemical performance from the mixed 2Kg SiO-Gr anode, the small jar SiO-Gr anode baseline and 8 of the 12 individual large jar SiO-Gr anode batches. The electrochemical performance from the scaled-up material is very similar to the small jar baseline suggesting that the process has been optimized and the material has been properly scaled-up.

Figure 58: Half Cell Electrochemical Performance from the SiO-Gr Scaled-Up 2Kg Batch, Small Jar Material and Individual Large Jars



Source: Envia Systems

Table 8 summarizes the physical, structural and electrochemical properties of the various SiO-Gr anode materials (2kg large batch, small jar material and large jar batches). The table shows nearly identical values for the particle size, surface area, lattice constant and electrochemical performance suggesting the scale-up process is well in control.

Table 8: Summary of Physical, Structural and Electrochemical Parameters of the Scale-up SiO-Gr Anode

Sample ID	Physical & Structural Properties			Half cell Electrochemical Data		
	Median Particle Size (µm)	Surface Area (m ² /g)	XRD-Lattice Parameter (Å)*	C/20-Discharge Capacity (mAh/g)	C/20-Charge Capacity (mAh/g)	IRCL (%)
Small jar baseline	3.7	9.1	No Si peak	2381	1560	34.50%
2Kg mixed batch	7.3	24.2	5.43	2335	1565	32.90%
Large jar #1	8.0	26.9	5.42	2345	1584	32.50%
Large jar #2	7.9	26.6	5.43	2336	1569	32.80%
Large jar #3	7.1	25.2	5.43	2305	1532	33.50%
Large jar #4	8.3	25.6	5.43	2315	1557	32.70%
Large jar #5	7.5	24.2	5.43	2292	1539	32.90%
Large jar #6	7.4	25.1	5.43	2333	1559	33.20%
Large jar #7	6.4	23.9	5.42	2274	1512	33.50%
Large jar #8	7.7	25.1	5.43	2267	1527	32.60%
Large jar #9	7.3	23.8	5.43	N/A	N/A	N/A
Large jar #10	7.0	23.0	5.44	N/A	N/A	N/A
Large jar #11	6.8	23.1	5.43	N/A	N/A	N/A
Large jar #12	6.4	N/A	5.43	N/A	N/A	N/A
Average Value	7.3	24.8	5.43	2308	1547	32.96%
Standard deviation	0.6	1.3	0.01	29	24	0.39%

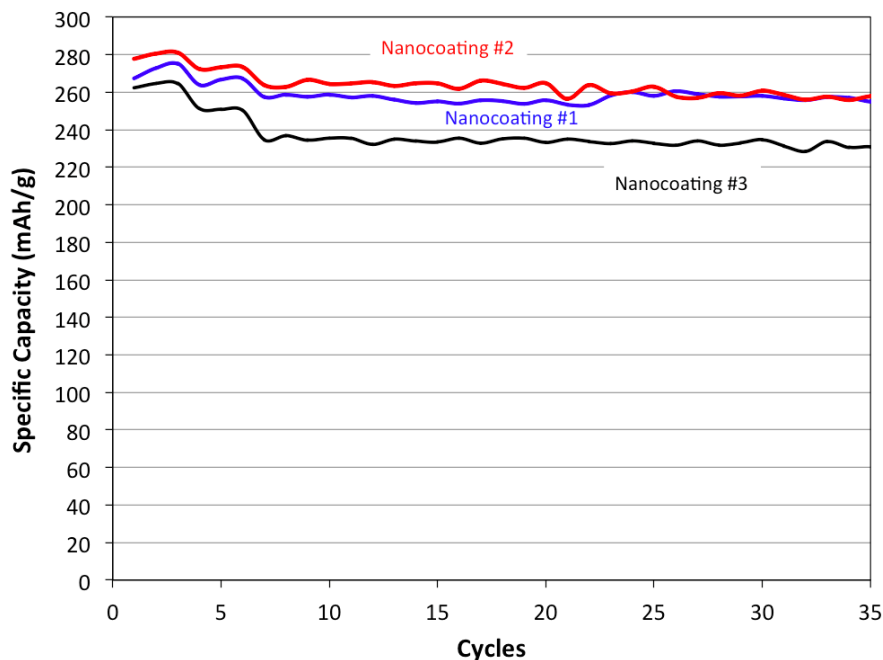
Source: Envia Systems

CHAPTER 3: Cathode Development

Envia Systems explored various HCMR™ cathode compositions, particle morphologies, and surface coatings to improve the reversible specific capacity, IRCL and cycle life of the cells. The reversible capacity for an optimized cathode composition ranged from 260mAh/g to 280mAh/g at low rate depending on the chosen conditions. The physical properties (tap density, surface area, particle size, etc.) were also controlled to enable high electrode density and loading levels required to reach the high energy density targets >400Wh/Kg. Through the life of the project the cathode material was scaled up to 3kg batches to be paired up with the developed anode and build large format high capacity pouch cells.

Figure 59 shows the cycling performance of cathode materials with an optimized composition and nanocoatings exhibiting a capacity of ~280mAh/g at C/10 and cell cycles with more than 90 percent efficiency at C/3 for approximately 35 cycles. For most of full cell studies described in the previous anodes sections, Envia used these cathodes to pair with the new composite and alloy anodes.

Figure 59: Specific Discharge Capacity versus Cycles for Optimized Cathode Materials

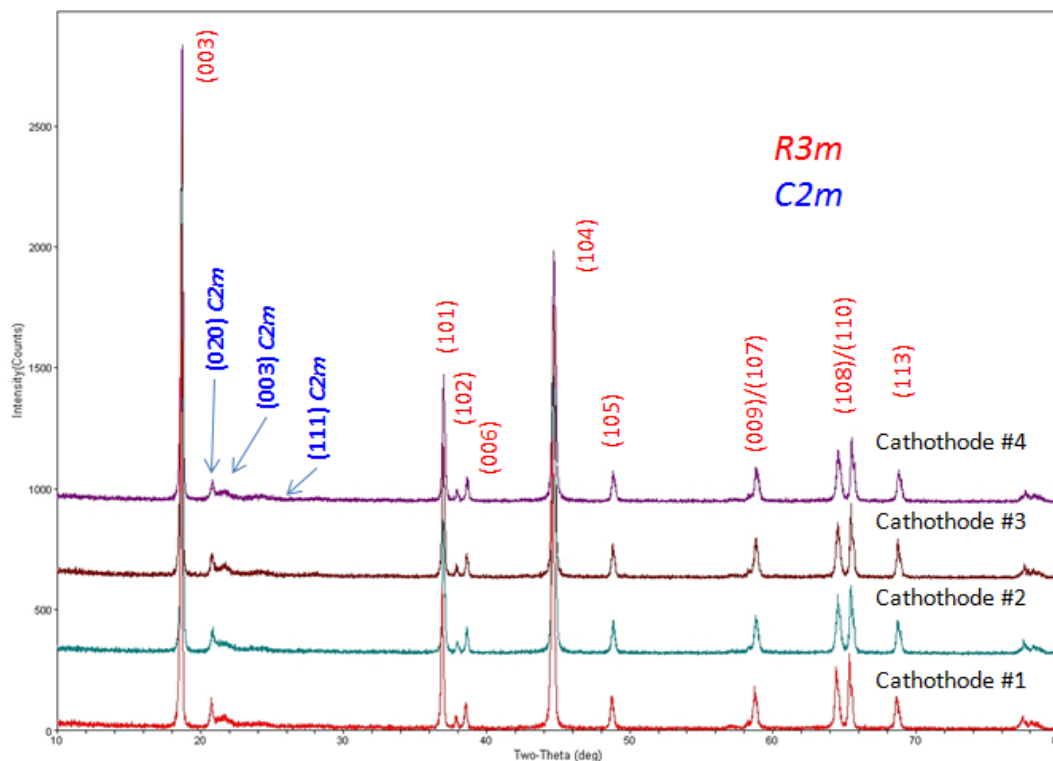


Source: Envia Systems

Figure 60 shows a number of XRD patterns for different cathode compositions that have been explored in this project. The patterns show nearly identical data for the different cathode

compositions, suggesting excellent control in the cathode synthesis. The data shows the expected signatures for the lithium-rich layer-layer cathode materials, with the distinctive R3m and C2m crystallographic groups clearly shown. The C2m crystallographic group corresponds to the monoclinic phase of Li_2MnO_3 and the R3m crystallographic group corresponds to the trigonal phase of LiMO_2 . The extracted lattice parameters (c , a , c/a and unit cell volume) of the cathode material are also nearly identical.

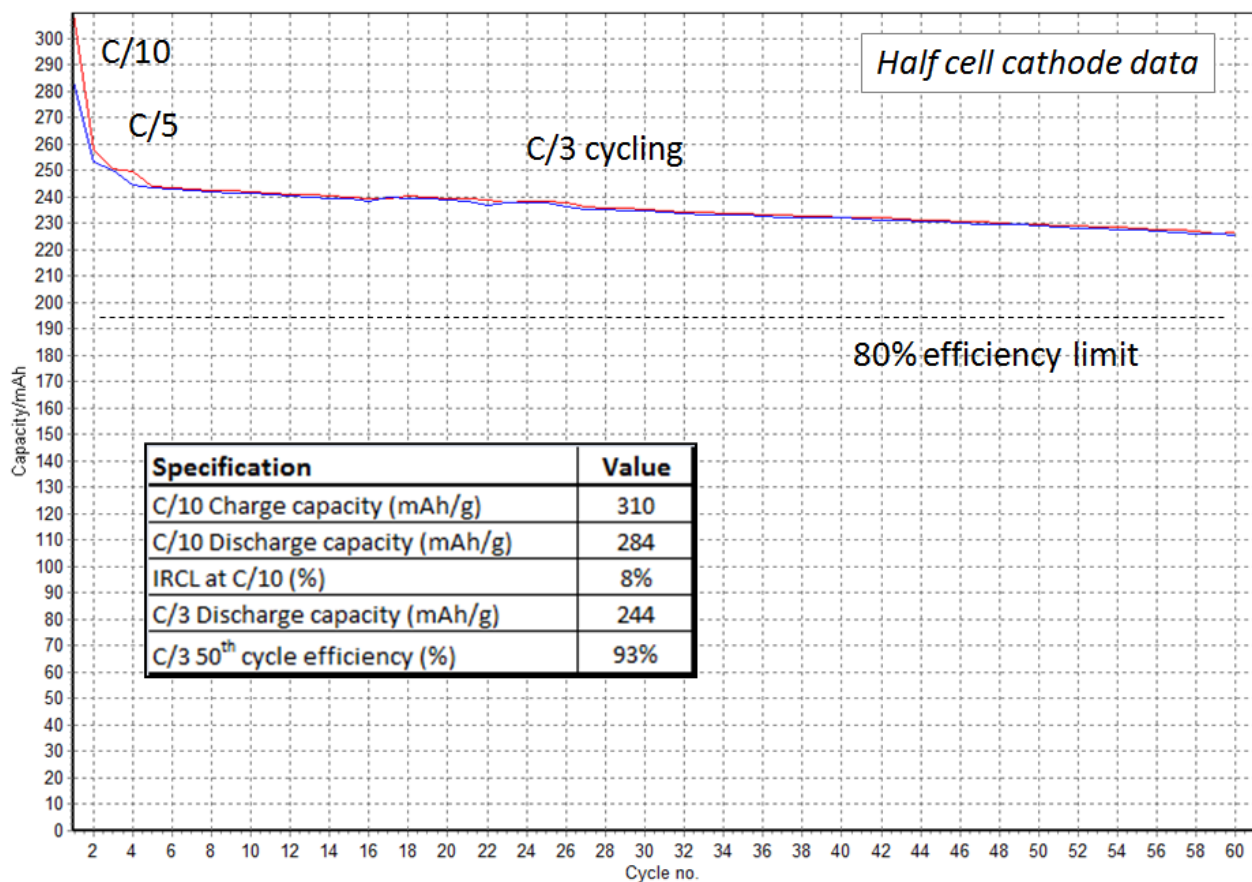
Figure 60: XRD Patterns of Different High Capacity Manganese Rich Cathodes



Source: Envia Systems

Figure 61 shows the half cell electrochemical performance of the optimized cathode material and selected to be scaled up for the large format cell builds. The figure shows a C/10 discharge capacity of 280mAh/g and a cycle life efficiency of 93 percent after 50 cycles.

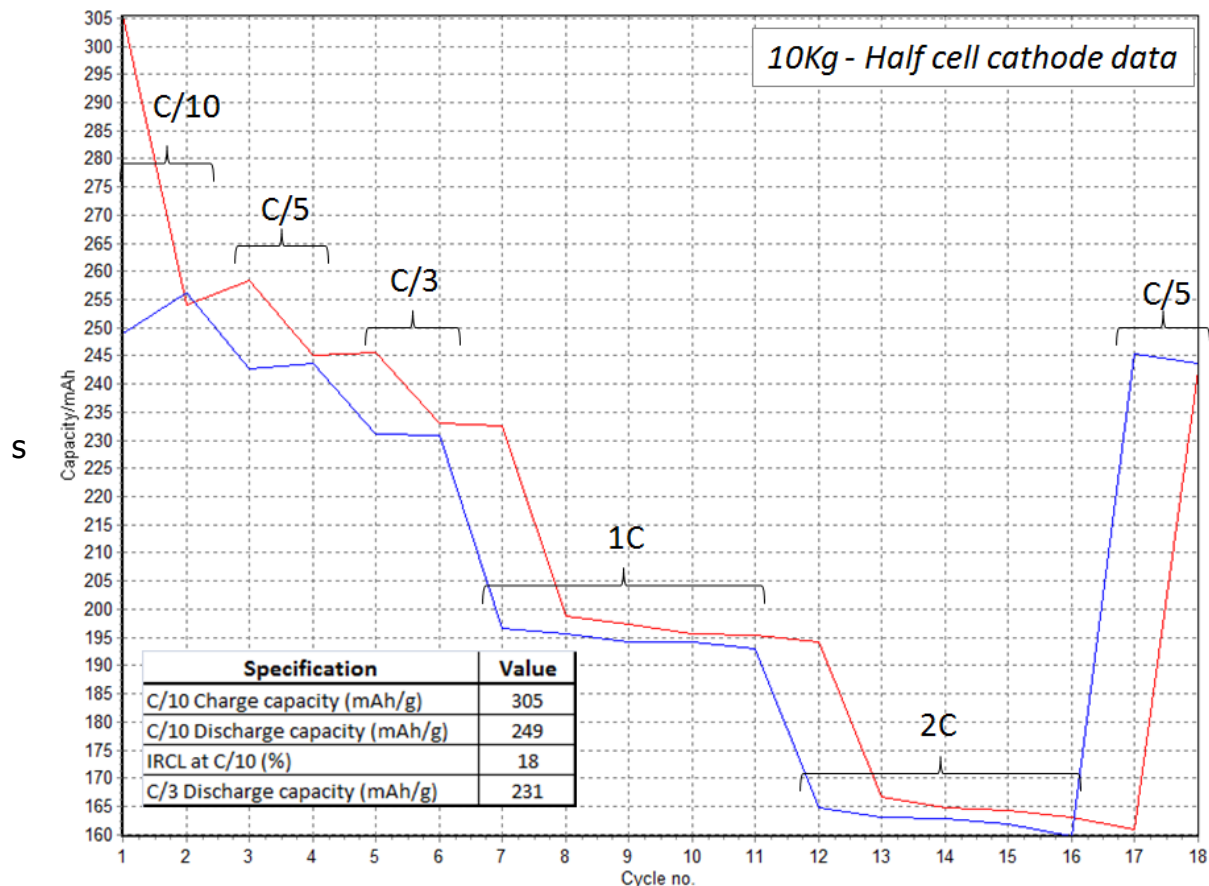
Figure 61: Half Cell Electrochemical Performance from the Optimized HCMR™ Cathode Material



Source: Envia Systems

The cathode material was scaled-up to 10Kg and shipped to our Cell Fabrication Facility where Envia used the material to build large capacity pouch cells with the high capacity SiO-Gr anode. Unfortunately as the cathode process was transferred from a smaller R&D reactor to a larger scale-up reactor, the cathode performance decreased. Figure 62 shows the electrochemical performance of the 10Kg cathode batch. The data shows that the specific capacity has decreased and the IRCL has increased. Envia continued to optimized the cathode process to reproduce the best cathode performance from the large scale-up reactors, but in the interim used the 10Kg of cathode to support the large cell builds.

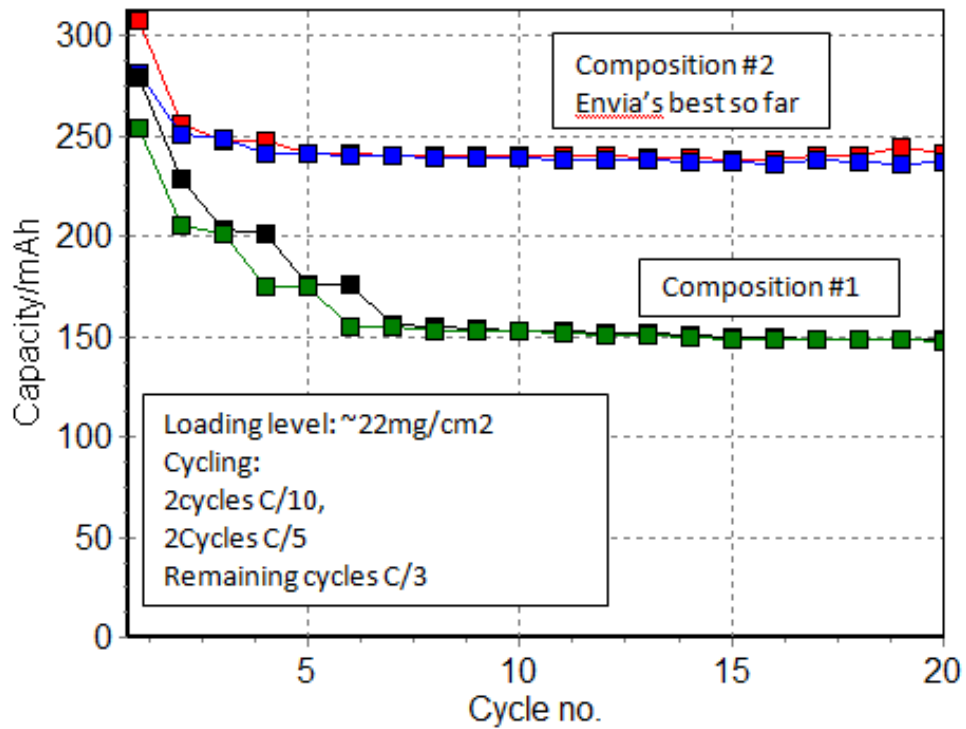
Figure 62: Half Cell Electrochemical Performance from the Scale-Up 10Kg Cathode Batch



Source: Envia Systems

Similar to the anode cell optimization, there is development in the cell engineering with respect to the cathode electrode. Since the anode has a very high capacity (>2000mAh/g at C/20), a matching high capacity cathode has to be developed. In order to balance against such a high capacity anode, the cathode needs to have high capacity, high electrode loading, high electrode density and high electrode conductivity to enable adequate cycling. The cycling performance of the heavy loaded cathodes greatly depends on the type of conducting material added while preparing the electrodes. Figure 63 shows the half cell cycling performance of HCMR™ cathode prepared with different conducting additives. Composition #1 consists of Super-P and KS-6 while composition #2 consists of Super-P and Carbon nanotubes. For a loading level of approximately 22mg/cm², the electrode with composition #2 cycled better with higher capacity compared to the electrode with composition #1.

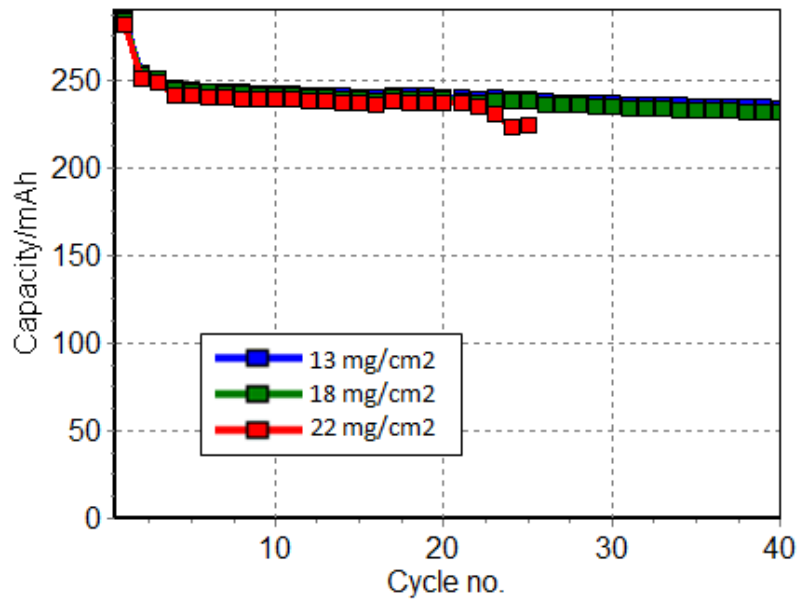
Figure 63: Half Cell Electrochemical Performance of HCMR™ Cathode with 2 Electrode Compositions at an Electrode Loading of Approximately 22mg/Cm²



Source: Envia Systems

In addition to conducting additives, the cycling performance of the cathode depends on the compression density of the electrode. Figure 64 shows the half cell cycling performance of the HCMR™ cathode with different electrode loading levels. All the electrodes were calendared to an electrode density of 2.7g/cc. The cells with loading levels of 13mg/cm² and 18mg/cm² cycled well, but when the loading level reached 22mg/cm² the cell faded and failed after 25 cycles. All cathode electrode formulations used composition #2.

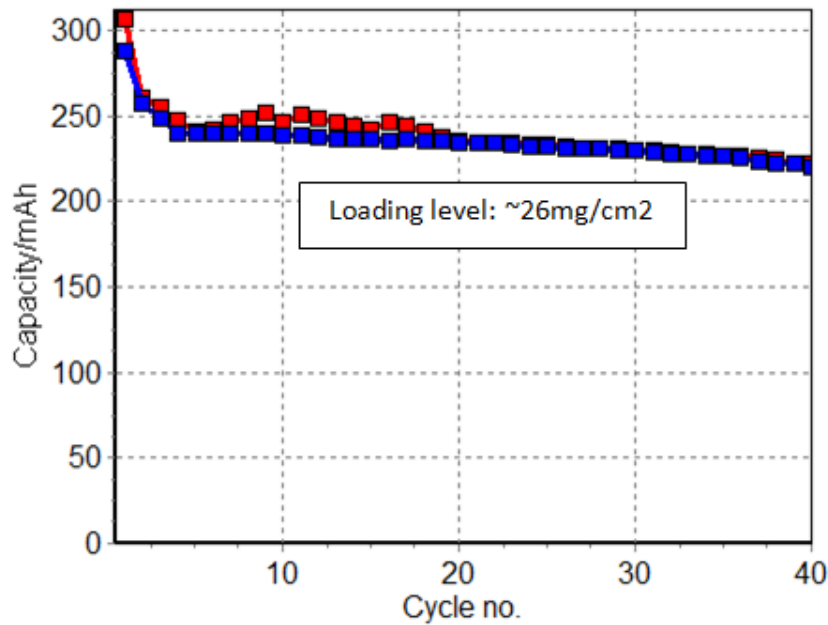
Figure 64: Half Cell Electrochemical Performance of HCMR Cathode with Various Electrode Loading Levels at an Electrode Density of 2.7g/Cc



Source: Envia Systems

When the electrode density is reduced from 2.7g/cc to about 2.4g/cc, it was noticed that the cells cycled even at loading levels of 26mg/cm² as shown in figure 65.

Figure 65: Half Cell Electrochemical Performance of an HCMR™ Cathode with an Electrode Loading of 26mg/Cm² and Electrode Density of 2.4g/Cc



Source: Envia Systems

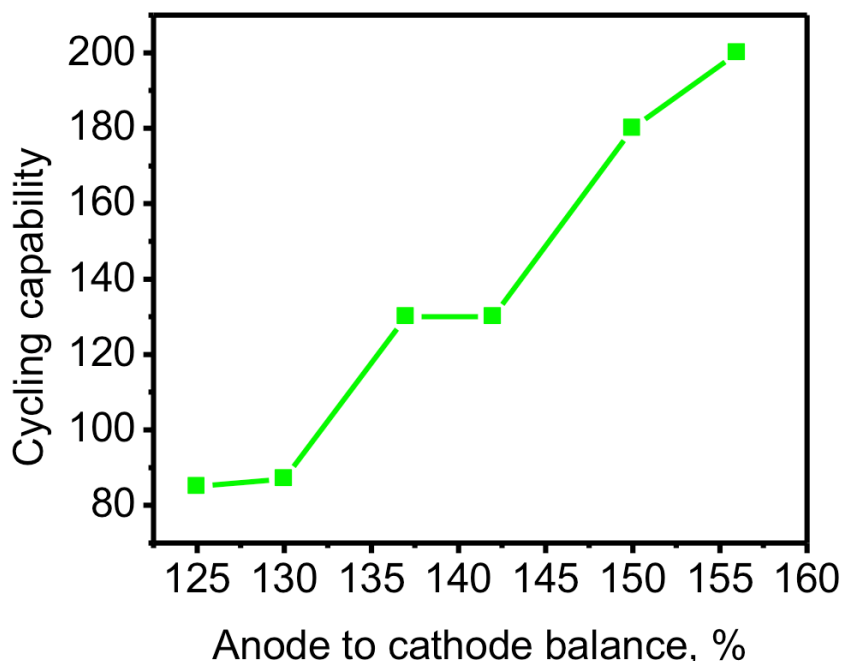
Decreasing the density of the electrode increases the porosity and thickness of the electrode. The higher porosity requires greater amounts of electrolyte, which will increase the cell weight and decrease the gravimetric energy density. Increasing the electrode thickness will increase the volume resulting in a decrease of the volume energy density of the battery. Understanding the different benefits and compromises of the cathode and anode electrodes specifications and how they relate to the cell performance is critical in achieving the target energy density ($>400\text{Wh/kg}$) and cycle life (>500 cycles) targets of the cells.

CHAPTER 4:

Large Cell Integration

Cell design and engineering is another key to reaching high energy density. One important cell design parameter is the balance between anode and cathode. The electrode balance plays a key role in the cycle life of the cell. The higher the cell balance, the better the cell cycling performance as shown in Figure 66. Unfortunately, a high cell balance always leads to lower energy density as more anode material is included in the cell increasing the weight of the cell. A trade-off between cycle life and energy density needs to be optimized when dealing with the cell balance.

Figure 66: Relationship of Cycling Capability and Cell Balance



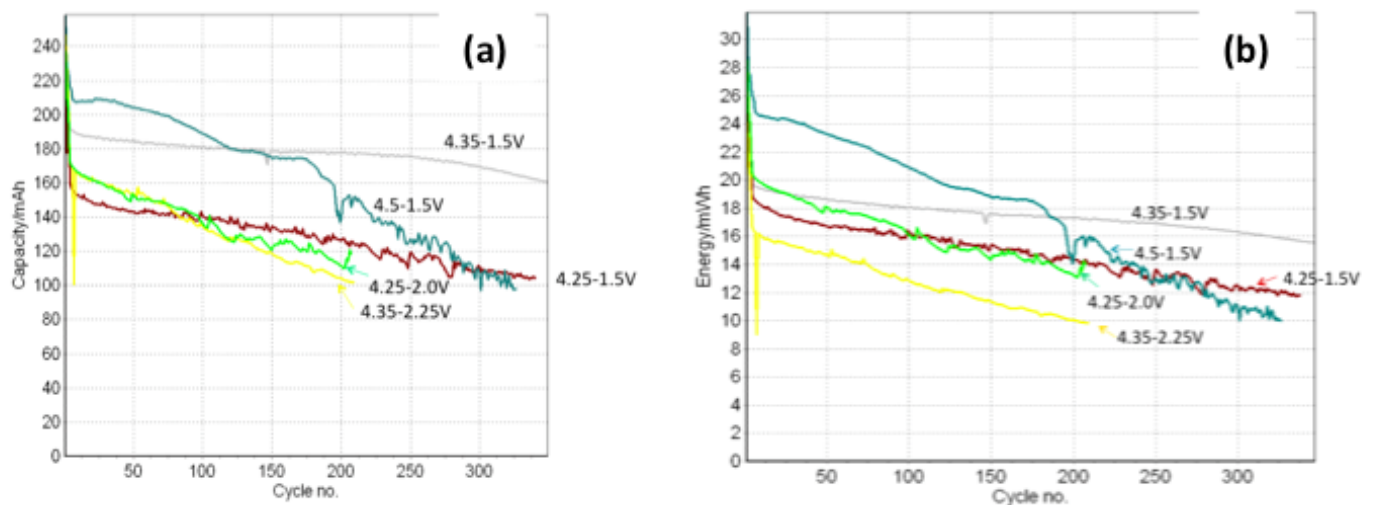
Source: Envia Systems

Another important cell design parameter is the cycling protocol of the cell, meaning the specific voltage window that will determine the depth of discharge (DOD) of the cell. Having an optimized cycling protocol will enable the cell to cycle longer. The voltage window was optimized using full cell coin cells with SiO-Graphite anode and HCMR™ cathode with a balanced of 150-155 percent of anode capacity to cathode capacity. The coin cells were cycled at different percent DOD while monitoring the cycle life. Figure 67 shows the cycling performance of these full cells at different percent DOD. Specifically, the DOD was controlled by different voltage cutoff window after the activation protocol of C/20 for 1 cycle, C/10 for 2

cycles, C/5 for 2 cycles and C/3 for one cycle. The voltage windows explored were: 4.5V-1.5V, 4.35V-1.5V, 4.25V-1.5V, 4.35V-2.25V, and 4.35V-2.0V.

As shown in Figure 67, the voltage window of 4.35V-1.5V shows the best cycling performance with respect to energy and capacity. Cycling the cell between 4.35V to 1.5V corresponds to about 85 percent DOD if 4.5V-1.5V is set as a full 100 percent depth of charge and discharge of the cell. The 4.35V to 1.5V voltage window shows approximately 83 percent capacity retention (Figure 67a) and approximately 80 percent energy density retention (Figure 67b) after 340 cycles. Similar results have been verified in small capacity pouch cells and as a result the voltage window of 4.35V-1.5V has been designed as the cut off voltage window to extend the cycle life in large format cells.

Figure 67: Relationship of (a) Specific Capacity versus Cycles and (b) Energy Versus Cycles for Different Voltage Windows

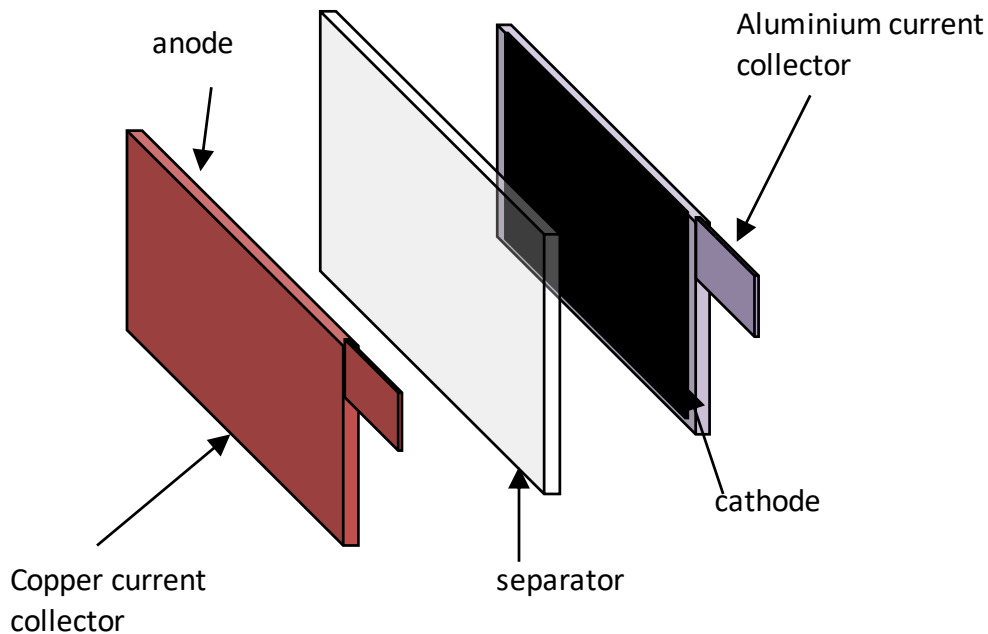


Source: Envia Systems

Due to some limitations in cell fabrication equipment (large coater, sealer and dry room) in our California facility, instead of building 1Ah pouch cells for cell development Envia assembled smaller capacity single layer pouch cells. 1Ah capacity cells could be built but the absence of a dry room made the process very difficult and unreliable since the multilayer cells need to be assembled in a glove box.

With the experience acquired from building 1Ah pouch cells, Envia started building single layer smaller capacity pouch cells. Figure 68 shows a schematic diagram of the single layer pouch cell design. Similar to the coin cell design, the single layer pouch cell has only one side of the electrode coated with anode and cathode with a separator in between. The idea behind building and studying single layer pouch cells is that the performance of these cells will be very representative to the target high capacity 10-40Ah pouch cells, as well as, Envia can routinely make these cells at its California facility.

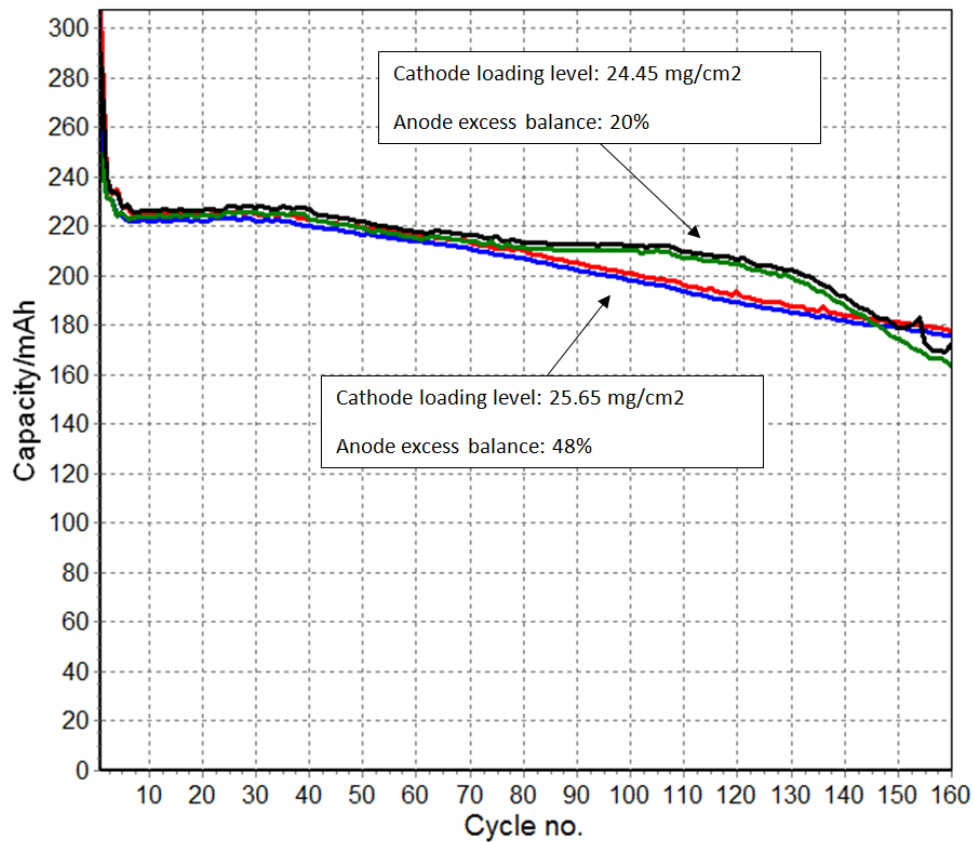
Figure 68: Schematic Representation of Single Layer Pouch Cells



Source: Envia Systems

Since the capacity of the cathode in a battery directly governs the energy density, it is very critical to push the upper limits on the loading levels of the cathode. With a regular graphite anode, Envia's high capacity cathode material loading levels fall in the range of 11-15mg/cm². In the present case, with high capacity Si anode, in order to reach an energy density of 400Wh/Kg the loading level of cathode may have to exceed 28mg/cm². Extensive studies were done to increase the loading levels of the cathode material and maintain adequate electrode adhesion and conductivity that will support the long cycling targets. Figure 69 shows the cycling performance of two single layer pouch cells with loading levels of cathode reaching close to 24-26mg/cm². Both cells have supplemental lithium and are at different anode excess balance. The cell with 20 percent excess anode balance appeared to cycle better initially with good cycle efficiency but faded rapidly after 130 cycles. The cell with 48 percent excess anode balance has a gradual fade in capacity and is still cycling even after 160 cycles. This shows that the excess anode balance is also critical in improving the cycle life of the battery but too much excess anode will compromise the energy density of the cell. Optimization of the anode balance and excess lithium loading are very critical in improving the energy density and cycle life of the battery.

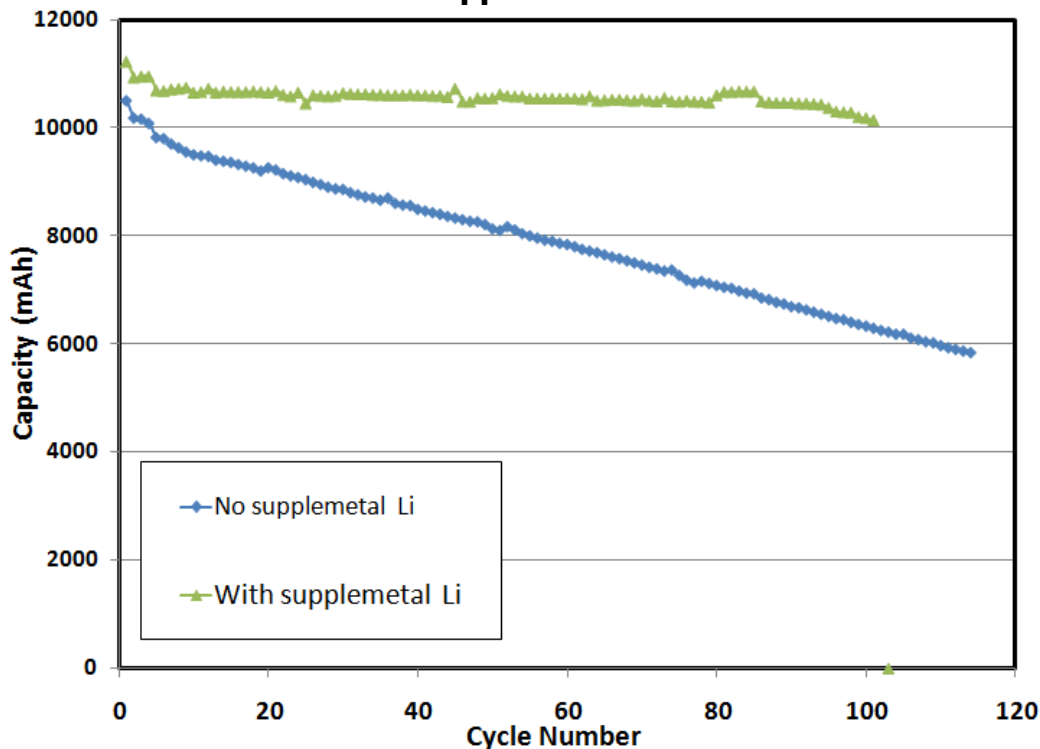
Figure 69: Electrochemical Performance of the Single Layer Pouch Cells with Heavy Loading Levels of the Cathode



Source: Envia Systems

With the learning from the single layer pouch cells from our California facility, the first large format cells built were 10Ah pouch cells. In our first large cell build with Si anode, the loading level of the cathode and anode were kept at lower levels in order to solve any problems that might arise from the basic cell build process. This was the first time Si based anodes were coated in our large coaters, where new polyimide binder and different drying protocols were established. On the cathode side, typical cathode loading levels for graphite-based cells are approximately 12mg/cm², and for this first build the target was 18mg/cm². Figure 70 shows the cycling performance of the 10Ah pouch cells, where the first cycle was run at the rate of C/10, the next two cycles at C/5 rate and the remaining cycles at a C/3 rate. The figure also shows 10Ah pouch cells with and without the incorporation of supplemental lithium.

Figure 70: Electrochemical Performance from 10Ah Capacity Pouch Cells With and Without Supplemental Lithium

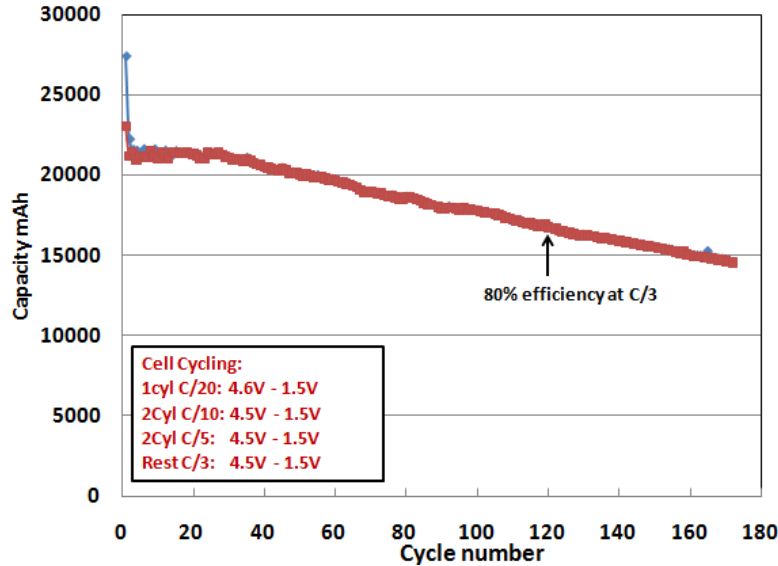


Source: Envia Systems

The cell with supplemental lithium showed excellent cycling performance with an energy density of about 246Wh/Kg at first C/3 rate and has a volume energy density of 400Wh/L. The cell finished 100 cycles with about 96 percent capacity efficiency. On the other hand the cell with no supplemental lithium showed a rapid capacity fade and the efficiency fell to about 63 percent after 100 cycles.

With the learning from the single layer pouch cells, large capacity 10-40Ah pouch cells were built in our Envia China facility with HCMR™ cathode and high capacity SiO-graphite anodes. The pouch cells were successfully built with a cathode loading level of approximately 22-27mg/cm². Figure 71 shows the cycling performance of 20Ah capacity pouch cells, where the first cycle was run at a rate of C/20, the next two cycles at a rate of C/10, followed by two cycles at a rate of C/5 and the remaining cycles at a C/3 rate. The cell was designed with an anode excess balance of 20 percent over the cathode and supplemental lithium additive added to the anode to compensate for the irreversible capacity loss in the anode.

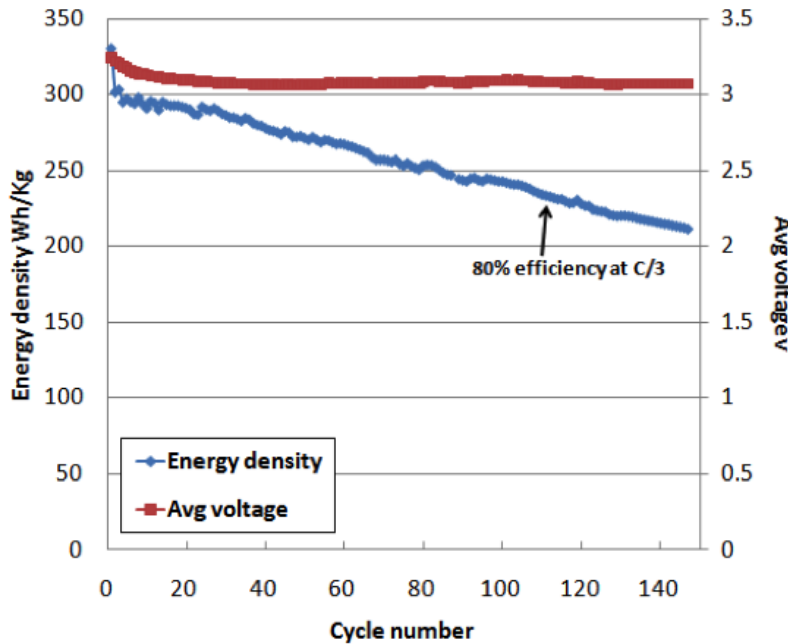
Figure 71: Electrochemical Performance of 20Ah Cells With Envia's HCMR™ Cathode and High Capacity Silicon-Based Anode



Source: Envia Systems

Figure 72 shows the corresponding cell average voltage and energy density of the 20Ah capacity pouch cells. The battery showed an energy density of 296Wh/Kg at a C/3 rate with an 80 percent retention in energy density and capacity observed at 110 cycles and 120 cycles, respectively. Achieving an energy density of approximately 300Wh/kg from a lithium ion cell was a significant accomplishment.

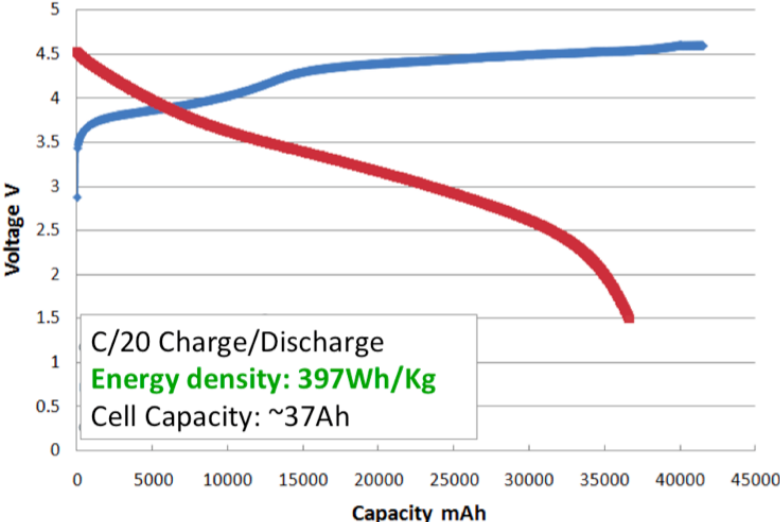
Figure 72: Energy Density and Average Voltage Versus Cycles for the 20Ah Capacity Pouch Cells with Envia's HCMR™ Cathode and High Capacity Silicon-Based Anode



Source: Envia Systems

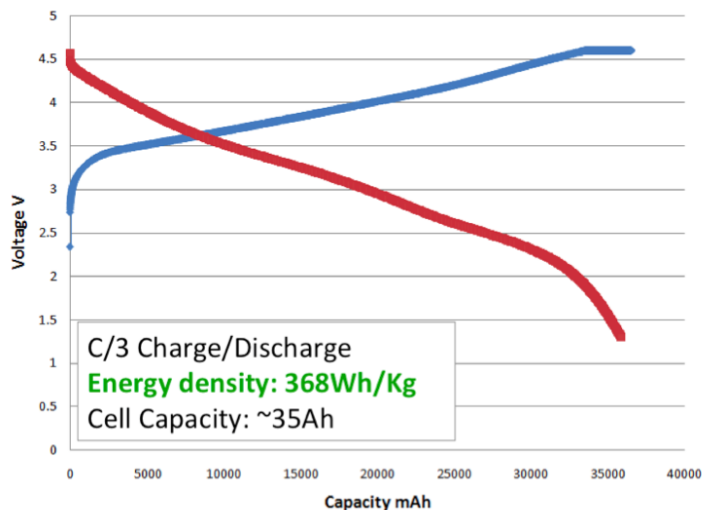
Subsequent to the 20Ah cell build, which reached an energy density of 300Wh/kg, Envia continued to improve the materials and cell design and constructed 37Ah capacity pouch cells at a C/20 rate. Electrochemical results from these cells show an energy density of 397Wh/Kg at the C/20 rate. At a C/3 rate the measured energy density was 368Wh/Kg, which was well above our 350Wh/kg target for the quarter. It should be noted that an energy density of 368Wh/kg at C/3 and 397Wh/kg at C/20 was already breaking the record of being the highest energy density lithium ion batteries in the world, but our target still continued to reach 400Wh/kg with a cycle life >500 cycles. Figure 73 shows the first charge-discharge curves at a C/20 rate (Figure 73a) and at a C/3 rate (Figure 73b).

Figure 73a: First C/20 Charge-Discharge Curves from 37Ah Capacity Pouch Cells Incorporating Envia’s HCMR™ Cathode and High Capacity Silicon-Based Anode



Source: Envia Systems

Figure 73b: C/3 Charge-Discharge Curves from 35Ah Capacity Pouch Cells Incorporating Envia’s HCMR™ Cathode and High Capacity Silicon-Based Anode



Source: Envia Systems

In order to continue to push the limits with respect to energy density, all aspects of the cell that contribute to the performance and weight need to be taken into account. Electrolyte density is an important parameter to vary in the cell design to improve the energy density of the battery. The density of the electrolyte could vary between 1.1g/cc and 1.4g/cc depending on the electrolyte composition and salt concentration. Various electrolyte compositions were explored to optimize the density of the electrolyte without compromising the battery performance.

Calendaring (compressing the material on the electrode) is very important to achieve good gravimetric and volumetric energy density in the battery. The density of the cathode could vary from 2g/cc to 3.4g/cc depending on the true density and tap density of the cathode powder. Increasing the electrode density by calendaring the electrode will reduce porosity and electrolyte consumption, therefore, lowering the weight of the battery. On the other hand, extensive compression could close the pores in the electrode and lead to particle cracking and mechanical instability, which can result in poor capacity and cycle life. Extensive studies were made to synthesize a cathode material with high tap density (2-3 g/cc) to enable high electrode densities and still maintaining good cycle life. Table 9 shows calculated energy densities of a battery at C/3 rate with respect to the electrode density and electrolyte density. The table is designed by assuming a specific cathode and anode loading level. For the cathode press density of 2.5g/cc and electrolyte density of 1.3g/cc, the energy density of the battery is 343Wh/Kg at C/3. The energy density could go up by more than 5 percent by increasing the density of the cathode electrode from 2.5g/cc to 3g/cc. Similarly the energy density will increase by about 3 percent if the electrolyte density decreases from 1.3g/cc to 1g/cc at a certain cathode electrode press density.

Table 9: Energy Density Calculations at C/3 With Respect to the Cathode Electrode Density and Electrolyte Density (The Cell Modeling Was Done by Assuming a Fixed Cathode and Anode Loading Level and a Specific Ah for The Cell Capacity)

Energy density (Wh/Kg) at C/3 variation w.r.t. cathode and electrolyte density		Electrolyte density g/cc			
		1.3	1.2	1.15	1.0
Cathode press density g/cc	2.5	343	349	352	355
	2.7	350	356	359	362
	2.9	356	362	365	368
	3	359	365	368	371

Source: Envia Systems

The specific capacities of the cathode and anode play an important role in determining the energy density of the battery. Table 10 calculates how the energy density of a battery at C/3 changes with the variation in the specific capacity of the anode and cathode. The energy density is calculated by assuming a fixed loading level of cathode and varying the anode so that the anode is balanced with 30 percent excess over the cathode. In order to reach the target 400Wh/Kg, the cathode capacity and the anode capacity needed to increase to the higher values in Table 10. For the cell modeling the cathode compression density and electrolyte density were assumed to be 2.5g/cc and 1.3g/cc respectively. Improvement in cell design, material electrochemical properties and cell energy density and cycle life were also critical considerations.

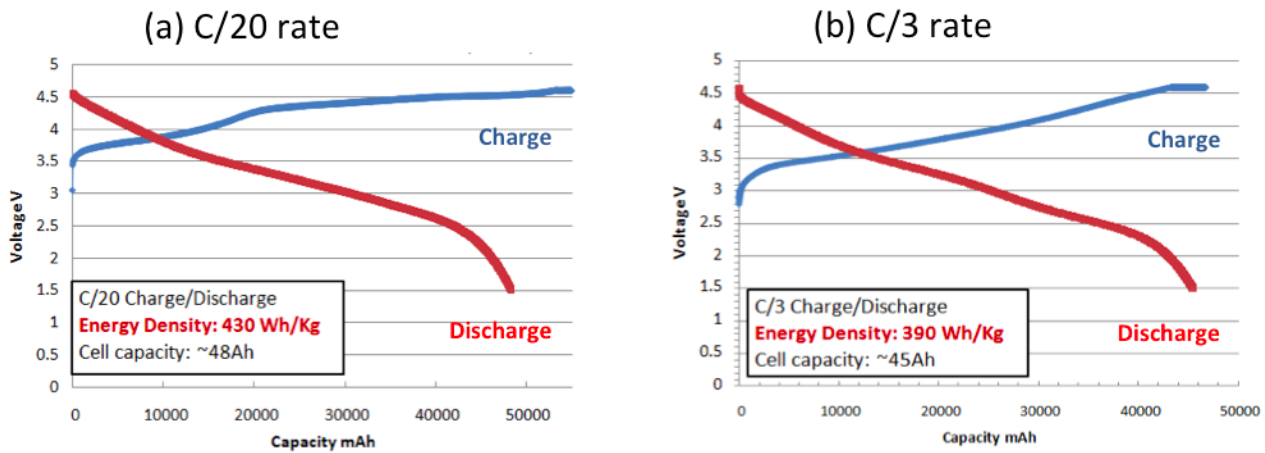
Table 10: Energy Density Calculations at C/3 With Respect to the Cathode and Anode Specific Capacities at a C/3 Rate (The Cell Modeling Was Done by Assuming a Fixed Cathode Loading Level and 30 Percent Excess Anode Balancing)

Energy density (Wh/Kg) at C/3 variation w.r.t. cathode and anode specific capacity for anode excess balance of 30% at C/20		Anode capacity at C/3 (mAh/g)			
		1550	1650	1750	1850
Cathode capacity at C/3 (mAh/g)	240	340	343	347	350
	250	354	358	361	364
	260	368	372	376	379
	270	382	386	390	394
	280	397	401	405	408

Source: Envia Systems

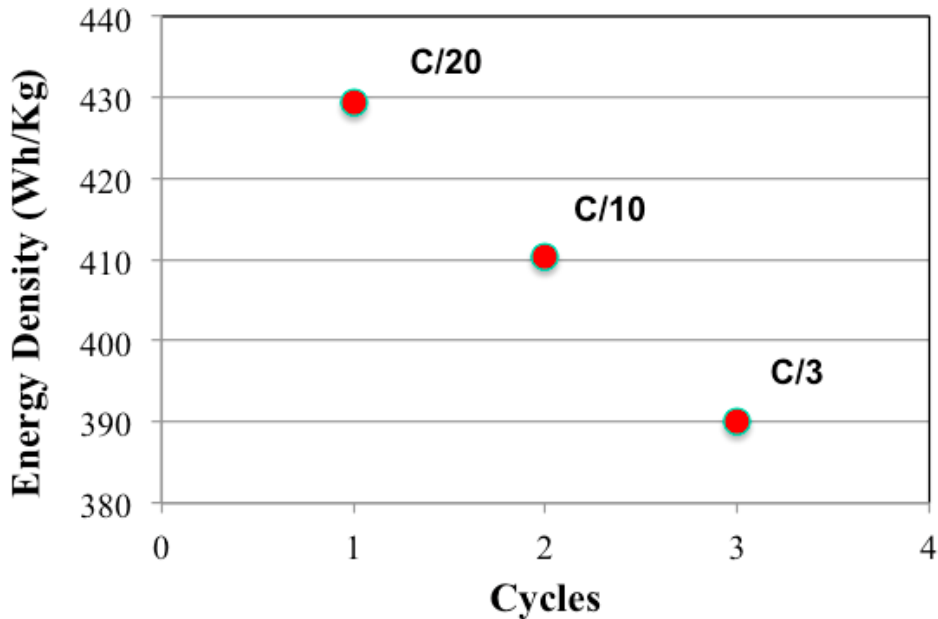
Incorporating all of the material development and improvements and optimized cell design and testing protocols, Envia was able to produce and deliver commercial format pouch cells with a capacity of 48Ah at a C/20 rate. These were the final cells fabricated that nearly met all of the project's targets. Figure 74 shows the charge discharge electrochemical results from these cells showing an energy density of 430Wh/Kg at the C/20 rate (Figure 74a) and a measured energy density of 390Wh/kg at a C/3 rate (Figure 74b) when cycled between 4.6V to 1.5V. The corresponding cell capacities were 48Ah and 45Ah at a C/20 and C/3 rate, respectively. The energy density values of 390Wh/Kg at C/3 nearly reached the final target of 400Wh/Kg. Figure 75 shows a plot of energy density versus cycles for a C/20, C/10 and C/3 rate cycled between 4.6V and 1.5V.

Figure 74: (A) Charge and Discharge Curves for the First Formation Cycle at a C/20 Rate and (B) Third Cycle Corresponding to a C/3 Rate



Source: Envia Systems

Figure 75: Energy Density versus Cycles at a C/20, C/10 and C/3 Rate Cycled at 100 Percent DOD (4.6V to 1.5V)

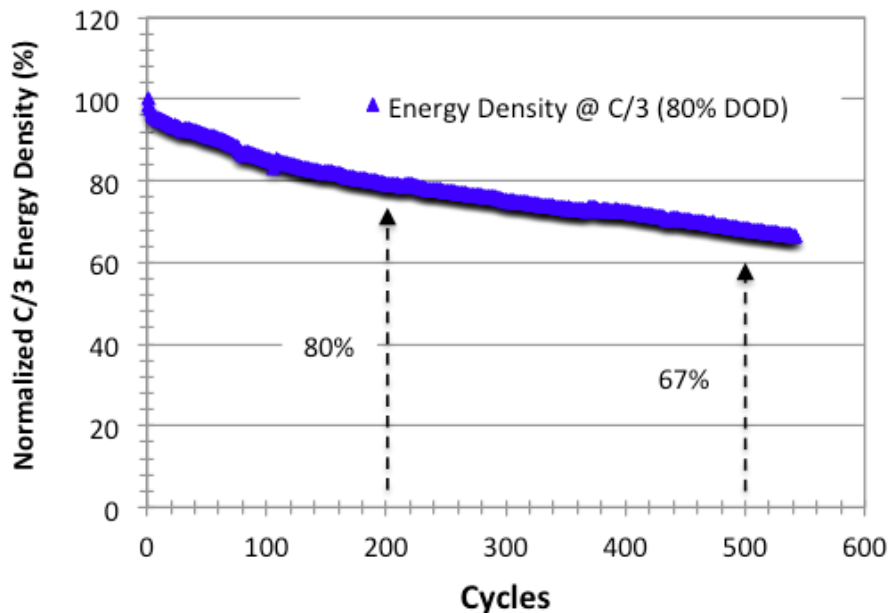


Source: Envia Systems

Figure 76 shows the normalized energy density versus cycles for the same approximately 45Ah pouch cell cycled at 80 percent depth of discharge at a C/3 rate between the voltage of 4.3V to 1.5V. The figure shows the cell reached more than 500 cycles, where 80 percent efficiency was reached approximately 200 cycles and approximately 67 percent efficiency being reached at cycle 500. Cycling the cells at 80 percent DOD at a C/3 rate was a project guideline and condition for the program. With this guideline in mind, the cell was precisely design to cycle at 80 percent DOD at a C/3 rate. If the goal of the cells was to cycle at a different rate, the cell

specifications will need to be redesigned. Envia recognizes that the goal of this program was to reach 500 cycles before reaching 80 percent efficiency, but obtaining 200 cycles at 80 percent efficiency and then the cell continuing to cycle past 500 cycles is still a great achievement from materials and a cell that few people expected to cycle past 50 cycles.

Figure 76: Normalized Energy Density versus Cycles for a 45Ah Cell Cycled at 80 Percent DOD at a C/3 Rate



Source: Envia Systems

To the best of Envia’s knowledge, a lithium battery with an energy density of 390Wh/Kg at a C/3 rate is the world’s highest energy density lithium battery, and moreover, this cell has achieved >500 cycles. This final program targets are achievable only when one combines the highest capacity electrode materials, cell engineering know-how and cell fabrication and testing expertise. Achieving the highest energy density from lithium ion batteries enables new opportunities for automotive, consumer electronics, military and grid applications addressing concerns about cost, size, weight and miles per charge. Envia looks forward to continue the development and commercialize the developed technology.

CHAPTER 5: Independent Cell Testing Validation

An important deliverable of the project was to demonstrate and deliver a minimum of two large format cells for independent testing. The project included an arrangement with the Naval Surface Warfare Center, Crane Division (NSWC Crane) Test & Evaluation Branch to independently test the cells. The idea was to have an unbiased third party validation of the test results from a nationally recognized expert testing laboratory. Envia fulfilled the deliverable by shipping five approximately 45Ah capacity cells (cell #5, #6, #9, #11 and #12) to the Naval Surface Warfare Center. The NSWC received, tested and verified the energy density, capacity and cycle life reported by Envia. Figure 77 shows the NSWC results showing cell energy density for the first 23 cycles from the received 5 cells. The figure also shows the results from cell #7 which was tested at Envia and used for comparison. The figure clearly shows that the energy density values (>400Wh/kg at C/20) obtained at Envia were also independently validated at the NSWC. Also, the initial cycling behavior was also reproduced. The data presented in Figure 77 corresponds to cells showing a 1st cycle at C/20 rate, 2nd cycle at C/10 rate, 3rd cycle at C/3 rate (100 percent DOD) and the consecutive cycles at C/3 rate (80 percent DOD).

Figure 77: Energy Density Versus Cycles for the 5 Cells Delivered to the NSWC (Cell #5, #6, #9, #11 & #12) Comparing to Cell #7 Which Was Tested at Envia

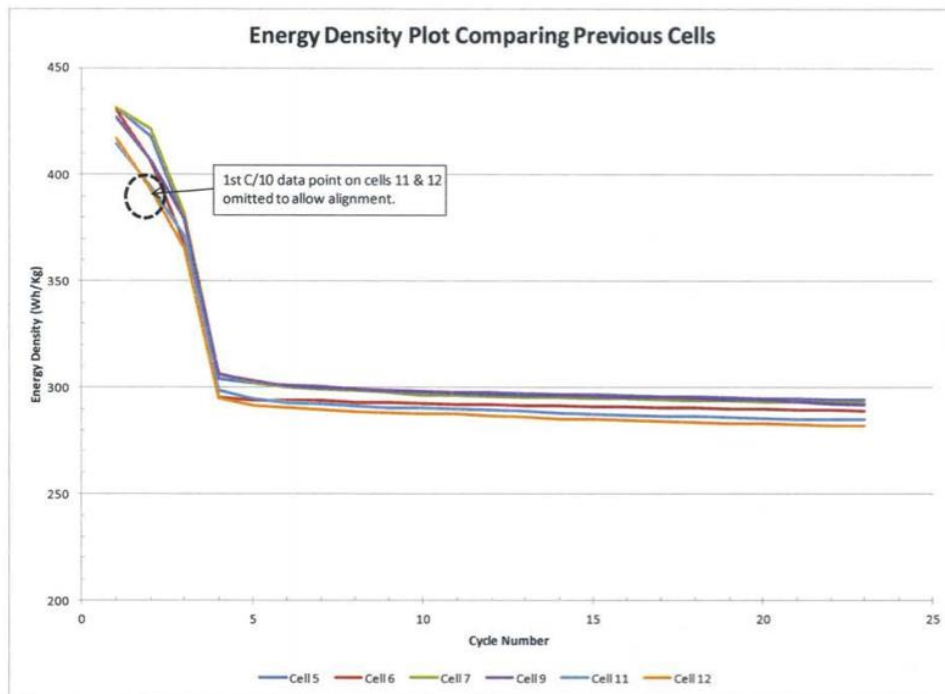


Figure Is From Official **NSWC** Report

Source: NWSC, Envia Systems

With respect to cycle life, the Naval Surface Warfare Center at Crane also tested the cycle life. Figure 78 shows the results obtained from cell #9, which was cycled more than 400 cycles with an efficiency of approximately 73 percent. Cell #9 tested at the NSWC showed improved cycling behavior when compared to the cells tested at Envia. Cell #9 showed 240 cycles before reaching an 80 percent energy density efficiency at 80 percent DOD at a rate of C/3.

Figure 78: Energy Density versus Cycles for Cell #9 Tested at the NSWC in Crane

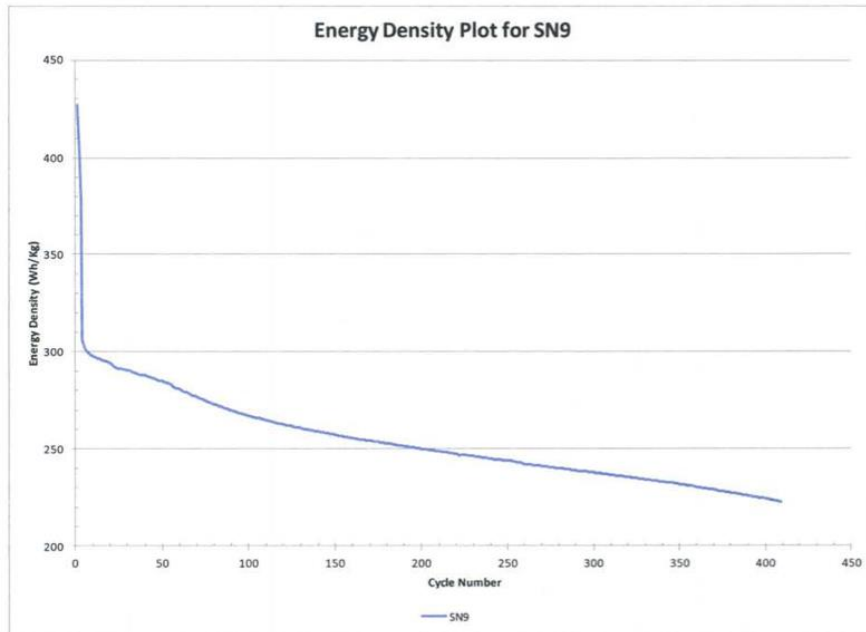
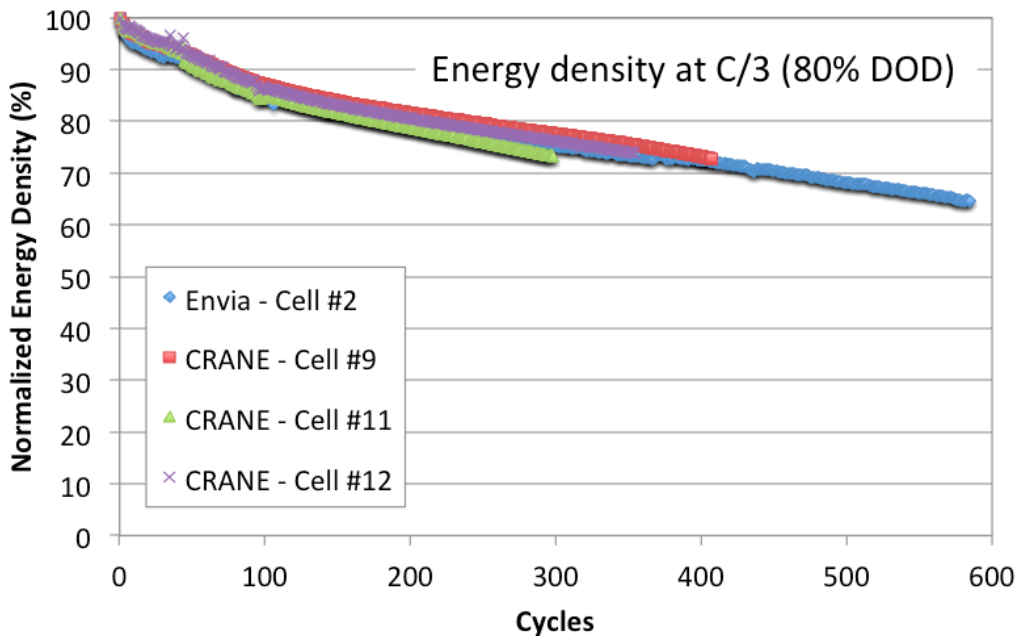


Figure Is From Official **NSWC** Report

Source: NSWC, Envia Systems

Figure 79 shows the comparison of the cycling data obtained at Envia in comparison to the cycling data obtained at the NSWC.

Figure 79: Comparison of the Normalized Energy Density Versus Cycles for 3 Cells Tested at NSWC (Cell #9, #11 And #12) and Tested at Envia (Cell #2)



Source: Envia Systems

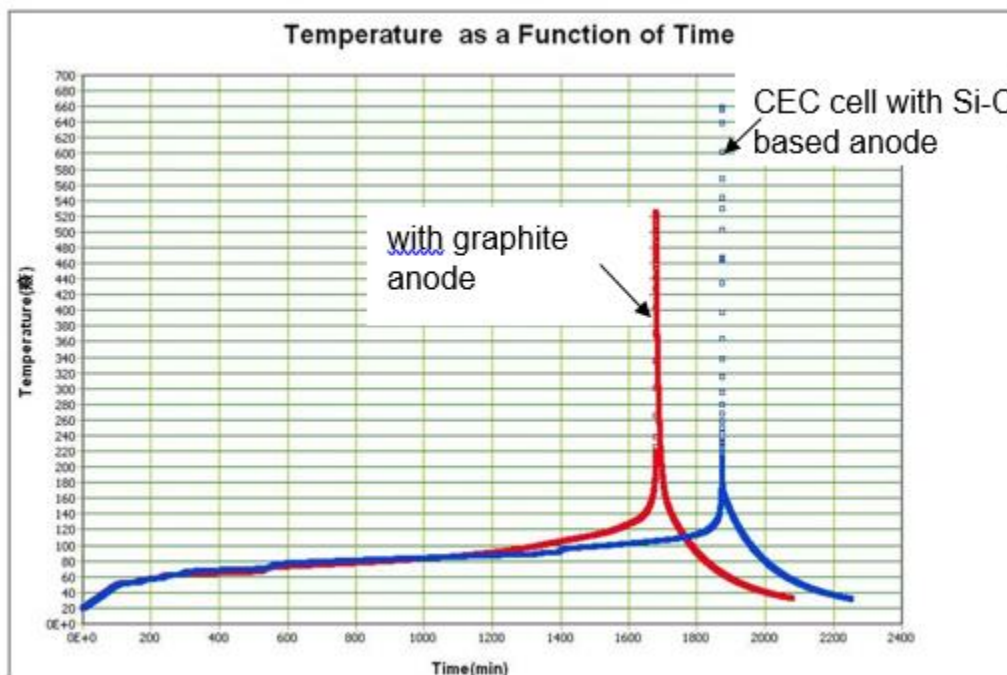
Once again 5 cells were delivered to the Naval Surface Warfare Center in Crane, IN for independent testing and validation of the results obtained by Envia. Similar to the results obtained at Envia, the NSWC obtained C/20 energy densities well above 400Wh/kg and C/3 energy densities of 393Wh/kg. With respect to cycle life testing, the Naval Surface Warfare Center obtained slightly better cycling performance than Envia. Cell #9 showed 240 cycles at a C/3 rate (80 percent DOD) before reaching an 80 percent energy density efficiency and 409 cycles before reaching an efficiency of approximately 73 percent. Which these results, the energy density and cycling results obtained at Envia were independently verified.

CHAPTER 6:

Thermal Stability and Abuse Testing

Envia purchased an Accelerating Rate Calorimeter (EV-ARC) from Thermal Hazard Technology to elucidate the thermal stability of the cells. The EV-ARC enables Envia to implement various safety tests on the high capacity batteries, including abuse and electro-thermal dynamics tests. Figure 80 shows the preliminary ARC results from a 45Ah cell combining Si based anodes and HCMR™ cathodes in comparison to a 20Ah graphitic cell that incorporates a comparable HCMR™ cathode.

Figure 80: Thermal Characteristics of a (Approximately 45Ah) Silicon-Based Cell in Comparison to a (Approximately 20Ah) Graphite Based Cell



Source: Envia Systems

The figure shows preliminary results were the onset temperature for thermal runaway happens at an earlier temperature for the graphite cell when compared to the Si cell. More detail analysis on the total heat generated is still ongoing, but this gives a first glimpse at the thermal and safety characteristics of the cells.

Nail penetration is a test used to mimic a collision or an impact where a fully charged cell is abruptly shorted by the introduction of a nail. Automotive specifications require passing of the nail penetration test without the presence of a fire. There is definitely a great deal of know-how and engineering that goes into the cell design and selection of specific cell components to allow the cell to pass this test. The cells produced during this program had a main goal that

was energy density and cycle life, not safety. In order to address safety, other aspect of the cell design need to be taken into account like type of separator, electrolyte, current collectors, etc. Even though the cells were not designed for safety, the nail penetration test was still performed at Envia and at the NSWC. Envia performed two tests where on of the two passed the nail penetration test. After this very promising result the test was performed at the NSWC on two cells where both cells failed the test. Again, the nail penetration results were as expected as the cells are prototype cells that were not designed with this test in mind. Envia is currently looking at the safety aspects of the cell with the intension to address and improve the safety performance of the cells.

CHAPTER 7: Future Direction

After three and a half years of the project Envia successfully showed the highest energy density lithium ion batteries in the world with a C/20 energy density >400Wh/kg and a C/3 energy density of 390Wh/kg. The cells cycled for more than 500 cycles at a C/3 rate (80 percent DOD) showing an efficiency approximately 70 percent. The cells' test results were also independently validated by the Naval Surface Warfare Center in Crane, IN, which was selected for the project.

Envia is excited to have achieved the audacious energy density goals of this project, especially given the short time period in which they were accomplished. However, Envia also recognizes that there is considerable engineering and development work to perform before this technology becomes an automotive product. Some of the areas that continue to be addressed are cell cycle life, calendar life, power and the safety characteristics of the cell. For this, Envia is exploring the failure modes of this project's cells from a materials (cathode, anode, electrolyte, separator), cell design (format, electrode loading, balancing, electrode density, voltage window) and a cell testing (voltage window and activation protocol) point of view. Efforts also continue to increase the specific capacity of both cathode and anode, reduce IRCL, optimize cell design and improve the morphology and surface passivation of both the electrode materials. Envia is committed to continue the development and successfully this this technology to market.

Much of the engineering development will now depend on the specific customer and application that will use this technology. Envia has been working with General Motors for the past 4 years on taking our first generation cathode technology and engineering it into a product for General Motors electric vehicles (such as the Chevy Volt). Envia anticipates a similar (possibly longer) timeline for developing this project's innovations into a product. General Motors (along with other automakers) has expressed excitement over our latest technology. Envia has already begun developing engineering plans with these automakers and is confident that they will result in industry leading electric vehicles at price points that truly enable mass proliferation of electric vehicles.

GLOSSARY

ADVANCED RESEARCH PROJECTS AGENCY–ENERGY (ARPA-E) - The Advanced Research Projects Agency-Energy (ARPA-E) advances high-potential, high-impact energy technologies that are too early for private-sector investment. ARPA-E projects have the potential to radically improve U.S. economic security, national security, and environmental well-being. The America COMPETES Act of 2007 authorized the establishment of ARPA-E within the U.S. Department of Energy. However, ARPA-E did not officially come into existence until early 2009, when it received \$400 million in funding through the American Recovery and Reinvestment Act.¹

ALTERNATING CURRENT (AC) - Flow of electricity that constantly changes direction between positive and negative sides. Almost all power produced by electric utilities in the United States moves in current that shifts direction at a rate of 60 times per second.

AMERICAN RECOVERY AND REINVESTMENT ACT OF 2009 (ARRA) - U.S. Congress passed the American Recovery and Reinvestment Act of 2009 on February 13, 2009, at the urging of President Obama, who signed it into law four days later. A direct response to the economic crisis, the Recovery Act strives to create new jobs and save existing ones, spur economic activity and invest in long-term growth, and foster unprecedented levels of accountability and transparency in government spending. Among its objectives, the act makes \$275 billion available for federal contracts, grants, and loans.

AMPERE (Amp) - The unit of measure that tells how much electricity flows through a conductor. It is like using cubic feet per second to measure the flow of water. For example, a 1,200 watt, 120-volt hair dryer pulls 10 amperes of electric current (watts divided by volts).

AMPERE-HOUR (Ah) - A unit of electric charge, usually used for batteries. This unit combines the amount of current with how long that current can be sustained until the battery completely discharges. Large batteries have several ampere hours but cell phones and other small devices have batteries with a total charge measured in milliampere hours. This measured quantity is called battery capacity.²

ANODE - The terminal or electrode from which electrons leave a system. In a battery or other source of direct current, the anode is the negative terminal.³

ARGONNE NATIONAL LABORATORY (ANL) - The first and the largest of the national labs chartered in 1946 in DuPage County, Illinois. The U.S. Department of Energy funds Argonne National Lab and University of Chicago Argonne, LLC manages the site. Argonne National Lab

¹ [Advanced Research Projects Agency – Energy Website](https://arpa-e.energy.gov) (https://arpa-e.energy.gov)

² [University of Calgary, Energy Education Website](https://energyeducation.ca/encyclopedia/Ampere_hour) (https://energyeducation.ca/encyclopedia/Ampere_hour)

³ [Encyclopedia Britannica](https://www.britannica.com/technology/anode) (https://www.britannica.com/technology/anode)

is the descendant of Chicago's Metallurgical Laboratory and the home of Enrico Fermi's first controlled nuclear chain reaction demonstration.⁴

CALIFORNIA ENERGY COMMISSION (CEC) - The state agency established by the Warren-Alquist State Energy Resources Conservation and Development Act in 1974 (Public Resources Code, Sections 25000 et seq.) responsible for energy policy. The Energy Commission's five major areas of responsibilities are:

- Forecasting future statewide energy needs
- Licensing power plants sufficient to meet those needs
- Promoting energy conservation and efficiency measures
- Developing renewable and alternative energy resources, including providing assistance to develop clean transportation fuels
- Planning for and directing state response to energy emergencies.

CATHODE - Negative terminal or electrode through which electrons enter a direct current load, such as an electrolytic cell or an electron tube, and the positive terminal of a battery or other source of electrical energy through which they return.⁵

DIRECT CURRENT (DC) - A charge of electricity that flows in one direction and is the type of power that comes from a battery.

ENERGY DENSITY - The amount of energy that can be stored in a given mass of a substance or system. The higher the energy density of a system or material, the greater the amount of energy stored in its mass.⁶

NAVAL SURFACE WARFARE CENTER, CRANE, IN - The mission of NSWC Crane Division is to provide acquisition engineering, in-service engineering and technical support for sensors, electronics, electronic warfare and special warfare weapons. NSWC Crane also works to apply component and system-level product and industrial engineering to surface sensors, strategic systems, special warfare devices and electronic warfare/information operations systems, as well as to execute other responsibilities as assigned by the Commander, Naval Surface Warfare Center.⁷

4 [Phys.Org Website](https://phys.org/partners/argonne-national-laboratory/) (https://phys.org/partners/argonne-national-laboratory/)

5 [Encyclopedia Britannica](https://www.britannica.com/technology/cathode) (https://www.britannica.com/technology/cathode)

6 [University of Calgary, Energy Education Website](https://energyeducation.ca/encyclopedia/Energy_density) (https://energyeducation.ca/encyclopedia/Energy_density)

7 [FLC Business Search](https://www.federalabs.org/labs/naval-surface-warfare-center-nswc-crane-division) (https://www.federalabs.org/labs/naval-surface-warfare-center-nswc-crane-division)

PLUG-IN ELECTRIC VEHICLE (PEV) - A general term for any car that runs at least partially on battery power and is recharged from the electricity grid. There are two different types of PEVs to choose from - pure battery electric and plug-in hybrid vehicles.

SCANNING ELECTRON MICROSCOPE (SEM) - Type of electron microscope designed for directly studying the surfaces of solid objects that utilizes a beam of focused electrons of relatively low energy as an electron probe that is scanned in a regular manner over the specimen. The action of the electron beam stimulates emission of high-energy backscattered electrons and low-energy secondary electrons from the surface of the specimen.⁸

UNITED STATES DEPARTMENT OF ENERGY (U.S. DOE) - The federal department established by the Department of Energy Organization Act to consolidate the major federal energy functions into one cabinet-level department that would formulate a comprehensive, balanced national energy policy. DOE's main headquarters are in Washington, D.C.

⁸ [Encyclopedia Britannica](https://www.britannica.com/technology/scanning-electron-microscope) (https://www.britannica.com/technology/scanning-electron-microscope)